



**The Abdus Salam  
International Centre for Theoretical Physics**



**2235-1**

**School and Conference on Mathematics and Physics of Soft and  
Biological Matter**

*2 - 13 May 2011*

**Notes on Elastomers, classical and neo-classical - the ultimate soft solids**

M. Warner  
*Cavendish Laboratory  
University of Cambridge  
UK*

Mathematics and Physics of Soft and Biological Matter  
notes on  
Elastomers, classical and neo-classical — the ultimate soft solids

M. Warner  
Cavendish Laboratory, University of Cambridge

April 21, 2011



## PREFACE

These notes are loosely based on the liquid crystals, polymers, elasticity and nematic elastomers sections of the book “Liquid Crystal Elastomers” by Warner and Terentjev, OUP (paperback edition 2007).

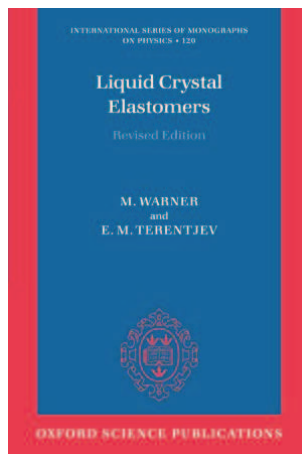


Figure 1: Warner and Terentjev: “Liquid Crystal Elastomers”: cover of the paperback edition 2007.

The notes have many exercises, some of which are solved and others of which have hints for their solution. It is suggested to the reader that these will help in understanding the subject, in particular where it diverges from classical elasticity theory (for instance when rotations are important in the elastic response because of the internal rotational degree of freedom, the director). The approach to elasticity is with the deformation gradient tensor because non-linear elasticity is used throughout (rubbers are capable of huge deformations). We use this tensor, rather than Cauch-Green tensors, also because it more directly records rotations which are so important.

The first chapter of the notes is a birds eye view of the whole field. It mentions areas not covered here, for instance smectic elastomers. Their elasticity is especially rich because the constraint of constant layer spacing is hard on the energy scale of elastomers. We thus have this and the constraint of constant volume governing the large deformations of those unusual elastomers.

The supersoft deformations of isotropic genesis nematic polydomain elastomers will hopefully be addressed in a research lecture after the material in these notes on nematic elastomers has been covered.

Mark Warner  
Cavendish Laboratory, University of Cambridge.  
April, 2011

## CONTENTS

---

<b>Contents</b>	<b>ii</b>
<b>1 An overview of liquid crystal elastomers</b>	<b>1</b>
<b>2 Liquid crystals</b>	<b>7</b>
2.1 Ordering of rod and disc fluids . . . . .	7
2.2 Nematic order . . . . .	8
2.3 Free energy and phase transitions of nematics . . . . .	10
2.4 Distortions of nematic order . . . . .	12
<b>3 Polymers, elastomers and rubber elasticity</b>	<b>15</b>
3.1 Configurations of polymers . . . . .	15
3.2 Classical rubber elasticity . . . . .	17
3.3 Liquid crystalline polymers . . . . .	21
<b>4 Classical elasticity</b>	<b>25</b>
4.1 The deformation tensor and Cauchy–Green strain . . . . .	25
4.2 Non-linear and linear elasticity; stresses . . . . .	27
4.3 Geometry of deformations and rotations . . . . .	28
4.3.1 Rotations . . . . .	29
4.3.2 Shears and their decomposition . . . . .	30
<b>5 Nematic rubber elasticity without director rotation</b>	<b>35</b>
5.1 Neo-classical theory . . . . .	35
5.2 Spontaneous distortions . . . . .	37
5.3 Nematic photoelastomers . . . . .	40
<b>6 Soft elasticity</b>	<b>43</b>
6.1 Director anchoring to the bulk . . . . .	43
6.1.1 Director rotation without strain . . . . .	43
6.1.2 Coupling of rotations to pure shear . . . . .	44
6.2 Soft elasticity . . . . .	45
6.2.1 Soft modes of deformation . . . . .	46
6.2.2 Symmetry arguments for soft response . . . . .	48
6.2.3 Forms of the free energy allowing softness . . . . .	49
6.2.4 Principal symmetric strains and body rotations . . . . .	49
6.3 Optimal deformations . . . . .	50
6.3.1 A practical method of calculating deformations . . . . .	50
6.3.2 Stretching perpendicular to the director . . . . .	52
6.4 Semi-soft elasticity and experiment . . . . .	54
6.4.1 A practical geometry of semi-soft deformation . . . . .	55
<b>7 How nematic elastomers distort</b>	<b>59</b>
7.1 Strain-induced microstructure: stripe domains . . . . .	60
7.2 General distortions of nematic elastomers . . . . .	62
7.2.1 One-dimensional quasi-convexification . . . . .	62
7.2.2 Full quasi-convexification . . . . .	64
7.2.3 Numerical and experimental studies . . . . .	66
<b>Bibliography</b>	<b>69</b>

## CHAPTER 1. AN OVERVIEW OF LIQUID CRYSTAL ELASTOMERS

Liquid crystal elastomers bring together, as nowhere else, three important ideas: *orientational order* in amorphous soft materials, *responsive molecular shape* and *quenched topological constraints*. Acting together, they create many new physical phenomena that are the subject of these notes. This bird's eye view sketches how these themes will come together.

Initially we introduce liquid crystals and polymers since they are our building blocks. A fuller primer for an undergraduate or graduate student embarking on a study of polymer or liquid crystal physics, or on complex fluids and solids, is found in the initial chapters of our book, "Liquid Crystal Elastomers" (Warner and Terentjev, 2007), hereafter referred to as WT. Then elastomers are discussed both from the molecular point of view, and briefly within continuum elasticity. We need to understand how materials respond at very large deformations for which only a molecular approach is suitable. Also one needs to understand the resolution of strains into their component pure shears and rotations, the latter also being important in these unusual solids. WT also provides a primer for the basics of these two areas that are otherwise only found in difficult and advanced texts.

Classical liquid crystals are typically fluids of relatively stiff rod molecules with long range orientational order. The simplest case is nematic – where the average ordering direction of the rods, the director  $\mathbf{n}$ , is uniform. Long polymer chains, with incorporated rigid anisotropic units can also order nematically and thus form liquid crystalline polymers. By contrast with rigid rods, these flexible chains elongate when their component rods align. This results in a change of average molecular shape, from spherical to spheroidal as the isotropic polymers become nematic. In the prolate anisotropy case, the long axis of the spheroid points along the nematic director  $\mathbf{n}$ , Fig. 1.1.

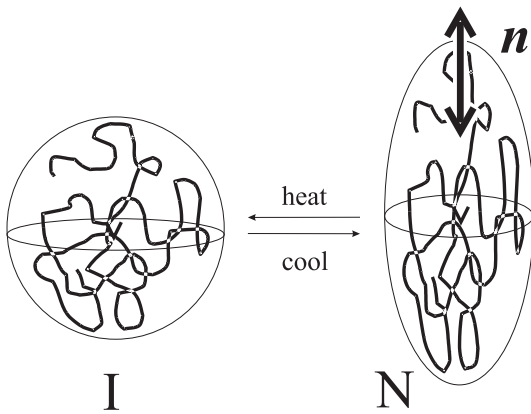


Figure 1.1: Polymers are on average spherical in the isotropic (I) state and elongate when they are cooled to the nematic (N) state. The director  $\mathbf{n}$  points along the principal axis of the shape spheroid. (The mesogenic rods incorporated into the polymer chain are not shown in this sketch, only the backbone is traced.)

So far we have no more than a sophisticated liquid crystal. Changes in average molecular shape induced by changes in orientational order do little to modify the properties of this new liquid crystal. Linking the polymer chains together into a gel network fixes their topology, and the melt becomes an elastic solid – a rubber. Radically new properties can now arise from this ability to change molecular shape while in the solid state. To understand this we have to consider rubber elasticity.

In rubber, monomers remain highly mobile and thus liquid-like. Thermal fluctuations move the chains as rapidly as in the melt, but only as far as their topological crosslinking constraints allow. These loose constraints make the polymeric liquid into a weak, highly extensible material. Nevertheless, rubber is a solid in that an energy input is required to change its macroscopic shape (in contrast to a liquid, which would flow in response). Equivalently, a rubber recovers its original state when external influences are removed. Systems where fluctuations are limited by constraints are known in statistical mechanics as 'quenched' - rigidity and memory of shape stem directly from this. It is a form of imprinting found in classical elastomers and also in chiral solids, as we shall see when thinking about cholesteric elastomers.

Can topology, frozen into a mobile fluid by constraints, act to imprint liquid crystalline order into the system? The expectation based on simple networks would be 'yes'. This question was posed, and qualitatively answered, by P-G. de Gennes in 1969. He actually asked a slightly more sophisticated question: Crosslink conventional

polymers (not liquid crystalline polymers) into a network in the presence of a liquid crystalline solvent. On removal of the solvent, do the intrinsically isotropic chains remember the anisotropy pertaining at the moment of genesis of their topology? The answer for ideal chains linked in a nematic solvent is ‘no’! Intrinsically nematic polymers, linked in a nematic phase of their own making, can also elude their topological memory on heating. How this is done (and failure in the non-ideal case) is a major theme of these notes.

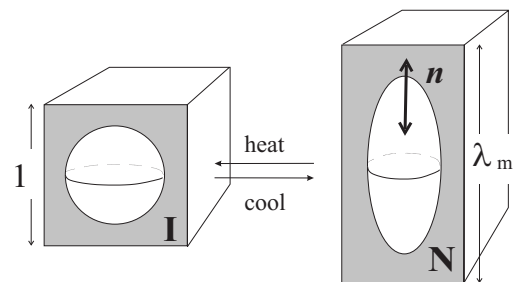
Second, what effects follow from changing nematic order and thus molecular shape? The answer is new types of thermal- and light-induced shape changes.

The third question one can ask is: While in the liquid-crystal state, what connection between mechanical properties and nematic order does the crosslinking topology induce? The answer to this question is also remarkable and is discussed below. It leads to entirely new effects – shape change without energy cost, extreme mechanical effects and rotatory-mechanical coupling. We give a preview below of these effects in the form of a sketch – details come later.

Rubber resists mechanical deformation because the network chains have maximal entropy in their natural, undeformed state. Crosslinking creates a topological relation between chains that in effect tethers them to the solid matrix they collectively make up. Macroscopic deformation then inflicts a change away from the naturally spherical average shape of each network strand, and the entropy,  $S$ , falls. The free energy then rises,  $\Delta F = -T\Delta S > 0$ . This free energy, dependent only on an entropy change itself driven by molecular shape change, explains why polymers are sometimes thought of as ‘entropic springs’. Macroscopic changes in shape are coupled to molecular changes. In conventional rubber it is always the macroscopic that drives the molecular; the induced conformational entropy of macromolecules offers the elastic resistance.

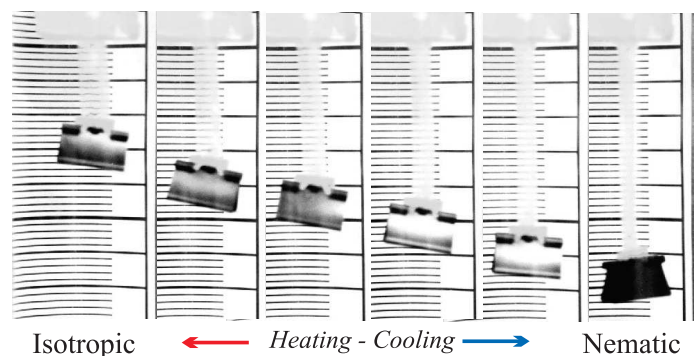
Nematic polymers suffer spontaneous shape changes associated with changing levels of nematic (orientational) order, Fig. 1.1. One now sees a reversal of influence: changes at the molecular level induce a corresponding change at the macroscopic level, that is induce mechanical strains, Fig. 1.2: a block of rubber elongates by a

Figure 1.2: A unit cube of rubber in the isotropic (I) state. Embedded in it is shown the average of the chain distribution (spherical). The block elongates by a factor  $\lambda_m$  on cooling to the nematic (N) state, accommodating the now elongated chains.



factor of  $\lambda_m > 1$  on cooling or  $1/\lambda_m < 1$  on heating. This process is perfectly reversible. Starting in the nematic state, chains become spherical on heating. But mechanical strain must now accompany the molecular readjustment. Very large deformations are not hard to achieve, see Fig. 1.3. Provided chains are in a broad sense ideal,

Figure 1.3: A strip of nematic rubber extends and contracts according to its temperature. Note the scale behind the strip and the weight that is lifted!



it turns out that chain shape can reach isotropy both for the imprinted case of de Gennes (on removal of nematic solvent) and for the more common case of elastomers formed from liquid crystalline polymers (on heating). Chains experiencing entanglement between their crosslinking points also evade any permanent record of their

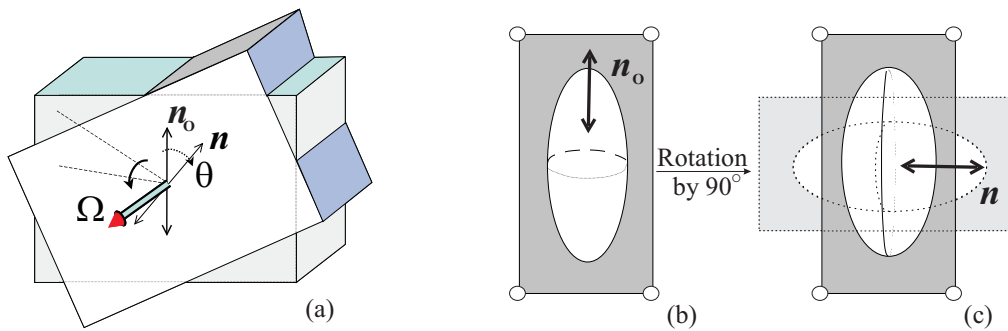


Figure 1.4: (a) Rotations of the director and matrix by angles  $\theta$  and  $\Omega$ , respectively. From (b) to (c) the director, and thus chain shape distribution, is rotated by  $90^\circ$  from  $\mathbf{n}_o$  to  $\mathbf{n}$ . The rubber is mechanically clamped and hence the chains in (c) that would be naturally elongated along  $\mathbf{n}$  must be compressed: the dotted spheroid in (c) is compressed to the actual solid spheroid.

genesis. Many real nematic elastomers and gels in practice closely conform to these ideal models. Others are non-ideal – they retain some nematic order at high temperatures as a result of their order and topology combining with other factors such as random pinning fields and compositional fluctuations. They still show the elongations of Fig. 1.3, but residues of non-ideality are seen in the elastic effects we review below.

This extreme thermomechanical effect, and the phenomena of Figs. 1.5 and 1.7, can only be seen in monodomain, well aligned samples. Without very special precautions during fabrication, liquid crystal elastomers are always found in polydomain form, with very fine texture of director orientations. The great breakthrough in this field, developing a first method of obtaining large, perfect monodomain nematic elastomers, was made by Küpfer and Finkelmann in 1991.

Nematic-elastic coupling was the third question we posed and gives rise to new rotational phenomena ubiquitous in liquid crystal elastomers. It is possible to rotate the director and the rubber matrix independently, see Fig. 1.4 (a). Such relative rotations of the body and of its internal anisotropy axis show that nematic elastomers are not simply exotic, highly-extensible, uniaxial crystals. Such materials belong to a class displaying so-called Cosserat elasticity, but with the distinction that deformations and rotations can be large in elastomers. Imagine now rotating the director while clamping the body so its shape does not change, Figs. 1.4(b) and (c). The natural, prolate spheroidal distribution, when rotated by  $90^\circ$  to be along  $\mathbf{n}$ , has a problem. Chains do not naturally fit, since the clamped body to which they are tethered is not correspondingly elongated along  $\mathbf{n}$  to accommodate their long dimensions. Chains in fact must have been compressed to fit, at considerable entropy loss if they were very anisotropic. A rotation of  $180^\circ$  recovers the initial state, so the free energy must be periodic, and turns out to be  $F = \frac{1}{2}D_1 \sin^2(\theta - \Omega)$ . The rotational modulus,  $D_1$ , was first given by de Gennes in the infinitesimal form  $\frac{1}{2}D_1(\theta - \Omega)^2$ . A rotation of the director in Fig. 1.4(b) would lead to a ‘virtual’ intermediate state depicted by dotted lines in Fig. 1.4(c). Subsequent squeezing to get back the actual body shape demanded by the clamp condition (full lines) of Fig. 1.4(c) costs an energy proportional to the rubber modulus,  $\mu$ , and to the square of the order,  $Q$ , (since  $Q$  determines the average chain shape anisotropy). Thus  $D_1 \sim \mu Q^2$ . In contrast to ordinary nematics, it costs energy to uniformly rotate the director independently of the matrix.

In liquid nematics it is director gradients that suffer Frank elastic penalties, and thus long-wavelength spatial variations of the rotation angle cost vanishingly small energy. Thermal excitation of these rotations causes even monodomain nematic liquids to scatter light and to be turbid. Not so monodomain nematic elastomers which are optically clear because even long wavelength director rotations cost a finite rubber-elastic energy  $\frac{1}{2}D_1 \theta^2$  and cannot be excited, see Fig. 1.5. The excitations have acquired a mass, in the language of field theory.

Local rotations, so central to nematic elastomers, yield a subtle and spectacular new elastic phenomenon which we call ‘soft elasticity’. Imagine rotating the director but now *not* clamping the embedding body, in contrast to Figs. 1.4(b) and (c). One simple response would be to rotate the body by the same angle as the director, and this would clearly cost no energy. However, contrary to intuition, there is an infinity of other ways by mechanical deformation to accommodate the anisotropic distribution of chains without its distortion

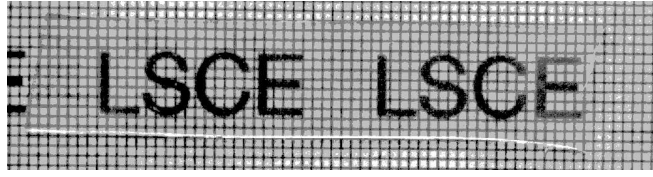


Figure 1.5: A strip of monodomain ‘single-crystal’ nematic rubber. It is completely transparent and highly birefringent (image: H. Finkelmann).

as it rotates. Thus the entropy of the chains does not change, in spite of macroscopic deformations. Figure 1.6 illustrates the initial and final states of a  $90^\circ$  director rotation. They are separated by a path of states, characterised by an intermediate rotation angle  $\theta$  and by a corresponding shape of the body, one of which is shown. This  $\theta$ -state is shown in the sketch (b) accommodating the spheroid without distorting it. A special combination of shears and elongations/compressions is required, but it turns out not very difficult to achieve in experiment!

One of the traditional ways to rotate the director in liquid crystals is by applying an electric (or magnetic) field and generating a local torque due to the dielectric anisotropy. Due to the nematic-elastic coupling, the director rotation is very difficult if an elastomer sample is mechanically constrained. Apart from a few exceptions (all characterised by a very low rubber-elastic modulus, such as in highly swollen gels) no electrooptical response can occur. However, if the elastomer is mechanically unconstrained, the situation changes remarkably. In a beautiful series of experiments, Urayama (2005,2006) has confirmed the prediction of soft elasticity: that the field-induced director rotation has no energy cost, can easily reach  $90^\circ$  rotation angles and has associated mechanical strains that almost exactly follow the sketch in Fig. 1.6.

Practically, when dealing with rubbers, one might instead impose a mechanical distortion (say an elongation,  $\lambda$ , perpendicular to the original director) and have the other components of strain, and the director orientation, follow it. The result is the same – extension of a rubber costs no elastic energy and is accompanied by a characteristic director rotation. The mechanical confirmation of the cartoon is shown in stress-strain curves in Fig. 1.7(a) and the director rotation in Fig. 1.7(b).

We have made liquid crystals into solids, albeit rather weak solids, by crosslinking them. Like all rubbers, they remain locally fluid-like in their molecular freedom and mobility. Paradoxically, their liquid crystallinity allows these solid liquid crystals to change shape without energy cost, that is to behave for some deformations like a liquid. Non-ideality gives a response we call ‘semi-soft’. There is now a small threshold before director rotation (seen in the electrooptical/mechanical experiments of Urayama (2005,2006), and to varying degrees in Fig. 1.7); thereafter deformation proceeds at little additional resistance until the internal rotation is complete. This stress plateau, the same singular form of the director rotation, and the relaxation of the other mechanical degrees of freedom are still qualitatively soft, in spite of a threshold.

There is a deep symmetry reason for this apparently mysterious softness that Fig. 1.6 rationalises in terms of the model of an egg-shaped chain distribution rotating in a solid that adopts new shapes to accommodate it. Ideally, nematic elastomers are rotationally invariant under separate rotations of both the reference state and of

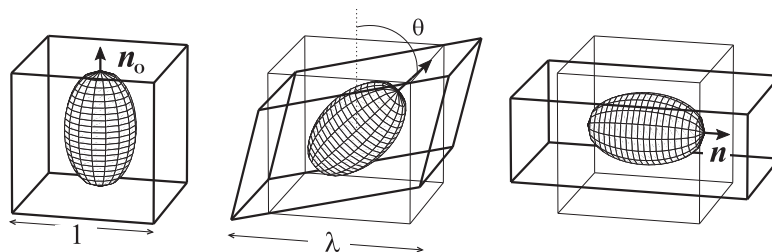


Figure 1.6: Rotation of chain shape distribution, from  $\mathbf{n}_0$  to  $\mathbf{n}$ , with an intermediate state  $\theta$  shown. The unconstrained rubber deforms to accommodate the rotating director without distorting the chain distribution.

the target state into which it is deformed. If under some conditions, not necessarily the current ones, an isotropic state can be attained, then a theorem of Golubović and Lubensky shows that in consequence soft elasticity must exist. It is a question of care with the fundamental tenet of elasticity theory, the principle of material frame indifference. We shall examine this theorem and its consequences many times in these notes, including what happens when the conditions for it to hold are violated, that is when semi-softness prevails.

Elastic softness, or attempts to achieve it, pervade much of the elasticity of nematic elastomers. If clamps or boundary conditions frustrate uniform soft deformation trajectories, microstructures will evolve to allow softness with the cost of interfaces being a relatively smaller price to pay. There are similarities between this so-called ‘quasi-convexification’ and that seen in martensite and other shape-memory alloys.

Cholesteric liquid crystals have a helical director distribution. Locally they are very nearly conventional nematics since their director twist occurs typically over microns, a much longer length scale than that associated with nematic molecular ordering. They can be crosslinked to form elastomers which retain the cholesteric director distribution. Several phenomena unique to cholesterics emerge: Being locally nematic, cholesteric elastomers would like on heating and cooling to lose and recover orientational order as nematic elastomers do. However, they cannot resolve the requirement at neighbouring points to spontaneously distort by  $\lambda_m$ , but in different directions. Accordingly, their chains cannot forget their topologically imprinted past when they attempt to reach a totally isotropic reference state (the second de Gennes’ prediction of 1969). Thus cholesteric rubbers also cannot deform softly in response to imposed strains. Their optical and mechanical responses to imposed stress are exceedingly rich as a result. They are brightly coloured due to selective reflection and change colour as they are stretched – their photonic band structure changes with strain. They can emit laser radiation with a colour shifted by mechanical effects. Further, the effect of topological imprinting can select and extract molecules of specific handedness from a mixed solvent. Such rubbers can act as a mechanical separator of chirality – a new slant on a problem that goes back to Pasteur.

We have sketched the essentials of nematic (and cholesteric) rubber elasticity. This survey leaves out many new phenomena dealt with in later chapters, for instance electromechanical Fredericks effects, photo-elastomers that drastically change shape on illumination, and so on.

Smectics are the other class of liquid crystal order. They have plane-like, lamellar modulation of density in one direction (SmA), or additionally a tilt of the director away from the layer normal (SmC). Many other more complex smectic phases exist and could also be made into elastomers. In many smectic elastomers, layers are constrained not to move relative to the rubber matrix. Deformations of a rubber along the layer normal are thus resisted by a layer spacing modulus,  $B$ , of the order of  $10^2$  times greater than the shear modulus of the matrix.

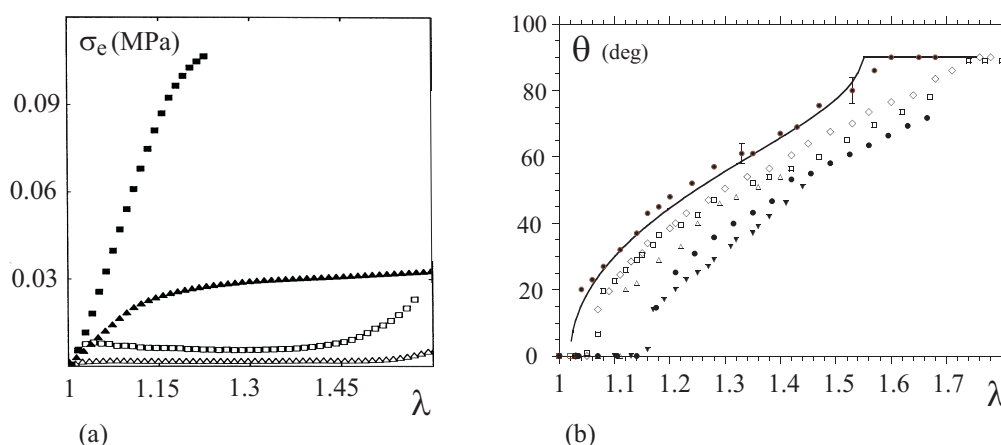


Figure 1.7: (a) Stress-deformation data of K pfer and Finkelmann (1994), for a series of rubbers with the same composition and crosslinking density, but differing in preparation history: some show a normal elastic response while others are remarkably soft. (b) The angle of director rotation on stretching nematic elastomer perpendicular to the director for a variety of different materials, from Finkelmann *et al.* (1997). The solid line from, theoretical modeling, accurately reproduces singular points and characteristic shape of data.

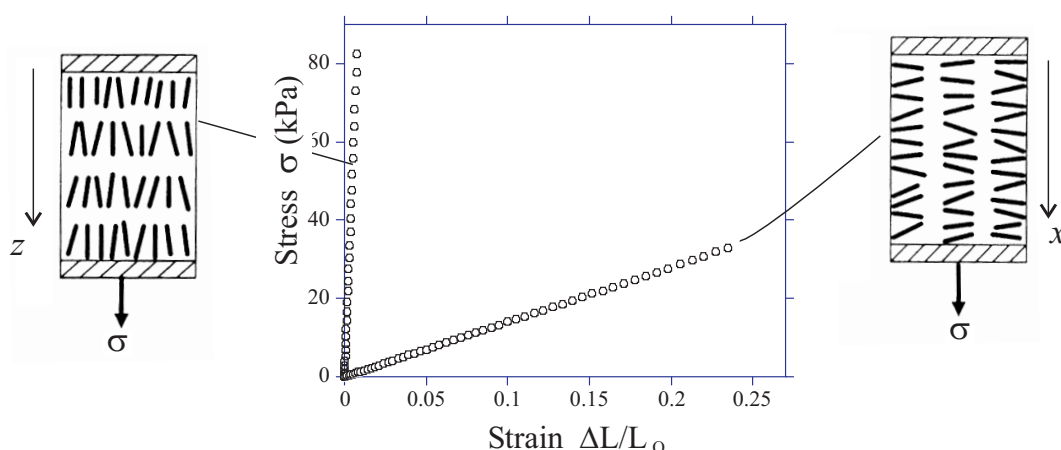


Figure 1.8: In-plane fluidity and parallel rigidity in a smectic A elastomer (Nishikawa *et al.*, 1997). The Young modulus parallel and perpendicular to the layer normals differ very greatly - the rubber elasticity is two-dimensional.

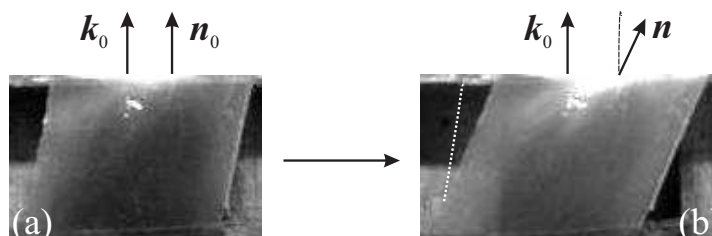


Figure 1.9: (a) A SmA elastomer (Hiraoka *et al.*, 2005). (b) Spontaneous shear  $\lambda_{xz}$  in achieving the SmC state.

Distortions in plane, either extensions or appropriate shears, are simply resisted by the rubber matrix. Thus SmA elastomers are rubbery in the two dimensions of their layer planes, but respond as hard conventional solids in their third dimension. Fig. 1.8 shows this behaviour. Such extreme mechanical anisotropy promises interesting applications.

The director tilt associated with the transition from SmA to SmC induces distortion in the polymer chain shape distribution. Since chain shape is coupled to mechanical shape for an elastomer, one expects, and sees in Fig. 1.9, spontaneous distortion. This response to order change is analogous to the elongations associated with orientational order of chains on entering the nematic state, but here we instead have shear. The amplitude is also large, of the order of 0.4 in the figure. As in the nematic case, the broken symmetry suggests a mechanism for SmC solids richer still than that of SmA elastomers, including SmC soft elasticity equivalent to that of Fig. 1.6.

The tilted, SmC, liquids also exist in chiral forms which must, on symmetry grounds be ferroelectric. Their elastomers are too. Ferroelectric rubber is very special: mechanically it is soft, about  $10^4$  times lower in modulus than ferro- and piezoelectrics because, as sketched above, its molecules are spatially localised by topological rather than energetic constraints. Distortions give polarisation changes comparable to those in ordinary ferroelectrics. But the response in terms of stress must necessarily be  $10^4$  times larger than in conventional materials. In these notes lack of space means we will not treat smectics. In WT their underlying liquid crystalline properties are reviewed in some detail. In Chapter 12, molecular picture of smectic elastomers valid to large distortions with strong layer constraints is given and the principal phenomena derived and discussed along with experiment. In Chapter 13 their continuum mechanics, which is also very complex, is developed.

We end our preview as we started – solids created by topological constraints are soft and highly extensible. Liquid crystal elastomers share this character with their important cousins, the conventional elastomers. But their additional liquid crystalline order gives them entirely new kinds of elasticity and other unexpected phenomena.

Liquid crystalline rubbery solids are polymer networks with nematic or smectic order. They display most of the complexities of conventional liquid crystals: directional but not translation long range order, optical birefringence and phase transitions. In fact they are liquid crystals with the exception that they cannot flow. Liquid crystal networks have many properties in addition to simple nematics and smectics, but to start understanding them, we briefly review conventional liquid crystals. WT (Warner and Terentjev, 2007) reviews more of the basics of what is a large and subtle subject. Excellent monographs exist, such as (de Gennes and Prost, 1994) and (Chandrasekhar, 1977). More specialist reviews explain corners of the field, for instance Landau theory or polarisational effects.

What are the essential differences when nematic liquid crystals are ‘solidified’ to form elastomers or gels? We shall see that rubber has all the mobility of liquids locally but not in a bulk sense – they cannot flow. The ordering thus remains mobile, albeit with some tethering to the solid matrix. All liquid crystal properties other than flow are manifested. We shall dwell here on properties of simple nematics, cholesterics and smectics that will be radically changed in networks.

Detailed molecular models play little role in nematic elastomers, apart from describing phase transitions and behaviour close to them, and for details of photoelastomers. Otherwise nematic, cholesteric and smectic elastomers, like conventional rubbers, are remarkably universal. We shall see that the properties of conventional elastomers depend essentially on the density of crosslinks and on temperature, much like an ideal gas. Liquid crystal elastomers depend upon these two factors, but also upon the shape anisotropy of their constituent polymer chains. This anisotropy is liquid crystalline (molecular) in origin, but can be measured directly or derived from macroscopic shape changes, a path we shall mostly follow. For this reason we do not dwell on detailed microscopic models of liquid crystals, and also not on models of polymers.

## 2.1 ORDERING OF ROD AND DISC FLUIDS

Nematics are anisotropic fluids. They derive their name from the thread-like defects in their anisotropy, i.e. disclinations that are observed under the microscope. The Greek word  $\nu\eta\mu\alpha$  for thread was taken by G. Friedel for the name of this phase. Molecular asymmetry is a precondition for macroscopic anisotropy. Weak asymmetry, for instance in the  $N_2$  molecule is insufficient to lead to spontaneous ordering. Increasing either the shape anisotropy (a *steric* influence), or the anisotropy of polarisability (a *thermotropic* influence), results in anisotropic liquids with long range directional ordering. The archetypical mesogenic molecule that forms such a fluid is para-azoxyanizole (PAA), see Fig. 2.1. Its shape is rod-like and its conjugated chemical bonds render it more polarisable along its long axis.

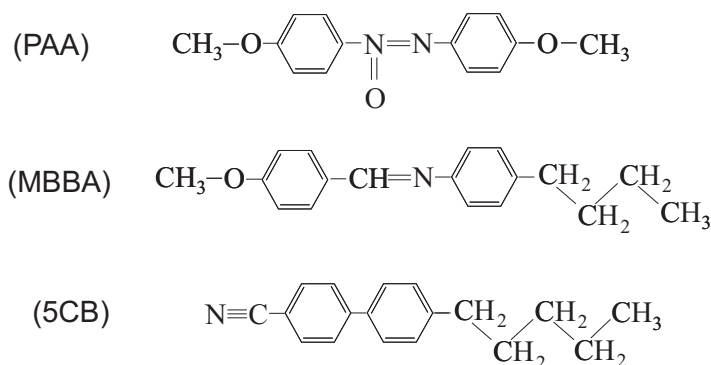


Figure 2.1: The chemical structure of para-azoxyanizole (PAA). This, and many other mesogenic (liquid crystal phase-forming) molecules are characterised by the same general pattern of two para-substituted aromatic rings rigidly linked into a rod-like structure. The terminal groups often vary, from a simple  $CH_3$  in PAA, to longer flexible chains in MBBA, or dipolar units, e.g. a  $CN$  group in cyanobiphenyls (5CB).

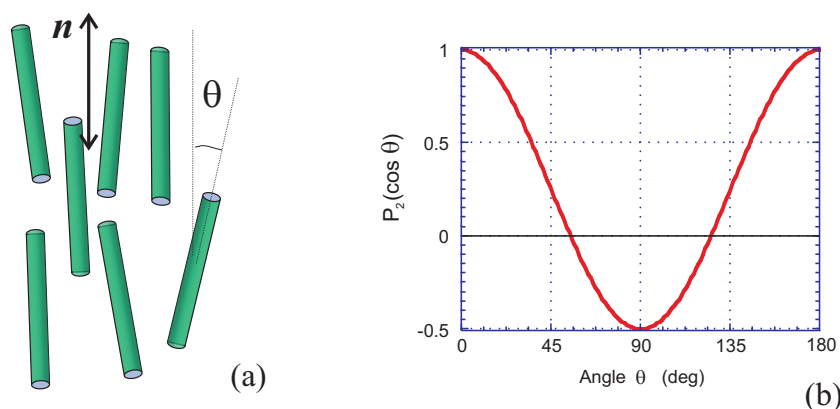


Figure 2.2: (a) The distribution of molecular axes around the average alignment direction  $\mathbf{n}$ . (b) The Legendre polynomial  $P_2$  as a function of angle  $\theta$  in the range  $0$  to  $180^\circ$ . Note that it varies between  $1$  and  $-0.5$ , that angles  $\theta$  and  $\pi - \theta$  are equivalent, and that positive and negative values of  $P_2$  refer to geometrically very different states.

When long-range van der Waals forces of anisotropic attraction are the dominant ordering influence, a reduction in temperature will lead to nematic ordering. Such systems are known as *thermotropic*. PAA is a good example of these. At a temperature  $T > 135^\circ\text{C}$ , even at the highest densities (in the melt, with no solvent at all), shape effects are insufficient to produce the nematic phase which can only result from cooling.

We shall be interested in directionally ordered molecules, irrespective of the mechanism by which they order (generally it is both). Rod-like molecules, similar to PAA, continue to order when incorporated into polymer chains and thereby create the essential alignment we require to obtain nematic (and later) smectic elastomers. For all the reasons given above, anisotropic disc-like molecules will generate nematic (and other) phases too. In some cases liquid crystal polymers have been created from incorporating discs into polymer chains.

## 2.2 NEMATIC ORDER

The sketch Fig. 2.2(a) of a nematic fluid shows rods correlated with a direction  $\mathbf{n}$ , the nematic director. The director is a unit vector, only showing the principal axis of alignment. In a fluid of rods, as in Fig. 2.2, the direction ‘up’ is not distinguished from ‘down’; indeed it could not be since the rods drawn are not themselves capable of making the distinction. For this reason  $\mathbf{n}$  is drawn as a double headed vector. In practice rods do have an internal direction, for instance a dipole moment along their long axis, but the up-down (quadrupolar) symmetry of nematics is not broken. If it were, we would have ferroelectric nematics with a spontaneous polarisation from the predominance of, say, ‘up’ molecular dipoles over those ‘down’. In nature uniaxial nematics are not polar but quadrupolar, with the symmetry described by the point group  $D_{\infty h}$  (a symmetry of a simple cylinder).

The orientational order can now be defined. In Fig. 2.2(a) a test rod’s spine is drawn with an angle  $\theta$  to  $\mathbf{n}$ . The nematic order parameter is defined via the average of second Legendre polynomial<sup>1</sup>, as

$$Q = \langle P_2(\cos \theta) \rangle = \left\langle \frac{3}{2} \cos^2 \theta - \frac{1}{2} \right\rangle \quad (2.1)$$

where  $\langle \dots \rangle$  denotes an average over rod directions  $\theta$ . From Fig. 2.2 one can see how  $Q = 1$  corresponds to perfect nematic order with rods directed up ( $\theta = 0$ ) or down ( $\theta = \pi$ ).  $Q = 0$  is when rods are randomly oriented, that is the phase is isotropic and  $\langle \cos^2 \theta \rangle = 1/3$ . Moderate nematic order of  $Q = 1/2$  sees rods with an average angle of  $\theta \sim 35^\circ$ , whereas  $Q = -1/2$  has all rods confined to the plane perpendicular to  $\mathbf{n}$ , that is all rods have ( $\theta = \pi/2$ ).

<sup>1</sup> The Legendre polynomials  $P_n(\cos \theta)$  naturally describe orientations since they are the eigenfunctions of the angular momentum operator (actually, its square) which is the generator of rotations. Dipolar order is described by  $\langle P_1(\cos \theta) \rangle = \langle \cos \theta \rangle$ . Since equal numbers of rods in a nematic have an angle  $\theta$  as  $\pi - \theta$ , and since  $\cos(\pi - \theta) = -\cos \theta$ , the dipolar order of a nematic vanishes,  $\langle P_1 \rangle = 0$ .  $P_2$  is the next function to try.

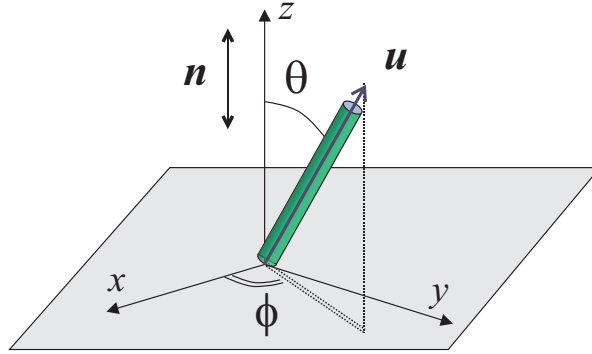


Figure 2.3: The coordinates of a rod used to define the order parameter tensor.

Nematic order can be measured directly by nuclear magnetic resonance (de Gennes and Prost, 1994), or more macroscopically, the fluid of aligned rods in Fig. 2.2(a) has a refractive index  $m_{\parallel}$  along  $\mathbf{n}$  typically greater than that,  $m_{\perp}$ , in all the perpendicular directions. This is because rods (see Fig. 2.1) are mostly more polarisable along their lengths and their long axes in a nematic are correlated with the director. Again ‘up’ and ‘down’ are not distinguished and the difference  $\Delta m = m_{\parallel} - m_{\perp}$  depends on the nematic order  $Q$  as:  $\Delta m = \Delta m_0 Q$ . The intrinsic anisotropy,  $\Delta m_0$ , depends on molecular factors and can be calculated, or estimated by extrapolation to low temperatures where the nematic order becomes high,  $Q \rightarrow 1$ .

We shall often deal with nematic order viewed from a general coordinate frame, not simply along the director as in the above example of refractive index. In fact, nematic order is tensorial in character and we have viewed in a principal frame where the director is along the  $z$  axis:

$$\underline{\underline{m}} = \begin{pmatrix} m_{\perp} & 0 & 0 \\ 0 & m_{\perp} & 0 \\ 0 & 0 & m_{\parallel} \end{pmatrix} \equiv \text{Diag}(m_{\perp}, m_{\perp}, m_{\parallel}) . \quad (2.2)$$

(For brevity we shall often denote diagonal tensors by the ‘Diag’ form). For a general orientation of  $\mathbf{n}$  we have for the refractive index tensor:

$$m_{ij} = m_{\perp} \delta_{ij} + (m_{\parallel} - m_{\perp}) n_i n_j \quad (2.3)$$

The microscopic definition of the order parameter tensor is the analogous extension from the scalar  $Q$ . Let  $\mathbf{u}$  be the unit vector describing the axis of the test rod. Using the  $\theta, \phi$  coordinates of Fig. 2.3, the projections of the rod are  $u_z = \cos \theta$ ,  $u_x = \sin \theta \cos \phi$  and  $u_y = \sin \theta \sin \phi$ . The mean square projections are  $\langle u_z u_z \rangle = \langle \cos^2 \theta \rangle$ ,  $\langle u_x u_x \rangle = \langle \sin^2 \theta \cos^2 \phi \rangle$ ,  $\langle u_y u_y \rangle = \langle \sin^2 \theta \sin^2 \phi \rangle$  and all other  $\langle u_i u_j \rangle$  with  $i \neq j$  vanish. Since we are interested in angular distributions rather than in the physical extent of an extended object, we have taken a unit vector,  $\mathbf{u}$ , for which one has  $1 = (\mathbf{u})^2 = \langle (\mathbf{u})^2 \rangle = \langle u_x u_x \rangle + \langle u_y u_y \rangle + \langle u_z u_z \rangle = \text{Tr}(\langle \mathbf{u}\mathbf{u} \rangle)$ . The above averages certainly satisfy this identity. In fact the identity adds nothing to the content of the tensor  $u_i u_j$ , so we subtract out the spherical part  $\frac{1}{3} \text{Tr}(\langle \mathbf{u}\mathbf{u} \rangle) \underline{\underline{\delta}} \equiv \frac{1}{3} \underline{\underline{\delta}}$  from the tensor  $\langle \mathbf{u}\mathbf{u} \rangle$ . Then the equivalent of eqn (2.3) is:

$$Q_{ij} = \langle \frac{3}{2} u_i u_j - \frac{1}{2} \delta_{ij} \rangle \quad (2.4)$$

(see Fig. 2.3). One can check that  $Q_{zz}$  is indeed the average  $\langle P_2(\cos \theta) \rangle = Q$  we defined before, if the coordinate axis  $\mathbf{z}$  is chosen along  $\mathbf{n}$ .

The other elements  $\langle u_x u_x \rangle$  and  $\langle u_y u_y \rangle$  are related to  $\langle u_z u_z \rangle$  since the average over the free angle  $\phi$  is trivial in the case of uniaxial order:  $\langle \cos^2 \phi \rangle = \langle \sin^2 \phi \rangle = 1/2$ . They can thus be written as  $\langle u_x u_x \rangle = \langle u_y u_y \rangle = (1 - \langle \cos^2 \theta \rangle)/2 = (1 - \langle u_z u_z \rangle)/2 = (1 - Q)/3$ . For this orientation of  $\mathbf{n}$  we have for the matrix representing the order parameter:

$$\underline{\underline{Q}} = \begin{pmatrix} -Q/2 & 0 & 0 \\ 0 & -Q/2 & 0 \\ 0 & 0 & Q \end{pmatrix} , \quad (2.5)$$

while in general the order parameter is

$$Q_{ij} = Q \left( \frac{3}{2} n_i n_j - \frac{1}{2} \delta_{ij} \right). \quad (2.6)$$

The order parameter tensor is, by construction, traceless and agrees with any of the macroscopic definitions of the ordering (for instance  $\underline{\underline{m}}$ ) if they too are made traceless. Let the average value of the refractive index be  $\bar{m} = \frac{1}{3} \text{Tr}(\underline{\underline{m}}) = \frac{1}{3}(m_{\parallel} + 2m_{\perp})$ . Then the new traceless  $\underline{\underline{m}}$  becomes

$$\underline{\underline{m}} = \begin{pmatrix} m_{\perp} - \bar{m} & 0 & 0 \\ 0 & m_{\perp} - \bar{m} & 0 \\ 0 & 0 & m_{\parallel} - \bar{m} \end{pmatrix} \equiv \frac{2}{3} \Delta m \begin{pmatrix} -\frac{1}{2} & 0 & 0 \\ 0 & -\frac{1}{2} & 0 \\ 0 & 0 & 1 \end{pmatrix} \equiv \frac{2}{3} \Delta m_0 \underline{\underline{Q}}. \quad (2.7)$$

The phase we have described is uniaxial. All angles  $\phi$  in Fig. 2.3 are equivalent and, as we have seen, for such nematics macroscopic average quantities such as the refractive index take the same values in all directions perpendicular to  $\mathbf{n}$ . Here this means  $m_{xx} = m_{yy} = m_{\perp}$ . In optics, the distinguished direction (along the director  $\mathbf{n}$ ) is called extraordinary (e) and the others ordinary (o). The refractive index tensor described by  $\underline{\underline{m}}$  governs the passage of the variously polarised light beams through the liquid crystal. It is known as the refractive index indicatrix and precisely mirrors the local nematic order parameter.

When there is no symmetry about  $\mathbf{n}$ , that is where all the perpendicular directions  $\phi$  are not equivalent, then we have a biaxial fluid with a more complex order parameter (Stephen and Straley, 1974) Such phases have not yet been observed in nematic elastomers and we do not discuss them further here; see WT for how biaxial order can be mechanically induced in nematic elastomers by applied stresses.

### 2.3 FREE ENERGY AND PHASE TRANSITIONS OF NEMATICS

In Fig. 2.2 we saw that an order parameter of  $Q = 1/2$  represented a nematic with a moderate degree of typical alignment of rods. By contrast a state with  $Q = -1/2$  is geometrically very different and physically very implausible in conventional nematics. The value  $\langle P_2(\cos \theta) \rangle = -\frac{1}{2}$  implies that all the rods would then be confined to the plane perpendicular to  $\mathbf{n}$ . Both the van der Waals and the excluded volume contributions to the free energy would be most unfavourable. Thus a system free energy depending on the equilibrium order parameter  $Q$  must distinguish between states of  $\pm Q$ , in contrast to magnetic (polar) systems where there is no distinction between positive and negative states. The general, Landau-de Gennes expansion of the free energy in powers of the full tensor order parameter,  $\underline{\underline{Q}}$ , is

$$F_{\text{nem}} = \frac{1}{3} A \text{Tr}(\underline{\underline{Q}} \cdot \underline{\underline{Q}}) - \frac{4}{9} B \text{Tr}(\underline{\underline{Q}} \cdot \underline{\underline{Q}} \cdot \underline{\underline{Q}}) + \frac{2}{9} C \text{Tr}(\underline{\underline{Q}} \cdot \underline{\underline{Q}} \cdot \underline{\underline{Q}} \cdot \underline{\underline{Q}}) + \dots \quad (2.8)$$

Inserting  $\underline{\underline{Q}}$ , from eqn (2.5) or (2.6), into eqn (2.8) yields the usual free energy density expressed as a function of the scalar order parameter,  $Q$ . As an important consequence of nematic symmetry, the Landau expansion of the nematic free energy density contains odd powers of  $Q$ :

$$F_{\text{nem}} = \frac{1}{2} A Q^2 - \frac{1}{3} B Q^3 + \frac{1}{4} C Q^4 + \dots - f Q \quad (2.9)$$

The linear term  $-fQ$  represents the effect of an external field, for instance  $f = \frac{1}{2} \delta \epsilon \epsilon_0 E^2$  where  $E$  is an applied electric field (which also has the effect of defining the direction of alignment, that is the director  $\mathbf{n}$ ) and where  $\delta \epsilon \propto Q$  is the anisotropic part of the relative dielectric constant. Without an applied field, the free energy density expansion  $F_{\text{nem}}$  is schematically shown in Fig. 2.4. As the temperature is lowered, a metastable minimum with  $Q > 0$  first appears at  $T_u$ . At  $T_{\text{ni}}$  the absolute minimum at  $Q = 0$  jumps discontinuously to an order  $Q_m > 0$ . The transition is thus of the first order. The existence of coexisting isotropic and nematic states around this transition creates the possibility of thermal hysteresis. The nominal transition point  $T_{\text{ni}}$  is defined where the two minima have equal depth. The second minimum at  $Q_m \neq 0$  exists in addition to the first at  $Q = 0$  because of the  $-\frac{1}{3} B Q^3$  term, that is because of the need to distinguish between states of  $\pm Q$ . This deep connection between the requirements of alignment geometry and the first order character of the phase transition was first recognised by Landau (Landau and Lifshitz, 1986).

In fact nematics are only weakly first order. Their latent entropy at the transition is very small. The sign of this is the smallness of the coefficient  $B$ . Normally the vanishing of  $B$  yields a so-called critical point where

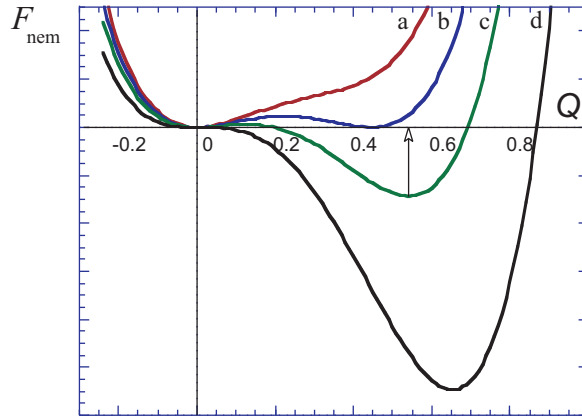


Figure 2.4: The Landau free energy density  $F_{\text{nem}}$  of a nematic liquid plotted against the scalar magnitude of order parameter  $Q$ . The plots correspond to characteristic points on the temperature scale: (a) the first appearance of  $Q_m$  on cooling at  $T = T_u$ , (b) the transition point  $T_{\text{ni}}$ , (c) at some temperature below  $T_{\text{ni}}$  the order parameter  $Q_m$  (shown by arrow) increases and the ordered phase has a lower free energy; (d) at the supercooling point  $T = T^*$  the disordered phase at  $Q = 0$  is no longer a metastable state.

a second order phase transition occurs, with the attendant critical divergence of many physical properties, for instance the specific heat and the correlation length of fluctuations. In nematics there is an incipient critical behaviour associated with a hidden second order transition at a temperature  $T^*$  just below  $T_{\text{ni}}$ , see curve (d) of Fig. 2.4. The most sensitive temperature behaviour in the problem can be encapsulated by writing  $A = A_0 \cdot (T - T^*)$ .

A full discussion of Landau theories applied to nematics, including their foundations, can be found in (Gramsbergen *et al.*, 1986) and in (Hornreich, 1985). Landau descriptions of (albeit weakly) first order systems are of qualitative rather than quantitative significance. Strictly, the Landau free energy is an expansion of  $F(Q)$  for small  $Q$ , valid for second order systems close enough to the transition where the order parameter becomes indefinitely small. First order systems, such as nematics, have however a discontinuous jump to a finite order parameter. Qualitatively, however, the Landau energy does give the right behaviour. The exercise shows that  $A_0, T^*, B$  and  $C$  determine the transition and can be fixed from measurements of  $Q_{\text{ni}}$ , of  $T_{\text{ni}} - T^*$  (from observing critical properties), of  $T_{\text{ni}}$  and of the latent entropy. It is better to take this phenomenological approach to  $F(Q)$  here than to attribute any deeper significance to the coefficients.

The minimum in  $F_{\text{nem}}$  at  $Q = 0$  becomes a maximum at  $T = T^*$  (the quadratic coefficient  $A$  reverses sign). Thus  $T^*$  is the limit to supercooling of the isotropic state. The other minimum at  $Q_m > 0$  is lost when  $A(T) > B^2/4C$  or equivalently when  $T_u = T^* + \frac{1}{4}(B^2/A_0C)$ , the limit to superheating of the nematic state, see Fig. 2.4. Superheating and supercooling are of course characteristic of a first order transition.

A large number of experiments have been performed to investigate the nematic-isotropic phase transition, which is often called the ‘clearing point’. The reason for this name will become clear in later sections of these notes. There is a degeneracy and the fluctuations of nematic director  $\mathbf{n}$  are very large at long wave lengths. Because  $\mathbf{n}$  is also the axis of optical birefringence, the light is strongly scattered by its fluctuations in the nematic phase – and so the material appears turbid. In the isotropic phase there is no director, no birefringence, no significant scattering of light – and so the liquid is clear, transparent. The mentioned degeneracy, when long wavelength director fluctuations are not penalised by elastic energy, is removed in nematic elastomers.

An external field, the  $-fQ$  contribution in eqn (2.9), can induce order at high temperatures (the paranematic state, in analogy to the effect of magnetic fields on spins at high temperatures). A linear term added to the curves of Fig. 2.4 shifts to higher  $Q$  both the minimum at  $Q = 0$  and those at finite  $Q$ . The transition is also shifted to higher temperatures since the minimum initially at finite  $Q$  is deepened (stabilised). The transition eventually disappears at a critical point  $(f_c, T_c)$ . The critical order parameter,  $Q_c$ , is half the order parameter jump,  $Q_{\text{ni}}$ , at the zero-field transition. See the sequence of  $f \neq 0$  curves in Fig. 2.5. Usually magnetic fields have a weak effect on the nematic transition. Electric fields are stronger, but seeing the critical point is still difficult (Hornreich, 1985). In contrast, mechanical fields can exert a powerful influence on the nematic behaviour of nematic elastomers;

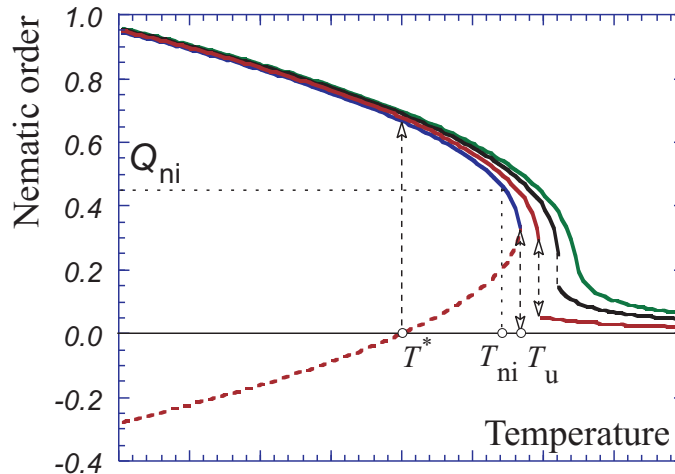


Figure 2.5: The order parameter  $Q_m(T)$  against temperature  $T$ . The dashed line shows the metastable solution  $Q_m < 0$ , dual to the principal order parameter branch  $Q_m$  corresponding to the deep minimum in  $F_{nem}$  in Fig. 2.4. The upper and lower limits of the transition  $T_u$  and  $T^*$  and the direction of hysteresis are shown by arrows; the zero-field transition point is at  $T = T_{ni}$ . The subsequent plots show the evolution of  $Q_m$  when an external field  $-f$  is applied: the paranematic phase at high temperatures becomes more pronounced as  $f$  increases, while the discontinuous jump of  $Q_m$  becomes smaller and disappears at the critical point.

see WT§6.6 — they are comparable in effective strength to molecular fields. Indeed many nematic elastomers appear to be in a supercritical state from the internal stresses they suffer. They do not have discontinuities in their order parameter at any temperature.

Nematic elastomers are much more complex than simple nematics. However, they possess the same uniaxial quadrupolar symmetry. ‘Up’ and ‘down’ are not distinguished for its director ( $\mathbf{n} \rightarrow -\mathbf{n}$ ). Thus Landau theory, which is based on symmetry considerations, tells us that their thermal properties will be qualitatively the same as those of simple nematics. We shall find that the free energy of nematic elastomers have a critical temperature  $T^*$  and the coefficient  $C$  modified from the values taken by the corresponding nematic polymer (uncrosslinked) melt. The modification depends on the network’s thermal and mechanical history. Networks are solids and thus the director can resist aligning along external fields, most drastically a mechanical (stress) field, even in the absence of anchoring at the boundaries. In simple nematics, where the orientation of the director  $\mathbf{n}$  is readjusted without resistance, ignoring anchoring at surfaces and other boundary effects for the moment, the external field (generally  $\mathbf{E}$  or  $\mathbf{B}$ ) sets this orientation. For more details and molecular theory, see WT §2

## 2.4 DISTORTIONS OF NEMATIC ORDER

Ignoring the effect of boundaries, the free energy of a nematic fluid is degenerate with respect to the direction of  $\mathbf{n}$ , which can be swung around by an infinitesimal guiding field, either  $\mathbf{E}$  or  $\mathbf{B}$ . However, since nematic fluids have long range directional order, there is a penalty associated with spatially varying the director,  $\mathbf{n}(\mathbf{r})$ . We stress both aspects in this section. In the next section we show that the loss of this degeneracy is central in nematic elastomers. Non-uniform directors will figure in a novel way later when we discuss instabilities in nematic elastomers.

The director can be splayed, twisted or bent, see Fig. 2.6(a), (b) and (c) respectively. The penalty for such distortions is the Frank elastic free energy density:

$$F_{Fr} = \frac{1}{2}K_1(\text{div } \mathbf{n})^2 + \frac{1}{2}K_2(\mathbf{n} \cdot \text{curl } \mathbf{n})^2 + \frac{1}{2}K_3(\mathbf{n} \times \text{curl } \mathbf{n})^2 \quad (2.10)$$

with the  $K_i$  being the corresponding splay, twist and bend curvature elastic constants respectively. Deriving this expression (de Gennes and Prost, 1994) requires care that it obeys all symmetry requirements, the most obvious

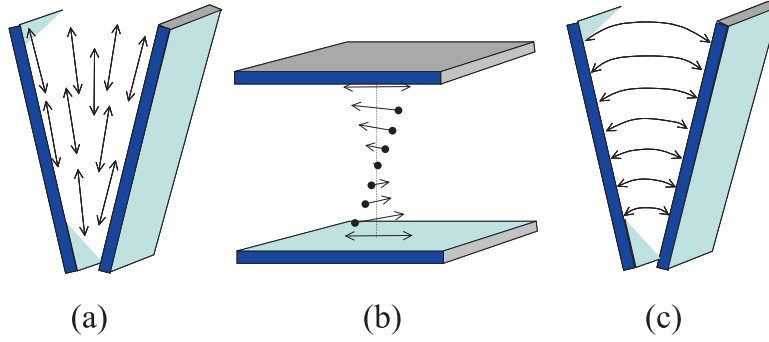


Figure 2.6: Three principal distortion modes in Frank elasticity: splay (a), twist (b), and bend (c) of the director  $\mathbf{n}$ .

being invariance with respect to  $\mathbf{n} \rightarrow -\mathbf{n}$ . With the simplification  $K_2 = K_3 = K$ , the Frank free energy density  $F_{\text{Fr}}$  reduces to

$$\frac{1}{2}K_1(\text{div } \mathbf{n})^2 + \frac{1}{2}K(\text{curl } \mathbf{n})^2,$$

apparently only quadratic in  $\mathbf{n}$ , but even then this free energy is not at all innocent. The requirement that  $\mathbf{n}(\mathbf{r})$  remains a unit vector,  $\mathbf{n}^2(\mathbf{r}) = 1$  at all points  $\mathbf{r}$ , means that  $F_{\text{Fr}}$  yields highly non-linear problems. Only few problems can be solved exactly; these special cases are catalogued in a series of beautiful and instructive illustrations (de Gennes and Prost, 1994).

In general is the full tensor order parameter  $Q_{ij}$  that is the proper field variable in the nematic phase. More than just the director is spatially varying; it is also the magnitude of the order. The Landau free energy density of the fluctuating nematic liquid crystal should be written as

$$F_{\text{nem}} = \frac{1}{3}A \text{Tr}(\underline{\underline{Q}} \cdot \underline{\underline{Q}}) - \frac{4}{9}B \text{Tr}(\underline{\underline{Q}} \cdot \underline{\underline{Q}} \cdot \underline{\underline{Q}}) + \frac{1}{9}C \text{Tr}(\underline{\underline{Q}} \cdot \underline{\underline{Q}})^2 + \frac{2}{9}\kappa_1 (\nabla_j Q_{ij})^2 + \frac{1}{9}\kappa_3 (\nabla_k Q_{ij})^2. \quad (2.11)$$

Linear gradient terms lead to spontaneous development of spatial variation of the nematic order — cholesteric phases; see WT §2.8 and §9.

The energy density cost of spatial variation over a distance  $\xi$  is  $\sim K/\xi^2$  whereas the energy density associated with elastic distortions is  $\mu$ , the rubber shear modulus. The rapidity of variation at which the energy costs are comparable is  $\xi = \sqrt{K/\mu}$ . For representative values  $K \sim 10^{-11}\text{N}$  and  $\mu \sim 10^6\text{J/m}^3$  one has  $\xi \sim 10^{-9}\text{m}$ , a very short length scale and we almost never meet Frank effects in elastomers.



In polymer melts, chain conformations are non-excluding, ideal random walks and thus are Gaussian. The self-avoidance problem of polymer solutions does not arise because of excluded volume screening. Elastomers too are conformationally ideal too and thus their statistical mechanics is relatively straightforward. Chains may however be entangled and these constraints will be felt when chains are extended. Polymers, and liquid crystal elastomers, are universal in most of their physical properties, which depend only weakly on their detailed structure — their complex chemistry can be at first neglected: for instance the shear modulus of a rubber is well described by  $\mu = n_s k_B T$  where  $n_s$  is the number of network strands per unit volume. A problem, at first sight of great complexity, has been reduced to counting ( $n_s$ ) and an energy scale set by temperature,  $k_B T$ . The relationship of ideal, equilibrium rubber elasticity has the same status and simplicity as the perfect gas law  $p = n k_B T$  and it is to this level of simplicity that we shall aspire in discussing the molecular basis of liquid crystal elastomers. The latter's properties are so radically different from conventional solids, to start with we don't need to consider entanglements, finite extensibility etc. that are needed to fine-tune descriptions of classical elastomers. Books that cover all aspects of polymers that we require are classics by Flory, de Gennes and Edwards (Flory, 1953; Flory, 1969; de Gennes, 1979; Doi and Edwards, 1986), the latter two being directed toward more advanced topics in polymers such as entanglements, dynamics and solutions.

Rubber is also capable of very large deformations and small strain elasticity is entirely inadequate. In liquid crystal elastomers many new phenomena emerge at large strains which is why we shall require a molecular theory.

### 3.1 CONFIGURATIONS OF POLYMERS

The classic example of a polymer is polyethylene, a long chain of segments shown in Fig. 3.1. The degree of polymerisation,  $N$ , may be quite large ( $N = 10^2 - 10^4$ ). The C-C bonds are nearly tetrahedral ( $109^\circ$ ), but there is a significant degree of crank motion generated in exploring the three possible positions of the next  $-\text{CH}_2-$  group. This generates an enormous number of equivalent configurations,  $3^N$  in total, for an ideal single chain of  $-(\text{CH}_2 - \text{CH}_2)_n-$ . For any chain, especially those with a complex chemical structure, the effective step length  $\ell$  over which the chain can essentially bend may be equivalent to many monomers. However, the principle of polymer chains possessing a vast number of conformations is preserved so long as the total number of monomers,  $N$ , is large compared with the number of monomers per effective step length. The rubbery response of networks (and indeed the characteristic response of polymers in general) depends on this separation of scales (the total length of a chain, often called the arc length  $L$ , being much greater than the effective step length  $\ell$ ). The opposite limiting case, of  $L \ll \ell$ , corresponds to an almost completely rigid rod molecule of length  $L$  (something that we have discussed in relation to ordinary nematic liquid crystals). We shall confine ourselves to sufficiently long chains where the entropic properties of polymers are pronounced. Figure 3.2 shows three schematic snapshots of such a chain with considerable internal flexibility in the joints. By considering the distribution,  $p(\mathbf{R})$ , of



Figure 3.1: The molecular unit (monomer) of a polyethylene chain. Covalent bonds of carbon make a tetrahedron — arrows on the two outgoing bonds show where this unit is connected to other identical monomers, thereby specifying the position of two more C atoms. (a) The *trans* conformation with the  $-\text{C}-\text{C}-$  links in one plane. (b) One of the *gauche* conformations where the first or last C atom is out of plane.

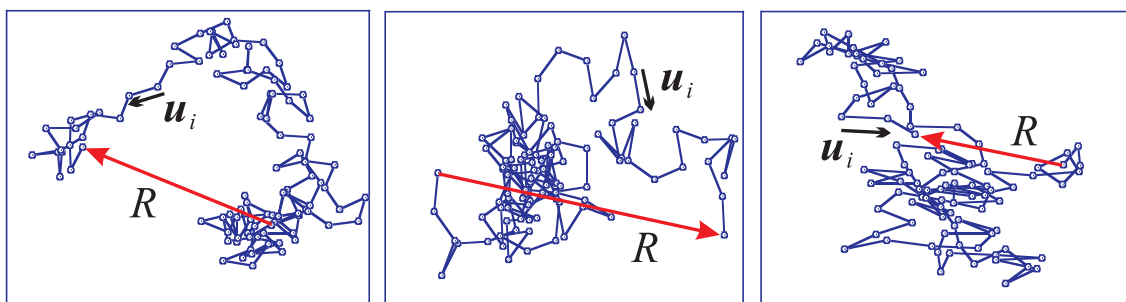


Figure 3.2: A random walk composed of freely jointed segments with  $N = 100$  such rods or ‘steps’. Three different trajectories in space are illustrated. The end-to-end vector,  $\mathbf{R}$ , is the sum of the steps  $\mathbf{u}$  of the component rods.

the chain’s end-to-end vector  $\mathbf{R}$ , one can make the idea of an effective jointed unit and the irrelevancy of local structure more precise.

Let us take a chain composed of  $N$  rods of length  $a$  freely jointed together as in Fig. 3.2. The whole chain conformation traces a path of a random walk with a fixed step length  $a$  (in this simple model, evidently,  $a = \ell$ ). Equivalently, this is a trajectory of a Brownian particle diffusing in space under the influence of a fixed-magnitude stochastic force. The mean square end-to-end vector for such a random walk of  $N$  steps is, in each direction,

$$\langle R_x^2 \rangle = \langle R_y^2 \rangle = \langle R_z^2 \rangle = \frac{1}{3} \langle R^2 \rangle = \frac{1}{3} a^2 N \equiv \frac{1}{3} aL \quad (3.1)$$

where  $L = Na$  is the actual arc length of the chain and corresponds to the total time of the analogous Brownian diffusion. In terms of the joint vectors  $\mathbf{u}_i$  of length  $a$ , the end-to-end distance  $\mathbf{R}$  is given by  $\mathbf{R} = \sum_i \mathbf{u}_i$ . Since vectors  $\mathbf{u}_i$  are uncorrelated with each other in their direction, the average  $\langle \mathbf{u}_i \mathbf{u}_j \rangle = \frac{1}{3} \delta_{ij} a^2$  and the result for  $\langle R^2 \rangle$  follows immediately.

Let the total number of possible conformations of such a chain, or the number of possible random walks with no restrictions on their starting and ending points, be  $Z_N$  (this is  $3^N$  in our simplistic 3-state model for polyethylene). Since energy plays no role in this idealised chain model, this number of conformations is also the partition function for the chain:  $Z_N = \sum_{\text{configs}} \exp(-\mathcal{H}/k_B T)$  with the energy  $\mathcal{H}$  of each configuration equal to zero or an irrelevant constant. The number of configurations with the ends fixed,  $Z_N(\mathbf{R})$ , is a great deal smaller:

$$Z_N(\mathbf{R}) = p_N(\mathbf{R}) Z_N \quad (3.2)$$

the  $p_N(\mathbf{R})$  expressing the probability a given conformation will have an end-to-end vector  $\mathbf{R}$ . It is easy to show from the central limit theorem that  $p_N(\mathbf{R})$  is a Gaussian distribution:

$$p_N(\mathbf{R}) = \left( \frac{3}{2\pi R_0^2} \right)^{3/2} e^{-3R^2/2R_0^2} \quad (3.3)$$

characterised by its variance  $R_0^2$ . The product of two parameters expressing the detail of chemical structure of a polymer, its step length  $a$ , and the arc length  $L$ , appears simply as the single parameter of probability distribution  $p(\mathbf{R})$ , namely as  $aL = R_0^2$ , reproduce eqn (3.1). This combination  $R_0$  is the only significant quantity associated with an idealised chain. It is directly measurable by neutron scattering in the melt and by light and neutron scattering in solution, as the average radius of chain gyration.

For a non freely-jointed chain, the effective step length will be increased beyond the physical length of a monomer  $a$  and, given a fixed overall arc length  $L$ , the number of effective steps in a chain will decrease from the full number of monomers  $N$  to a lower value. We now more precisely define an effective step length, denoted by  $\ell_o$ , from the measurable quantities  $R_0$  and  $L$ :

$$\ell_o = R_0^2/L \quad (\text{by analogy with } R_0^2 = aL). \quad (3.4)$$

Flory’s coefficient  $C_\infty = \ell_o/a$  (Flory, 1953) is a direct measure of just how much local chemical structure can stiffen and extend a chain beyond what it would be, if freely jointed. Whatever the stiffening,  $R_0$  remains the

single measure of the chain size distribution. This is true if  $L$  is long enough compared with  $\ell_o$  so that the distribution is Gaussian.

The free energy of the single polymer chain we have described above is  $\mathcal{F} = -k_B T \ln Z_N(\mathbf{R})$ , where we use eqn (3.2) and (3.3) for  $Z$  to obtain:

$$\mathcal{F}(\mathbf{R}) = \mathcal{F}_o + k_B T (3\mathbf{R}^2/2R_o^2) + C. \quad (3.5)$$

$\mathcal{F}_o = -k_B T \ln Z_N$  is the free energy of an unconstrained chain and is an additive constant.  $C$  is another additive constant arising from the normalisation of probability distribution  $p_N$ .  $\mathcal{F}_o$  and  $C$  simply make a reference point of free energy and we neglect it, since it does not depend on the chain end-to-end distance  $\mathbf{R}$ .

We have obtained  $\mathcal{F}(\mathbf{R})$  by simply counting configurations, assuming that they all have equal internal energy. The free energy (3.5) is purely entropic, the prefactor of  $k_B T$  being a signal of this. However, energy is involved in the distortion of chemical bonds. If the internal energy per molecule associated with bond distortion were  $\mathcal{U}(\mathbf{R})$ , then we would instead have:

$$\mathcal{F}(\mathbf{R}) = \mathcal{U}(\mathbf{R}) - T\mathcal{S}(\mathbf{R})$$

with  $\mathcal{S}$  the entropy per molecule. The classical freely jointed model evidently has  $U = 0$  and an entropy

$$\mathcal{S}(\mathbf{R}) = -k_B (3\mathbf{R}^2/2R_o^2). \quad (3.6)$$

In fact the free energy (3.5), quadratic as it is in  $\mathbf{R}$ , represents Hooke's law for the extension of a single chain. One indeed thinks of polymers as entropic springs with Hooke's constant  $3k_B T/R_o^2$ . The stored (free) energy is entropic, because it measures a change (reduction) in the number of possible conformations (and thus – the entropy) when the ends of such a chain are pulled apart ( $R$  increases). Ultimately one would reach a state of a fully extended chain with  $R = L$  and, thus, only *one* possible configuration. This very unfavourable situation is, of course, well beyond the limit of applicability of the Gaussian law (3.3) for a truly random walk. In addition to this very basic argument, there is some residual temperature dependence in  $R_o$  in eqn (3.5) and (3.6) since thermal energy determines the effective stiffness of chemical bonds and hence the effective step length  $\ell$ . The dependence is weak compared with the dramatic effects of nematic ordering leading, for instance, to spontaneous shape changes of between 10 and 400% in elastomers. Moreover, for most of these notes, we only require that chains have some anisotropy. As usual in polymers, most effects are universal and do not depend on specific chain properties. We accordingly mostly discard stiffness variation effects.

The free energy for an isolated polymer chain with free ends extended by a distance  $R$  is a paradigm for a polymer network where the macroscopic deformation ultimately leads to the extension of constituent chains. The internal energy contribution to  $\mathcal{F}$  turns out to be small and we can consider network chains as purely entropic springs.

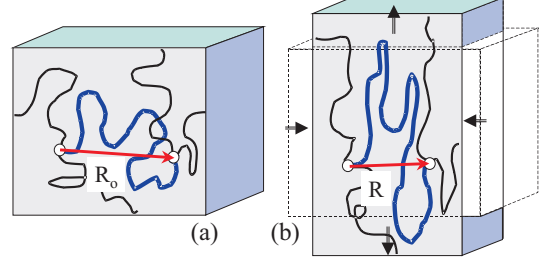
In the melt and in elastomers chain configurations are those of phantom, single Gaussian chains (Arrighi *et al.*, 1992). However, despite their ideal conformations in the concentrated state, chains are not really phantoms - they are entangled with each other. In networks, as chains are extended their configurations are restricted more powerfully than simply by their ends being fixed. The fixing of chain ends to other chains means that, unlike in the corresponding melt, knots cannot be untied and their frozen-in topology must be respected. One can examine (Deam and Edwards, 1976; Ball *et al.*, 1981) topological effects in networks in order to explain the experimental deviation from classical predictions. For sufficiently long chains crosslinked in the melt such deviations are important. However, we shall find that liquid crystal order leads to deviations from classical behaviour that are much more significant than the role of entanglements, even in short solution-crosslinked chains.

### 3.2 CLASSICAL RUBBER ELASTICITY

Let us now return to the classical picture of simple, isotropic and long polymer chains. Most of the unusual, characteristically polymeric properties we associate with polymers of high molecular weight derive from their resistance to distortion of their average shape. The entropy of a single chain, eqn (3.6), is lowered as the distance between its ends is extended. Fewer conformations implies that the free energy rises. This stored elastic free energy is at the root of the entropic-mechanical effects of rubber elasticity. We present the classical picture of rubber here, because we aim to develop an analogous simple view for nematic elastomers – a straightforward

extension of the classical approach describing isotropic polymer networks. Consider a network of crosslinked chains sketched in Fig. 3.3. The number of crosslinks is sufficient to ensure a percolating path of elastically active chains across the whole block of rubber. Distortion of the block causes the component strands between

Figure 3.3: A block of rubber with the underlying polymer network. (a) The chains of the network are shown linked. A test chain (heavy curve) has a span at formation  $\mathbf{R}_f$  between two successive crosslinks along its contour. (b) The block of rubber is extended by factors  $\lambda_{ii}$  in the three principal directions. The test network span is now  $\mathbf{R} = \underline{\underline{\lambda}} \cdot \mathbf{R}_f$ .



crosslinks to distort with respect to their equilibrium average shapes, which costs a free energy due to the loss of configuration entropy. Departure from equilibrium corresponds to a reduction from the maximal entropy allowed by network constraints. The material is thereby a solid rather than a liquid, which would accommodate any distortion in its shape at constant energy. We shall return to this rather obvious remark later, since we shall find that it is not true for some distortions of nematic elastomers.

Returning to simple rubber: without crosslinks it would be a polymer melt – a fluid that would eventually flow under stress. Relatively so few monomers are locally constrained by crosslinking that chains continue to have great mobility and explore the myriad of conformations characteristic of such a melt. Rubber is in effect a liquid in all regards except that it cannot flow! In nematic networks this observation is of central importance since the associated mobility of the director  $\mathbf{n}$  is also great and will largely determine the mechanical response.

The mobility of chains means, in particular, that they continue to explore many conformations and the drive to maximise entropy outweighs other influences. Change of average shape continues to be resisted, as in the single chain example given above. Consider the junction points in Fig. 3.3 to be fixed relative to the body. This implies that a selected strand's end-to-end vector, connecting a pair of crosslinks, will deform in geometric proportion to the body's deformation (the affine deformation approximation). Suppose a selected strand at network formation has been given an end-to-end distance  $\mathbf{R}_f$ . The deformation,  $\underline{\underline{\lambda}}$ , is defined such that any separation vector in the body, e.g. initially  $\mathbf{R}_f$ , will deform to a new value  $\mathbf{R}$  given by:

$$\mathbf{R} = \underline{\underline{\lambda}} \cdot \mathbf{R}_f . \quad (3.7)$$

For instance in Fig. 3.3 if the sides are initially of unit length and deform to dimensions  $\lambda_{xx}, \lambda_{yy}, \lambda_{zz}$  in the directions  $x, y$  and  $z$  respectively (and no shear deformations are present), then each dimension of the chain is multiplied by the same geometric factors:

$$R_x = \lambda_{xx} R_x^f, \quad R_y = \lambda_{yy} R_y^f \quad \text{and} \quad R_z = \lambda_{zz} R_z^f .$$

The one test strand of Fig. 3.3 is shown in the deformed body in its affinely deformed state. The free energy of this particular strand is, as in the corresponding eqn (3.5):

$$\mathcal{F}_s(\mathbf{R}) = k_B T \left( \frac{3\mathbf{R}^2}{2R_0^2} \right) .$$

Recall that the mean square size,  $R_0$ , is the single parameter describing the Gaussian chain statistical properties. Using the affine relationship (3.7), we obtain

$$\mathcal{F}_s(\mathbf{R}) = \frac{3k_B T}{2} \frac{\mathbf{R}_f \cdot \underline{\underline{\lambda}}^T \cdot \underline{\underline{\lambda}} \cdot \mathbf{R}_f}{R_0^2} . \quad (3.8)$$

Several constants, exposed and then neglected in eqn (3.5), such as the constant  $C$  from the normalisation of the Gaussian chain probability, have also been suppressed here. The current free energy of the selected network strand depends on the deformation  $\underline{\underline{\lambda}}$  and on the initial end-to-end separation  $\mathbf{R}_f$  (the subscript  $f$  denotes the state

at the network formation). The overall elastic free energy of the block of rubber adds together contributions like eqn (3.8) for all other network strands. All different strands have their own initial end-to-end distance  $\mathbf{R}_f$ , but we know the proportion of chains with any given  $\mathbf{R}_f$  among the whole ensemble – it is the probability distribution of chains having this end-to-end distance before crosslinking, at the moment of network formation:

$$p(\mathbf{R}_f) = \left( \frac{3}{2\pi R_0^2} \right)^{3/2} e^{-3(\mathbf{R}_f)^2/2R_0^2}. \quad (3.9)$$

Naturally, it is the same Gaussian as in Sect. 3.1, eqn (3.3). Thus, the summing of individual chain free energies (3.8) in the deformed body is equivalent to the *averaging* of  $\mathcal{F}_s$  over their distribution and then multiplying the resulting average free energy per strand by the total number of network strands in the system. Since  $\mathbf{R}$  is derived from  $\mathbf{R}_f$ , the probability to find a strand currently with end-to-end separation  $\mathbf{R}$  is simply the probability of finding the appropriate span  $\mathbf{R}_f$  at the moment of network formation, that is  $p_N(\mathbf{R}_f)$ . The average free energy per strand,  $\mathcal{F}$ , is:

$$\mathcal{F} = \frac{3k_B T}{2R_0^2} \langle \mathbf{R}_f \cdot \underline{\lambda}^T \cdot \underline{\lambda} \cdot \mathbf{R}_f \rangle_{p(\mathbf{R}_f)}. \quad (3.10)$$

This amounts to averaging of a quadratic form (in  $\mathbf{R}_f$ ) with the corresponding Gaussian distribution,  $p(\mathbf{R}_f)$ . The integration is of the form  $\int x^2 e^{-\alpha x^2} dx$ , and yields the appropriate averages:

$$\langle R_i^f R_j^f \rangle = \frac{1}{3} R_0^2 \delta_{ij}. \quad (3.11)$$

We have assumed here that the mean square chain size at formation is the same as that which is current,  $R_0^2$ , when we are distorting the rubber, eqn (3.8). If for instance, temperature were to change between formation and current conditions, then the mean square size,  $R_f^2$ , at formation might be different from the current value,  $R_0^2$ . Substituting the average (3.11) back in to eqn (3.10) and multiplying by the average number of strands per unit volume  $n_s$ , the free energy density (the free energy per unit volume) of a deformed rubber becomes

$$F = \frac{1}{2} n_s k_B T \text{Tr} \left( \underline{\lambda}^T \cdot \underline{\lambda} \right) \equiv \frac{1}{2} n_s k_B T (\lambda_{ij} \lambda_{ji}) \quad (3.12)$$

$$= \frac{1}{2} n_s k_B T (\lambda_{xx}^2 + \lambda_{yy}^2 + \lambda_{zz}^2). \quad (3.13)$$

[We follow the Einstein convention of summation over the pairs of repeated indices in expressions involving matrices – such as in (3.12).]

Equation (3.13) is the result of the particular extension shown in Fig. 3.3, that is the case where  $\underline{\lambda}$  is diagonal, with no shear deformations. Note that the mean square size in each spatial direction,  $R_0^2$ , has cancelled out between expressions (3.10) and (3.11) and, as promised, the energy is just  $k_B T$  times geometrical factors ( $\lambda^2$ , the squares of the extensions). Nothing remains of the structure of the component chains, except that they must be long enough (and flexible enough) to satisfy laws of Gaussian statistics.

Chapter 4 is concerned with classical elasticity. We show there that the free energy density of a material deforming at constant volume is of the form of eqn (3.12) where the coefficient is  $\frac{1}{2}\mu$ , with  $\mu$  the solids's shear modulus. Thus eqn (3.12) allows us to define, for the first time in these notes, the characteristic rubber modulus:

$$\mu = n_s k_B T.$$

We shall constantly use this quantity. The magnitude of this static, equilibrium rubber modulus may vary greatly depending on the value of  $n_s$ . It is, however, useful to give at least a crude estimate of  $\mu$ . The number of chain strands per unit volume,  $n_s$ , is equal to the inverse volume occupied by an average chain between two connected network crosslinks. Let us take a network of rather flexible polyethylene chains (see Fig. 3.1) with, on average,  $N = 100$  units between crosslinks and a monomer size of, say  $a \sim 3 \text{ \AA}$ . Then  $n_s \simeq 1/(Na^3) \sim 3 \times 10^{26} \text{ m}^{-3}$ . This is a high estimate – it leads to a modulus  $\mu \sim 10^6 \text{ Pa}$  at room temperature. (The units of elastic moduli are commonly taken as Pa, which is the same as  $\text{J/m}^3$  or  $\text{N/m}^2$ ). In practice, the rubber modulus is often much lower. There are two common reasons, both serving to reduce the density of strands  $n_s$ : simple flexible chains with a small monomer size ( $a \sim 2\text{-}3 \text{ \AA}$ ) often have much lower crosslinking density and thus very long chain strands – often with monomer numbers  $N \geq 10^4$  between crosslinks. Polymers with a more complex molecular

structure, in particular with long rigid rod elements necessary for liquid crystallinity, have the monomer volume 10-20 times greater than that of, say, polyethylene. Accordingly, one often finds rather weak rubbers with  $\mu$  as low as  $10^4$  Pa, but hardly less than that. This identifies the characteristic range of possible magnitudes,

$$\mu \sim 10^4 - 10^6 \text{ Pa.}$$

At first sight the free energies (3.12) and (3.13) are unfortunate results. The lowest free energy density,  $F = 0$  would apparently be at  $\lambda_{xx} = \lambda_{yy} = \lambda_{zz} = 0$ . Rubber should shrink to a point under the action of the entropic springs of the network! Of course, the repulsion arising when the molecules overlap eventually balances the attractive forces, as in any liquid or solid. The bulk modulus has the same dimensions (Pa) as the rubber modulus  $\mu$ , and for a polymeric liquid, as for simple liquids, is roughly of the order  $10^9 - 10^{10} \text{ J/m}^3$ . The characteristic scale of rubber elastic energies is about  $10^{-4}$  times that of the compressional modulus. Thus entropic effects of rubber elasticity are insignificant, compared with those causing or penalising volume change, and distortions of rubber must accordingly occur at constant volume (to within 1 part in  $10^4$ ). The difficulty that the rubber should shrink to a point under elastic forces is thus avoided. The example of Fig. 3.3 is instructive. Assuming the sides of the rubber block are along the coordinate axes  $x, y, z$ , the constancy of volume requires that the product of extensions is fixed:

$$\lambda_{xx}\lambda_{yy}\lambda_{zz} \equiv \text{Det}(\underline{\underline{\lambda}}) = 1. \quad (3.14)$$

If we extend the sample by the factor  $\lambda$  in the  $z$  direction ( $\lambda_{zz} = \lambda$ ) and let the  $x$  and  $y$  dimensions simply be slaves to the condition of constant volume, then the constraint (3.14) demands  $\lambda_{xx} = \lambda_{yy} = 1/\sqrt{\lambda}$  and the free energy density (3.13) becomes:

$$F = \frac{1}{2}\mu \left( \lambda^2 + \frac{2}{\lambda} \right). \quad (3.15)$$

Having put in the conservation of volume by hand, this of course has  $\lambda = 1$  as its relaxed, undeformed state. The higher energy scale associated with change of volume can be ignored if we always choose  $\underline{\underline{\lambda}}$  with the constraint (3.14) in mind. Figure 3.4 shows the reduced energy density (3.15), in units of  $\frac{1}{2}\mu$ , increasing from the ground-state level  $\lambda^2 + 2/\lambda = 3$  in both elongation ( $\lambda > 1$ ) and compression ( $\lambda < 1$ ) modes of deformation.

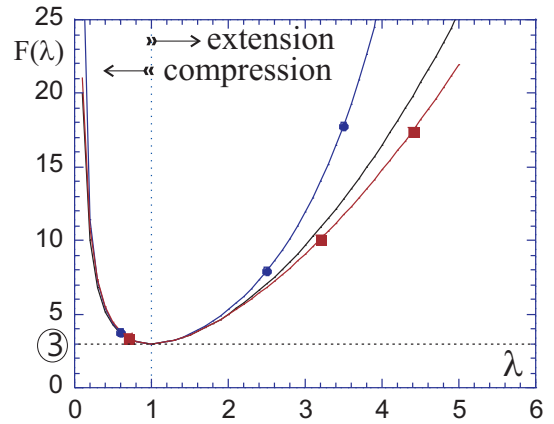


Figure 3.4: The plot of free energy density of incompressible rubber under uniaxial elongation and compression  $\lambda$ , in units of  $\frac{1}{2}\mu$ ; the absolute minimum is  $F = \frac{3}{2}\mu$  at  $\lambda = 1$ . Three curves correspond to the classical rubber-elastic expression (3.15), the middle solid line, and two its modifications, due to the ‘finite extensibility’ (curve labelled by solid circles), and the chain entanglements (solid squares).

The energy density as a function of deformation determines the force per unit area (see later for definitions of stress) as deformation is imposed. Take for example simple extension along the vertical axis,  $z$ , of a classical rubber, sketched in Fig. 3.3, that is initially a *unit* cube. Its current length in the  $z$  direction is  $\lambda$ . The force  $f_z$  acting on the  $z$  ends of the body is the rate of change of energy, eqn (3.15), with length  $\lambda$ , times the area of the initial sample cross-section perpendicular to  $z$ -direction:

$$f_z = A \frac{\partial F}{\partial \lambda} = A \mu \left( \lambda - \frac{1}{\lambda^2} \right). \quad (3.16)$$

Taking a unit cube ( $A = 1$ ) allowed us to consider forces and stresses interchangeably in this sketch.

## 3.3 LIQUID CRYSTALLINE POLYMERS

Nematic and smectic elastomers are networks of polymer chains with intrinsic liquid crystalline ordering. Such polymer liquid crystals (PLCs) combine the spontaneous orientation of liquid crystals with the entropically driven behaviour of polymers. Creating a PLC is delicate; too much chain stiffness eliminates the large number of configurations of a chain that makes it an entropic spring. Too stiff, it becomes a simple rod, albeit a long one. Too little stiffness or too few nematic-forming rods eliminates orientational order and results in an ordinary isotropic melt of chains.

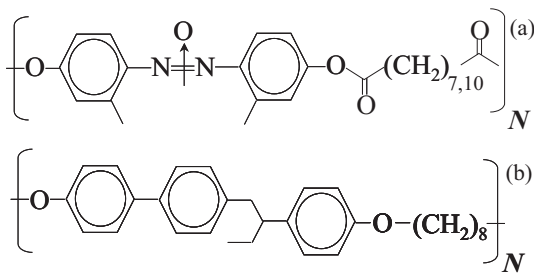


Figure 3.5: Typical main chain polymer liquid crystals with rod-like, nematic-forming sections in the middle of each monomer, flexible  $-(CH_2)_n-$  spacers between the rods allowing for many conformations. Polymer (a) with the 10-spacer is known as DDA-9, with the 7-spacer it is AZA-9; their monomers are not unlike the nematic PAA, Fig. 2.1. Polymer (b), with a different rigid rod structure, occurs in several main chain nematic elastomers.

Two strategies can be followed. Rigid rod-like elements can be linked together in a head-to-tail fashion to form a main chain (MC) polymer with linkages between the rods giving sufficient flexibility to ensure a Gaussian chain, and thus a random walk as in Fig. 3.2. Examples of the chemical structure of main-chain PLCs are shown in Figs. 3.5(a) (d'Allest *et al.*, 1988) and (b) (Percec and Kawasumi, 1991).

Rods can otherwise be pendant to a flexible backbone to give a comb or side-chain (SC) PLC (Plate and Shibaev, 1987). Again, nematic order and flexibility compete.

## SHAPE OF LIQUID CRYSTALLINE POLYMERS

The average shape of the nematic polymer backbone, distorted by the nematic ordering of the associated rods, generates the equilibrium elastic response of a network into which it is linked. The aligned rod-like segments of a main-chain polymer elongate the average shape of gyration, essentially stretching the backbone, along their principal axis the director  $\mathbf{n}$ ; see Fig. 3.6(a). Side-chain polymers may have the backbone in different

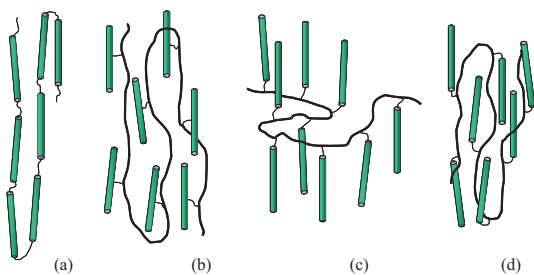


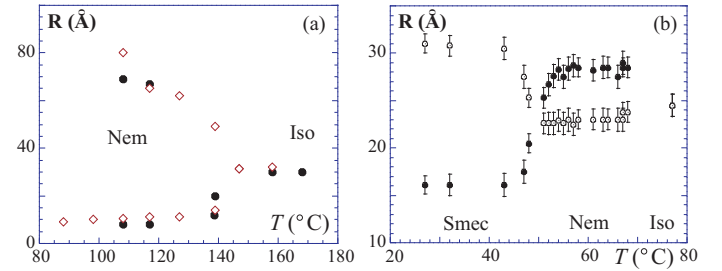
Figure 3.6: The shapes of nematic polymer backbones. The MC polymer (a) shows very high backbone anisotropy, the intermediate case of side-on PLC (b) shows weaker, but still substantial backbone alignment, while in the two end-on SC PLCs (c,d) the mesogenic groups may be only weakly coupled to the backbone; here the choice between the oblate (c) and the prolate (d) backbone arrangement is made by the spacer selection.

conformations for the same degree of nematic ordering of pendant rods depending on the type of linking the mesogenic groups to the backbone, Figs. 3.6(b)-(d). The local uniaxial symmetry of a nematic is preserved whatever the coupling.

The mean square end-to-end vector remains sufficient to characterise the shape of a chain and its probability distribution, if it is long enough to be Gaussian. In a principal frame there are now three such mean square quantities and in general we have:

$$\langle R_i R_j \rangle = \frac{1}{3} \ell_{ij} L \quad (3.17)$$

Figure 3.7: Nematic polymer radii of gyration from neutron scattering. (a) MC nematic polymers DDA-9 (filled circles) and AZA-9 (open diamonds) in the isotropic and nematic states.  $R_{\parallel} \sim \sqrt{\ell_{\parallel}L}$  along  $\mathbf{n}$  becomes much larger than that perpendicular,  $R_{\perp} \sim \sqrt{\ell_{\perp}L}$ . (b) A side-on polysiloxane in the isotropic, nematic and smectic states. The backbone's  $R_{\parallel}$  (filled circles) flattens to become shorter than  $R_{\perp}$  (open circles) when smectic.



where now the effective step lengths form a tensor  $\ell_{ij}$  [compare with the analogous isotropic form, eqn (3.1)] and define an anisotropic Gaussian distribution  $p_N(\mathbf{R})$ , uniaxial if the mesogenic units form an ordinary nematic phase. Neutron scattering from deuterated test chains in melts gives the mean square radii of gyration.

Figure 3.7(a) shows the shape anisotropy of the polymer DDA-9, Fig. 3.5(a) (d'Allest *et al.*, 1988). The main-chain PLC melt anisotropy jumps from zero to a finite value on cooling through the transition temperature  $T_{ni}$ . With ever increasing nematic order at low temperatures, the anisotropy can increase to very high values as the main chain polymer stretches out its backbone, see Fig. 3.6(a). For instance at  $T = 108^\circ\text{C}$ , the ratio of radii of gyration is  $R_{\parallel}/R_{\perp} \sim 8$  giving a ratio of effective step lengths  $\ell_{\parallel}/\ell_{\perp} \sim 60$ . Still larger values obtain below this temperature. This ratio determines mechanical effects in nematic elastomers.

Side chain polymers of both the extended and flattened backbone varieties have been studied as well (Ohm *et al.*, 1988; Cotton and Hardouin, 1997). In general their anisotropy is less extreme because the backbones are less strongly coupled to the ordering rods – see Fig. 3.7(b) (Lecommandoux *et al.*, 1997).

In uniaxial polymers, mean square sizes in all directions in the plane perpendicular to  $\mathbf{n}$  are identical,  $R_x = R_y = R_{\perp}$ . For such nematic polymer melts with the director  $\mathbf{n}$  along  $z$  we have the accordingly uniaxial tensor of step lengths:

$$\underline{\underline{\ell}}_0 = \begin{pmatrix} \ell_{\perp} & 0 & 0 \\ 0 & \ell_{\perp} & 0 \\ 0 & 0 & \ell_{\parallel} \end{pmatrix} \rightarrow \ell_{\perp} \underline{\underline{\delta}} + [\ell_{\parallel} - \ell_{\perp}] \mathbf{n}\mathbf{n} \text{ in a general coordinate system.} \quad (3.18)$$

where  $\ell_{\parallel}$  and  $\ell_{\perp}$  are the effective lengths of steps in the directions parallel and perpendicular to  $\mathbf{n}$  and depend on  $Q$ . Thus  $\langle R_z^2 \rangle = \frac{1}{3} \ell_{\parallel} L$  and  $\langle R_x^2 \rangle = \langle R_y^2 \rangle = \frac{1}{3} \ell_{\perp} L$  (cf. Figs. 3.6 and 3.7).

The tensor  $\underline{\underline{\ell}}$  defines the spheroid of gyration  $\langle R_i R_j \rangle$ , eqn (3.17). Figure 3.8 extracts only the backbone from the sketches in Fig. 3.6, in particular ignoring the rods in side-chain polymers. We then have the appropriate uniaxial prolate and oblate spheroids, with  $\delta\ell > 0$  and  $\delta\ell < 0$ , respectively. The isotropic phase has its gyration tensor in the shape of a sphere and hence has  $\delta\ell = 0$ . The Gaussian distribution of chain conformations,  $p(\mathbf{R})$ ,

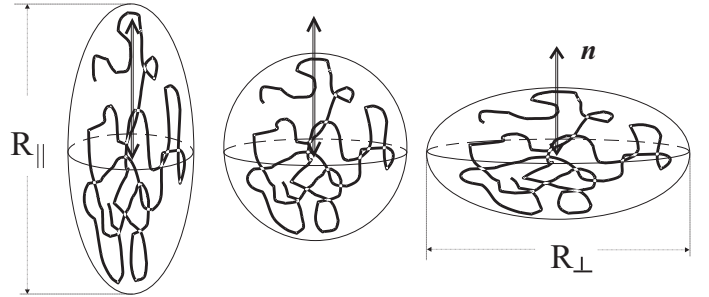


Figure 3.8: The gyration tensor spheroids. The arrow indicates the nematic director. The rods are suppressed in the diagram. Their coupling to the backbone may produce prolate (elongated along  $\mathbf{n}$ ) or oblate chain conformations.

must be generalised for the anisotropic case:

$$p(\mathbf{R}) = \left[ \left( \frac{3}{2\pi L} \right)^3 \frac{1}{\text{Det}[\underline{\underline{\ell}}]} \right]^{1/2} \exp \left( -\frac{3}{2L} R_i \ell_{ij}^{-1} R_j \right). \quad (3.19)$$

The inverse step length tensor is  $\underline{\underline{\ell}}^{-1} = \text{Diag}(\ell_{\perp}^{-1}, \ell_{\perp}^{-1}, \ell_{\parallel}^{-1})$  in its diagonal frame (see eqn (2.2) for a reminder of this notation), with the distribution in this frame being:

$$p(\mathbf{R}) \sim \exp\left(-\frac{3R_x^2}{2\ell_{\perp}L} - \frac{3R_y^2}{2\ell_{\perp}L} - \frac{3R_z^2}{2\ell_{\parallel}L}\right). \quad (3.20)$$

This distribution determines nematic rubber elasticity, just as the isotropic distribution (3.3) led to the entropic spring energy (3.8) and thus to classical rubber elasticity.

It is possible to give explicit expressions for the step length tensor  $\underline{\underline{\ell}}$  within specific models of polymers that turn out to work very well. See for instance that of a freely jointed nematic main chain polymer treated in WT§3.2, exercise 3.1. The anisotropy for a nematic main chain freely jointed polymer is

$$r = \frac{\ell_{\parallel}}{\ell_{\perp}} = \frac{1+2Q}{1-Q} \sim 1+3Q \quad \text{for } Q \text{ small.} \quad (3.21)$$

Experimentally, side chain polymers in fact obey the same kind of dependence of shape tensor on order parameter although one would expect for such polymers the angular relationship between chain steps and the rod alignment to be different.



The deformation tensor  $\underline{\lambda}$  has arisen naturally in the derivation of classical rubber elasticity. In the form given by eqn (3.7) it is appropriate for small and large strains alike, which is as well since rubber is capable for strains up to many hundreds of percent. Since we are concerned with elasticity of a new and unexpected form, with hitherto unsuspected phenomena to be summarised in the next chapter, we devote some space to reviewing the symmetry character of  $\underline{\lambda}$ , from whence the effects will arise. We also examine the structure of non-linear elasticity and the connection with linear elasticity commonly used to describe solids at small strains. In contrast to classical elasticity, nematic rubber elasticity relies on the coupling of the rotations of internal degrees of freedom (the director  $\mathbf{n}$ ) to not only elastic strains but also body rotations. We thus illustrate the geometry of deformations and local rotations in order to prepare for this new type of elasticity. We note that incompressible distortions are all essentially shears; even the simple extensions and compressions of the rectangular block in Fig. 3.3 are shears, just viewed from a rotated coordinate frame. Deformations, not in general symmetric or anti-symmetric, can be broken down into symmetric (pure shear) and rotational components. This will be useful in considering the mechano-orientational responses and instabilities of nematic elastomers. Intimately related to this symmetric/anti-symmetric resolution of strains are the square roots of tensors. We discuss them in this context, though principally to introduce them for the later treatment of soft elasticity.

There is a large literature on the fundamentals of elasticity, for instance, the book by Atkins and Fox (1980) gives a good and compact overview, including the definitions of the various distortion and strain tensors and the more general requirements of invariance. Murnaghan (1967) discusses non-linear elasticity, symmetry requirements and the roots of tensors. Treloar (1975) also reviews elasticity in the context of rubber.

#### 4.1 THE DEFORMATION TENSOR AND CAUCHY–GREEN STRAIN

Consider a reference space  $S_R$  of the relaxed body before deformation to a target space  $S_T$ . A material point  $\mathbf{R}_0$  in  $S_R$  becomes  $\mathbf{R} = \mathbf{R}_0 + \mathbf{u}(\mathbf{R}_0)$  in  $S_T$ , see Fig. 4.1. The deformation records how differently neighbouring points are displaced (by  $\mathbf{u}$ ) and hence how their relative separation is deformed from its relaxed value. The deformation gradient tensor is defined as:

$$\lambda_{ij} = \frac{\partial R_i}{\partial R_{0j}}, \quad (4.1)$$

see Fig. 4.1 [compare with eqn (3.7)]. It is clear that only the gradients of displacement contribute to physical effects: the uniform displacement field  $\mathbf{u}$  corresponds to the movement of the body as a whole. Some authors denote  $\underline{\lambda}$  by  $\underline{F}$ . We shall sometimes refer to it simply as the deformation tensor.

If the target space transforms under rotations, represented by the matrix  $\underline{U}$ , as  $\mathbf{R}' = \underline{U} \cdot \mathbf{R}$ , and the reference space transforms under rotations  $\underline{V}$  as  $\mathbf{R}'_0 = \underline{V} \cdot \mathbf{R}_0$ , then the deformation tensor deforms as

$$\lambda'_{kl} = U_{ki} \frac{\partial R_i}{\partial R_{0j}} V_{jl}^T \quad (4.2)$$

$$\underline{\lambda}' = \underline{U} \cdot \underline{\lambda} \cdot \underline{V}^T \quad \text{or conversely} \quad \underline{\lambda} = \underline{U}^T \cdot \underline{\lambda}' \cdot \underline{V}. \quad (4.3)$$

See Sect. 4.3.1 for more on rotations, in particular the end of that section for explicit forms of matrix representations  $\underline{U}$  and  $\underline{V}$  of finite rotations. Thus  $\underline{\lambda}$  records the character of both the target and reference states. The connection with both spaces is quite different in character from the Cauchy tensors to be introduced below. Approaching large amplitude elasticity through  $\underline{\lambda}$  makes dealing with non-linearities easier than via retaining non-linear terms in the Cauchy strain formalism of conventional elasticity which we outline in Sect. 4.2. Also rotational information about the map  $S_R \rightarrow S_T$  is retained.

Isotropic systems are invariant under rotations  $\underline{V}$  of  $S_R$  and the system's final energy must be invariant under rotations of  $S_T$ . (If  $S_R$  is crystalline, the invariance under the relevant point group instead of under  $\underline{V}$  is required). The rubber free energy (3.13) is a good vehicle to discuss this.  $F$  is a function of the combination

$$\underline{\lambda}^T \cdot \underline{\lambda} = \underline{V}^T \cdot \underline{\lambda}'^T \cdot \underline{U} \cdot \underline{U}^T \cdot \underline{\lambda}' \cdot \underline{V} = \underline{V}^T \cdot \underline{\lambda}'^T \cdot \underline{\lambda}' \cdot \underline{V}.$$

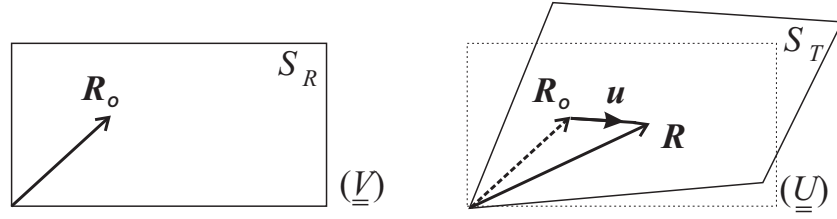


Figure 4.1: The deformation of an elastic body. A point with the coordinate  $\mathbf{R}_o$  in a reference space  $S_R$  is moved to a new position  $\mathbf{R}$  in a target space  $S_T$ . The deformation is fully described by a field of displacement vectors  $\mathbf{u}(\mathbf{R}_o)$  at each point in the initial body shape. The material point  $\mathbf{R}_o$  is thereby displaced by  $\mathbf{u}(\mathbf{R}_o)$  to  $\mathbf{R}$ . The matrices  $\underline{\underline{V}}$  and  $\underline{\underline{U}}$  are the rotations relevant for  $S_R$  and  $S_T$  respectively.

Thus the product  $\underline{\underline{\lambda}}^T \cdot \underline{\underline{\lambda}}$  is invariant under body rotations  $\underline{\underline{U}}$  of the final (target) space  $S_T$ ; it is called the right Cauchy–Green deformation tensor

$$\underline{\underline{C}} = \underline{\underline{\lambda}}^T \cdot \underline{\underline{\lambda}}, \quad \underline{\underline{C}} = \underline{\underline{V}}^T \cdot \underline{\underline{C}}' \cdot \underline{\underline{V}}. \quad (4.4)$$

Evidently  $\underline{\underline{C}}$  transforms as a second rank tensor in the reference space  $S_R$ .

The rubber elastic free energy in the initial (unprimed) frame can be expressed in terms of  $\underline{\underline{C}}'$ :

$$\begin{aligned} F &= \frac{1}{2}\mu \operatorname{Tr}(\underline{\underline{C}}) = \frac{1}{2}\mu \operatorname{Tr}(\underline{\underline{V}}^T \cdot \underline{\underline{C}}' \cdot \underline{\underline{V}}) \\ &= \frac{1}{2}\mu \operatorname{Tr}(\underline{\underline{C}}' \cdot \underline{\underline{V}} \cdot \underline{\underline{V}}^T) = \frac{1}{2}\mu \operatorname{Tr}(\underline{\underline{C}}') \end{aligned} \quad (4.5)$$

(by cyclical properties of the trace).  $F$  is invariant under rotations of the reference state because the trace of the product  $\underline{\underline{\lambda}}^T \cdot \underline{\underline{\lambda}}$  is. The form of the free energy in terms of  $\underline{\underline{C}}$  is then identical to that in terms of  $\underline{\underline{C}}'$ .

For completeness, the left Cauchy–Green tensor is  $\underline{\underline{B}} = \underline{\underline{\lambda}} \cdot \underline{\underline{\lambda}}^T$ . In contrast to  $\underline{\underline{C}}$ , it is invariant under rotations of the reference state and transforms like a second rank tensor in the target state  $S_T$ :

$$\underline{\underline{B}} = \underline{\underline{\lambda}} \cdot \underline{\underline{\lambda}}^T; \quad \underline{\underline{B}} = \underline{\underline{U}}^T \cdot \underline{\underline{B}}' \cdot \underline{\underline{U}}. \quad (4.6)$$

Importantly, the elastic energy can be equivalently expressed in terms of the left Cauchy–Green deformation tensor, although this is much less common approach because the invariance of the current (target) state is often a more relevant condition (Lubensky *et al.*, 2002).

In general, the scalar free energy density  $F$  must be a function purely of the rotational invariants of  $\underline{\underline{C}}$  (or  $\underline{\underline{B}}$ , if this is the chosen representation). Such invariants of a second-rank  $3 \times 3$  tensor  $C_{ij}$  are well known in linear algebra, and are usually called  $I_1$ ,  $I_2$  and  $I_3$ . Explicitly:

$$I_1 = \operatorname{Tr}(\underline{\underline{C}}), \quad I_2 = \frac{1}{2} \left[ \left( \operatorname{Tr}(\underline{\underline{C}}) \right)^2 - \operatorname{Tr}(\underline{\underline{C}}^T \cdot \underline{\underline{C}}) \right], \quad I_3 = \operatorname{Det}(\underline{\underline{C}}). \quad (4.7)$$

Since these are rotational invariants, they are the same in all frames, including the diagonal frame. It is therefore sufficient to write their expressions in terms of the eigenvalues  $C_1$ ,  $C_2$  and  $C_3$  of  $\underline{\underline{C}}$ . This yields  $I_1 = C_1 + C_2 + C_3$ ,  $I_2 = C_1C_2 + C_2C_3 + C_3C_1$  and  $I_3 = C_1C_2C_3$ .

We have seen that the separation of compressional and rubber-elastic energy scales ensures that distortions are at essentially constant volume, that is  $I_3 = \left( \operatorname{Det}(\underline{\underline{\lambda}}) \right)^2 = 1$  and is not considered further. Classical molecular theory, eqn (3.12), produces  $F = \frac{1}{2}\mu I_1$  which is a reasonable first approximation, valid up to surprisingly high extensions into the non-linear (large strain) regime. It is impossible to adopt a simpler result. The Mooney–Rivlin attempt to account phenomenologically for deviations due to entanglements and other causes, invokes the simplest possible correction, giving for  $F$ :

$$F = c_1 I_1 + c_2 I_2. \quad (4.8)$$

This modification is not entirely successful and gives no clue about the origins of the deviation from purely classical behaviour measured by the phenomenological coefficient  $c_2$  in eqn (4.8). More fitting scope is given by the Ogden rubber elastic free energy (Ogden, 1972). However, we are concerned with much more dramatic departures from classical behavior than those like  $c_2 I_2$  and concentrate on generalisations of  $I_1$  contributions.

We shall re-examine the above rotational symmetry requirements for nematic elastomers in Sect. 6.2.3: there is, in fact, an additional hidden symmetry that leads to so-called ‘soft elasticity’ or a ‘Goldstone mode’ of their mechanical response. This is the subject of Chapter 6. For large deformations and for these new elastic modes, considerations at the level of  $I_1$ , or rather its generalisation for nematics, will turn out to be sufficient.

#### COMPATIBILITY CONSTRAINTS

Distortions are in general non-uniform and thus  $\underline{\lambda}(\mathbf{R}_o)$  depends on the position in the body where it is measured. There are then certain conditions of *geometric compatibility* that the components of  $\underline{\lambda}$  must satisfy. The elements of this matrix cannot be completely independent because, in effect, there are only three independent components of the vector  $\mathbf{u}(\mathbf{R}_o)$  that determine all components of  $\lambda_{ij}$ . Mathematically, this geometric compatibility is most obvious when one calculates the second derivative, in which the order of derivatives is immaterial:

$$\begin{aligned} \frac{\partial \lambda_{ij}}{\partial R_{ok}} &= \frac{\partial^2 R_i}{\partial R_{oj} \partial R_{ok}} \equiv \frac{\partial^2 R_i}{\partial R_{ok} \partial R_{oj}} \\ \text{i.e.} \quad \frac{\partial \lambda_{ij}}{\partial R_{ok}} &= \frac{\partial \lambda_{ik}}{\partial R_{oj}} \end{aligned} \quad (4.9)$$

for all possible combinations of indices  $i, j, k$  from the set  $x, y, z$ . Of course, when the components of strain tensor are constant, all second derivatives are zero and compatibility is satisfied automatically. However, in many cases, for instance in modulated structures such as cholesteric elastomers or around topological defects, the deformations are naturally non-uniform and have to comply with this constraint.

In cholesteric elastomers with the pitch axis along  $\mathbf{z}$ , the director and the anisotropy associated with it rotate in the  $xy$ -plane as  $z$  advances. One might expect elastic deformations such as  $\lambda_{xy}(z)$  which would demand shears  $\lambda_{xz}(y)$  from compatibility, while  $\lambda_{xz}(z)$  can freely exist without the need for further attendant, compatibility-induced shears.

#### 4.2 NON-LINEAR AND LINEAR ELASTICITY; STRESSES

Strain-based descriptions of elasticity break down the deformation tensor  $\underline{\lambda}$  into a unit tensor  $\underline{\delta}$  (no deformation) plus a displacement gradient tensor  $u_{ij} = \partial u_i / \partial R_{oj}$ :

$$\lambda_{ij} = \delta_{ij} + u_{ij} . \quad (4.10)$$

Considering the change in squared distances between neighbouring points on distortion leads to the right, finite, symmetric strain tensor  $\varepsilon_{ij}$ :

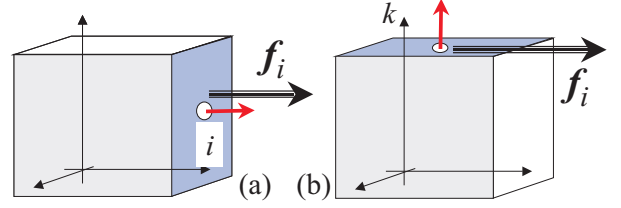
$$\varepsilon_{ij} = \frac{1}{2} \left( \underline{\lambda}^T \cdot \underline{\lambda} - \underline{\delta} \right)_{ij} \equiv \frac{1}{2} \left( \frac{\partial u_i}{\partial x_j} + \frac{\partial u_j}{\partial x_i} + \frac{\partial u_i}{\partial x_j} \frac{\partial u_j}{\partial x_i} \right) \rightarrow \frac{1}{2} (u_{ij} + u_{ji}) , \quad (4.11)$$

the latter being the small strain limit. The strain is symmetric by construction.

The right strain tensor  $\underline{\varepsilon}$  has the symmetry of  $\underline{\lambda}^T \cdot \underline{\lambda}$  – it is invariant under rotations  $\underline{U}$  of  $S_T$  and transforms like  $\underline{V}^T \cdot \underline{\varepsilon} \cdot \underline{V}$  under rotations of the reference state,  $S_R$ . The left strain tensor  $\underline{\varphi}$  could be derived from  $\underline{\lambda} \cdot \underline{\lambda}^T$ ; it would be invariant under rotations  $\underline{V}$  of  $S_R$  and transforms like  $\underline{U}^T \cdot \underline{\varphi} \cdot \underline{U}$  under rotations of  $S_T$ . Thus when nematic order  $\underline{Q}_o$  arises in  $S_R$  and  $\underline{Q}$  arises in  $S_T$ , we can couple  $\underline{Q}_o$  to  $\underline{\varepsilon}$  to form true scalars, such as  $\text{Tr}(\underline{\varepsilon} \cdot \underline{Q}_o)$ , and  $\underline{Q}$  couples to  $\underline{\varphi}$ , since each transforms as tensors in the same space. These symmetry requirements are vital for developments of nematic rubber elasticity using Cauchy strains, rather than  $\underline{\lambda}$ .

In the linear case, consider forces  $\mathbf{f}$  acting on the surfaces of a small volume element in a body, see Fig. 4.2. The stress  $\sigma_{ik}$  at this point is the component of force,  $f_i$  acting in the  $i^{\text{th}}$  direction, divided by the area of the

Figure 4.2: Stress  $\underline{\sigma}$  — a force per unit area of a body element. (a) Forces  $\mathbf{f}$  acting normally to the  $i^{\text{th}}$  element of surface generate diagonal (extensional) components of stress,  $\sigma_{ii}$ , the normal stresses. (b) Forces acting in the plane of the surface element yield shear stress, off-diagonal components of stress,  $\sigma_{ik}$ .



element of the surface with normal in the  $k^{\text{th}}$  direction on which the force is acting. Diagonal elements of the stress tensor are normal forces divided by the relevant surface area, the surface normal vector defined to be outwards from the body. The hydrostatic pressure is  $p = -\frac{1}{3} \text{Tr}(\underline{\sigma})$ , that is the average of the normal stresses with a minus sign since pressure acts inwards. Since force depends on the change of energy with extension, actual expressions for the stress turn out to depend on derivatives of the free energy density  $F$  with respect to the strain:  $\sigma_{ik} = (\partial F / \partial \epsilon_{ik})_T$ . See WT§4.2 where these issues are discussed with reference to rubber.

However, conventional elasticity breaks down for large strains on physical and geometrical grounds (Landau and Lifshitz, (i) The harmonic approximation to  $F$  is inadequate. Additional powers of invariants can be used in its expansion, but ultimately at hundreds of percent strain only a molecularly based  $F$  will be adequate. (ii) One has to be more careful finding the stress than we have been above. The true stress is the ratio of the force to the *current* area, that is the area in the deformed state. The engineering stress is the ratio of the force to the *initial* area. As area changes at large distortions, there are distinctions between the two.

Murnaghan, 1967, explicitly derives the expression for stress in terms of derivatives of the free energy density with respect to strain in the non-linear regime, taking into account changes in area. Take for example simple extension along the vertical axis (call it  $z$ ) of a classical rubber, sketched in Fig. 3.3. We consider an initially unit cube so we can use the energy density in place of the total energy. Its current length in the  $z$  direction is  $\lambda$ . The force  $f_z$  acting on the  $z$  ends of the body is the rate of change of energy,  $F$ , with length  $\lambda$ , eqn (3.15):

$$f_z = A \frac{\partial F}{\partial \lambda} = A \mu \left( \lambda - \frac{1}{\lambda^2} \right)$$

where  $A$  is the initial area of the sample cross-section facing the  $z$ -direction ( $A = 1$  in the unit cube). However the real surface area of the cross-section in this  $xy$ -plane is no longer unity, but has been reduced by  $1/\lambda$  because of constancy volume (the two perpendicular dimensions each contract by a factor  $1/\sqrt{\lambda}$ ). The current area is thus  $A_\lambda = A/\lambda$ . Dividing the force by this *current* area we obtain for the *true* local stress in the elastic material:

$$\sigma_{zz} = f_z / A_\lambda = \lambda \partial F / \partial \lambda = \mu (\lambda^2 - 1/\lambda). \quad (4.12)$$

Microscopically, as the rubber is extended there is the same number of strands (connecting crosslink points) crossing an  $xy$ -section of the rubber and conveying force (proportional to  $\partial F / \partial \lambda$ ), but the sectional area is diminishing thereby increasing the force per unit area. Clearly  $\lambda \partial F / \partial \lambda$  increases more rapidly than  $\partial F / \partial \lambda$ .

By contrast, the *engineering* stress is the current force divided by the *initial* area,  $A$ , at  $\lambda = 1$  which makes it much easier to measure. Whence

$$\sigma_{zz}^e = \mu (\lambda - 1/\lambda^2); \quad f_z = \sigma_{zz}^e A.$$

Accordingly, the production of mechanical work on such an extension is simply  $\delta w = -\sigma_{zz}^e \delta \lambda$ , using the engineering stress if we only measure the extension factor and not the change in cross-section area. To account for this, and for the true stress, the work density should be written taking into account the changing area of the element at constant volume:

$$\delta w = -\sigma_{zz} \left( \frac{1}{\lambda} \right) \delta \lambda = -\sigma_{zz} \delta (\ln \lambda). \quad (4.13)$$

Of course, both versions converge to the same linear expression at small deformations: when  $\lambda = 1 + \epsilon$  with  $\epsilon \ll 1$  one obtains  $\delta \lambda \approx \delta (\ln \lambda) \approx \delta \epsilon$ . (Both the stresses expand to  $\sigma_{zz} \approx \sigma_{zz}^e = 3\mu \epsilon$  for a rubber in this limit.)

### 4.3 GEOMETRY OF DEFORMATIONS AND ROTATIONS

In conventional elasticity of isotropic bodies, the energy is invariant under body rotations. We illustrate below how body rotations reflect the anti-symmetric part,  $\underline{\lambda}^A$ , of the deformation tensor  $\underline{\lambda}$ . To automatically render rotations irrelevant, one can take the symmetric part  $\underline{\lambda}^S$  of  $\underline{\lambda}$ . Alternatively, one can work with  $\underline{C} = \underline{\lambda}^T \cdot \underline{\lambda}$  which is symmetric by construction and where any rotations of the target state, which would appear as a multiplicative factor as  $\underline{U} \cdot \underline{\lambda}$ , are also removed by construction. In liquid crystal elastomers there exists an internal rotational freedom (the director) with respect to which body rotations are important, see Chapter 1, page 3. Accordingly we recall the geometry of rotations and of pure shears in more detail than is usual in elasticity. We then give examples of the decomposition of  $\underline{\lambda}$  into its two components ( $\underline{\lambda}^S$  and rotations). A more mathematical treatment, Sect. 4.3.2, on how this decomposition is achieved in general, can be skipped. It is however ultimately related to the question of the square roots of tensors, which we discuss. Roots of tensors are needed later in soft elasticity.

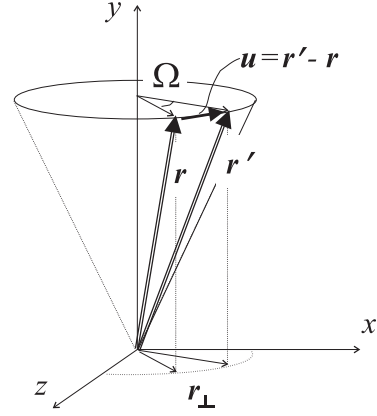


Figure 4.3: The geometry of rotations.

#### 4.3.1 ROTATIONS

Consider infinitesimal rotations about a particular axis,  $\Omega$ , depicted in Fig. 4.3. The displacement  $\mathbf{u}$  is  $\mathbf{u} = \Omega \times \mathbf{r} = \mathbf{r}' - \mathbf{r}$  where the magnitude of the displacement is  $u = r_{\perp} \Omega$ , given by the rotation of an arm of length  $r_{\perp}$  by an infinitesimal angle  $\Omega$  about the axis  $\Omega$ . Returning to the definition  $\lambda_{ij} = \partial r'_i / \partial r_j$  we find the  $\underline{\lambda}$  corresponding to body rotations to be:

$$\lambda_{ij} = \partial r'_i / \partial r_j = \delta_{ij} + \frac{\partial}{\partial r_j} (\Omega \times \mathbf{r})_i . \quad (4.14)$$

One can write this more simply using the totally anti-symmetric Levi-Civita tensor  $\epsilon_{ijk}$  since then  $(\Omega \times \mathbf{r})_i = \epsilon_{ilm} \Omega_l r_m$ . Using  $\partial r_m / \partial r_j = \delta_{jm}$  we have

$$\lambda_{ij} = \delta_{ij} + \epsilon_{ilj} \Omega_l \equiv \delta_{ij} + \Omega_l \epsilon_{lji} . \quad (4.15)$$

We can invert this relation to give:

$$\Omega_k = -\frac{1}{2} \epsilon_{ijk} \lambda_{ij} = -\lambda_{ij}^A \quad (i \neq j \neq k) \quad (4.16)$$

since the Levi-Civita tensor  $\epsilon_{ijk}$  selects out the antisymmetric part,  $\underline{\lambda}^A$ , of  $\underline{\lambda}$ . For instance, for infinitesimal rotations (about the axis  $\mathbf{y}$ ), we have:

$$\underline{\lambda} = \begin{pmatrix} 1 & -\Omega_y \\ \Omega_y & 1 \end{pmatrix} = \delta_{ij} + u_{ij}^A \quad (i, j = z, x) . \quad (4.17)$$

Here, and in the worked examples below in Sect. 4.3.2, we suppress for compactness  $y$  and just present the non-trivial,  $2 \times 2$  part of matrices describing effects in the  $xz$ -plane. The appearance in eqn (4.17) of the anti-symmetric component of strain,  $\underline{u}^A = \begin{pmatrix} 0 & -\Omega \\ \Omega & 0 \end{pmatrix}$  is the signal that rotation is involved.

The matrix representing rotation by a finite angle  $\Omega$  about the axis  $\mathbf{y}$ , in the  $xz$ -plane, is

$$\underline{\mathbf{W}}_{\Omega} = \begin{pmatrix} \cos \Omega & 0 & -\sin \Omega \\ 0 & 1 & 0 \\ \sin \Omega & 0 & \cos \Omega \end{pmatrix} . \quad (4.18)$$

In the most general case, the rotation matrix  $\underline{\mathbf{W}}$  is determined by three Euler angles: two defining the orientation of the axis,  $\Omega$ , and one specifying the amount of rotation,  $\Omega$ , about this axis. It clearly agrees with eqn (4.15) at  $\mathcal{O}(\Omega)$ . Recall that matrices  $\underline{\mathbf{W}}$  representing rotations have the properties  $\underline{\mathbf{W}} \cdot \underline{\mathbf{W}}^T = \underline{\mathbf{W}}^T \cdot \underline{\mathbf{W}} = \underline{\delta}$  and

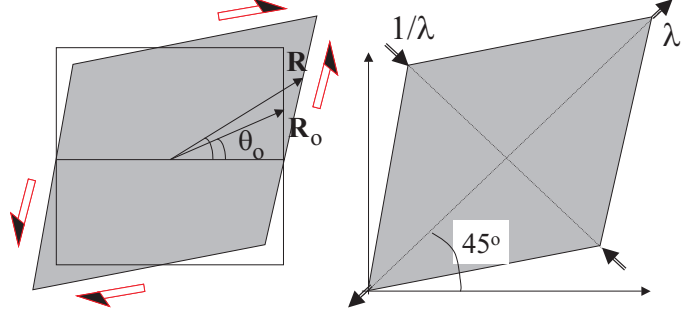
$\text{Det}(\underline{\mathbf{W}}) = 1$ , that is they are proper orthogonal matrices. The above example was of transforming a body, that is a position vector  $\mathbf{R}$  transforms as  $\mathbf{R}' = \underline{\mathbf{W}} \cdot \mathbf{R}$ . More discussion of finite rotations and their coordinate-independent representation is in WT Appendix E, on-line.

## 4.3.2 SHEARS AND THEIR DECOMPOSITION

## PURE SHEAR IS COMPOSED OF STRETCH AND CONTRACTION

The symmetric part of  $\underline{\lambda}$ , at constant volume, is pure shear. Despite appearances, simple extension and compression at right angles are in fact pure shear (at constant volume), but viewed in a rotated coordinate system. In the infinitesimal case the rotation is by  $45^\circ$ . This is a trivial observation since any symmetric tensor is diagonalisable and in diagonal form the elements are only stretch or compression. For the illustration below, we are rotating  $S_R$  and  $S_T$  in the same way.

Figure 4.4: Small, simple extension and compression (broken lines; arrows indicate the principal extensions and compressions) when rotated by  $45^\circ$  is pure shear. The original coordinate axes are shown unbroken. Pure shear rotates vectors  $R_o$  embedded in the solid towards the stretch axis.



*Exercise 4.1:* Confirm that the pure,  $xz$ -planar shear  $\begin{pmatrix} A & \lambda \\ \lambda & A \end{pmatrix}$ , sketched in Fig. 4.4, is simply a uniform extension/compression viewed at  $45^\circ$ . When at constant volume, determine the values  $\lambda'_{xx}$  and  $\lambda'_{zz}$  in the associated diagonal frame.

*Solution:* Transform as  $\underline{\lambda}' = \underline{W} \cdot \underline{\lambda} \cdot \underline{W}^T$  with  $\underline{W}_{(\pi/4)} = \frac{1}{\sqrt{2}} \begin{pmatrix} 1 & 1 \\ -1 & 1 \end{pmatrix}$  whence:  $\underline{\lambda}' = \begin{pmatrix} A+\lambda & 0 \\ 0 & A-\lambda \end{pmatrix} = \begin{pmatrix} \lambda' & 0 \\ 0 & 1/\lambda' \end{pmatrix}$  where  $A$  is fixed by  $\text{Det}(\underline{\lambda}) = 1$  as  $A = \sqrt{1 + \lambda^2}$ . At lowest order as shears are small,  $\lambda \ll 1$ , then  $A \approx 1$ . In its original frame  $\underline{\lambda}$  is recognisable as a familiar form of pure shear  $\begin{pmatrix} 1 & \lambda \\ \lambda & 1 \end{pmatrix}$ . In the new frame, it corresponds to an extension  $\lambda' (= A + \lambda)$  along  $x'$  and a compression  $1/\lambda' (= A - \lambda)$  along  $z'$ , at constant volume, see Fig. 4.4. Infinitesimally,  $\underline{\lambda}' \approx \begin{pmatrix} 1+\lambda & 0 \\ 0 & 1-\lambda \end{pmatrix}$ .

When the original diagonal elements are not equal, then the principal axes are not at  $45^\circ$  and  $135^\circ$ , but must still be orthogonal, since  $\underline{\lambda}$  is symmetric. For  $\begin{pmatrix} A & \lambda \\ \lambda & B \end{pmatrix}$ , with  $A > B$  say, the principal extensions  $\lambda_\pm$  and their angles  $\chi_\pm$  to the  $x$ -axis are:

$$\lambda_\pm = \frac{1}{2} \left( A + B \pm \sqrt{(A+B)^2 - 4} \right) \quad \text{and} \quad \chi_\pm = \pm \cos^{-1} \left[ \frac{2(AB-1)}{(A+B)^2 - 4 \mp (A-B)\sqrt{(A+B)^2 - 4}} \right]^{1/2}. \quad (4.19)$$

We have invoked incompressibility, that is  $\lambda^2 = AB - 1$ . The two angles  $\chi_\pm$  differ by  $\pi/2$ .

*Exercise 4.2:* An example of shear strains in the context of rubber elasticity. Consider a pure, planar  $x-z$  shear of magnitude  $\lambda$ . The deformation gradient is  $\underline{\lambda} = \begin{pmatrix} A & \lambda \\ \lambda & A \end{pmatrix}$  and the equivalent small strain is  $\underline{\epsilon} = \begin{pmatrix} A-1 & \lambda \\ \lambda & A-1 \end{pmatrix}$  (suppressing the unchanging  $y$  components for compactness in  $\underline{\lambda}$  and in  $\underline{\epsilon}$ ). Show that the elastic energy density is  $F = \mu(A^2 + \lambda^2) = \mu(1 + 2\lambda^2)$ . Hence the modulus associated with this distortion is  $4\mu$  which derives from the curvature of the free energy density,  $\partial^2 F / \partial \lambda^2|_{\lambda=0}$  at zero shear.

## SIMPLE SHEAR IS COMPOSED OF PURE SHEAR PLUS ROTATION

Consider a deformation  $\underline{\lambda}^S = \begin{pmatrix} a & \lambda \\ \lambda & a \end{pmatrix}$  acting in the  $xz$ -plane. Then  $\lambda_{yy} = 1$  and we suppress the  $y$  parts of  $\underline{\lambda}$  in the discussion. Figure 4.4 shows the body initially and after a pure *shear*. At  $45^\circ$  these are shown to be simple extensions and compression, at least approximately for this finite deformation. Figures 4.5(a) and (b) show *simple shears*  $\underline{\lambda}^a = \begin{pmatrix} 1 & \lambda \\ 0 & 1 \end{pmatrix}$  and  $\underline{\lambda}^b = \begin{pmatrix} 1 & 0 \\ \lambda & 1 \end{pmatrix}$ . For infinitesimal  $\lambda$ , since deformations are then additive, we can

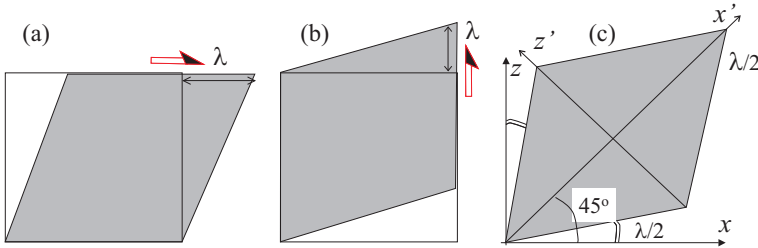


Figure 4.5: Simple shears (a) and (b) add to give pure shear, Fig. 4.4. Simple shear can also be decomposed into the rotation and the pure shear components (c): *Small* simple shears  $\lambda$  are pure shears in a coordinate system  $(x'-z')$ , followed by a rotation of  $-\frac{1}{2}$  the shear angle ( $\lambda/2$ ) from the original  $(x-z)$  system.

regard the pure shear  $\underline{\lambda}^S = \begin{pmatrix} a & \lambda \\ \lambda & a \end{pmatrix}$ , Fig. 4.5(c), as being made up of two such simple shears in the two relevant directions:

$$\begin{pmatrix} a & \lambda \\ \lambda & a \end{pmatrix} \approx \begin{pmatrix} 1 & 0 \\ 0 & 1 \end{pmatrix} + \begin{pmatrix} 0 & \lambda \\ 0 & 0 \end{pmatrix} + \begin{pmatrix} 0 & 0 \\ \lambda & 0 \end{pmatrix} \quad (4.20)$$

The entry  $a \sim 1 + \mathcal{O}(\lambda^2)$  in  $\underline{\lambda}^S$  ensures volume conservation:

$$\text{Det}(\underline{\lambda}^S) = 1 = a^2 - \lambda^2 \rightarrow a = \sqrt{1 + \lambda^2} \quad (4.21)$$

Material points  $\mathbf{R}_0$  at a  $\theta_0 \neq 45^\circ$ , see Fig. 4.4, are transformed to points  $\mathbf{R}$  which have a different final angle which increases,  $\theta > \theta_0$ , for initial angles  $\theta_0 < 45^\circ$ . The angle diminishes,  $\theta < \theta_0$ , for initial angles  $\theta_0 > 45^\circ$ . Thus vectors  $\mathbf{R}_0$  are drawn toward the extension diagonal and repelled from the compression diagonal. Overall, there is no rotation of the body. Recall Chapter 1, where a penalty  $D_1$  for director rotation relative to body rotation of the solid was anticipated. We can regard the  $D_1$  coupling as being that of the director to the anti-symmetric part of deformations. Figure 4.4 and the above discussion of the attraction of  $\mathbf{R}_0$  toward the extension axis suggests another coupling,  $D_2$  of  $\mathbf{n}$  to  $\underline{\lambda}$ , but this time to  $\underline{\lambda}^S$  rather than to  $\underline{\lambda}^A$ .

Simple shear has been seen to possess a component of pure shear. Additionally, simple shear has a component of rotation. For example in the limit of *small* distortions  $\lambda$ :

$$\begin{pmatrix} 1 & \lambda \\ 0 & 1 \end{pmatrix} = \begin{pmatrix} 1 & \lambda/2 \\ -\lambda/2 & 1 \end{pmatrix} + \begin{pmatrix} 0 & \lambda/2 \\ \lambda/2 & 0 \end{pmatrix} \quad (4.22)$$

$$\approx \underline{\mathbf{W}}_{-\lambda/2} + \underline{\boldsymbol{\epsilon}}_{\lambda/2}. \quad (4.23)$$

Thus,  $\underline{\lambda}^a$  of Fig. 4.5(a) is a rotation  $\underline{\mathbf{W}}_{-\lambda/2}$  through an angle  $-\lambda/2$  and a pure, symmetric shear  $\underline{\boldsymbol{\epsilon}}_{\lambda/2}$  of small amplitude  $\lambda/2$ , see Fig. 4.5(c). Simple shear is not so simple as pure shear!

## THE POLAR DECOMPOSITION THEOREM

For finite deformations the decomposition is more complicated, but it is still true by the polar decomposition theorem that any non-singular, non-symmetric  $\underline{\lambda}$  can be broken down into products of a symmetric deformation gradient tensor and an orthogonal tensor, in effect a pure shear preceded or followed by a body rotation:

$$\underline{\lambda} = \underline{\lambda}^L \cdot \underline{\mathbf{V}} \quad \text{or} \quad \underline{\mathbf{U}} \cdot \underline{\lambda}^R. \quad (4.24)$$

The rotations are denoted as before by  $\underline{V}$  or  $\underline{U}$  depending upon which space they act on. The form of the accompanying symmetric deformations  $\underline{\lambda}^S$  will also depend on whether they precede or follow rotations and have been denoted by  $\underline{\lambda}^R$  and  $\underline{\lambda}^L$  because they yield the Cauchy-Green tensors  $\underline{C}$  and  $\underline{B}$  respectively. Since they are symmetric, a frame can be found in which they are diagonal, and in which the deformations are therefore simple:

$$\underline{\lambda}^S = \begin{pmatrix} \lambda_1 & 0 & 0 \\ 0 & \lambda_2 & 0 \\ 0 & 0 & \lambda_3 \end{pmatrix} \quad \text{thus } R_1 = \lambda_1 R_{01}, \quad R_2 = \lambda_2 R_{02}, \quad R_3 = \lambda_3 R_{03}. \quad (4.25)$$

Hence all deformations are extensions ( $\lambda_i > 1$ ) or compressions ( $\lambda_i < 1$ ). Thus  $\underline{\lambda}^R$  and  $\underline{\lambda}^L$  are the right and left stretching tensors, respectively. This procedure is an example of the polar decomposition theorem (Horn and Johnson, 1991) which holds for non-singular matrices  $\underline{\lambda}$ . One requires that  $\text{Det}(\underline{\lambda}) > 0$ , which means geometrically (i) that deformations do not shrink a body to a point,  $\text{Det}(\underline{\lambda}) = 0$ ; or (ii) cause the body to pass through itself,  $\text{Det}(\underline{\lambda}) < 0$  (Atkins and Fox, 1980).

*Exercise 4.3:* Show that simple shear can be broken down into a combination of symmetric distortion and body rotation, that is:

$$\begin{pmatrix} 1 & \lambda \\ 0 & 1 \end{pmatrix} = \begin{pmatrix} \cos \Omega & \sin \Omega \\ -\sin \Omega & \cos \Omega \end{pmatrix} \cdot \frac{1}{\sqrt{4 + \lambda^2}} \begin{pmatrix} 2 & \lambda \\ \lambda & 2 + \lambda^2 \end{pmatrix} \equiv \underline{U} \cdot \underline{\lambda}^S$$

where  $\sin \Omega = \lambda / \sqrt{4 + \lambda^2}$ . Check that the symmetric shear tensor is volume-preserving, that is  $\text{Det}(\underline{\lambda}^S) = 1$ . Note that for small amplitudes the rotation is  $\Omega \sim \lambda/2$ , see Fig. 4.5. For large shears the rotation is  $\Omega = \pi/2$ .

*Exercise 4.4:* Break down a *general*  $xz$ -distortion  $\underline{\lambda}$  into a combination of symmetric distortion,  $\underline{\lambda}^S$ , followed by body rotation,  $\underline{U}_\Omega$ , about  $y$ .

*Solution:* Let  $\underline{\lambda}$  be broken down as:

$$\begin{pmatrix} \lambda_{xx} & \delta \\ \delta' & \lambda_{zz} \end{pmatrix} = \begin{pmatrix} \cos \Omega & \sin \Omega \\ -\sin \Omega & \cos \Omega \end{pmatrix} \begin{pmatrix} a & d \\ d & b \end{pmatrix} \equiv \underline{U}_\Omega \cdot \underline{\lambda}^S.$$

Multiplying out the right-hand side and comparing with the corresponding elements on the left-hand side, one obtains four simultaneous equations. Eliminating between them in pairs one obtains equations for each of  $a$  and  $b$  and two equations for  $d$ . Equating the latter two, one obtains for the rotation:

$$\tan \Omega = (\delta - \delta') / (\lambda_{xx} + \lambda_{zz}) \quad (4.26)$$

Thus  $\sin \Omega = (\delta - \delta') / \Delta$  where  $\Delta = \sqrt{(\lambda_{xx} + \lambda_{zz})^2 + (\delta - \delta')^2}$  and similarly for  $\cos \Omega$  in the rotation matrix. Note, there is no body rotation for  $\underline{\lambda}$  symmetric, that is  $\delta = \delta'$ . Restoring sin and cos to the expressions for  $a$ ,  $b$  and  $d$  gives for the symmetric shear tensor:

$$\underline{\lambda}^S = \frac{1}{\Delta} \begin{pmatrix} \lambda_{xx}(\lambda_{zz} + \lambda_{xx}) - \delta'(\delta - \delta') & \lambda_{xx}\delta + \delta'\lambda_{zz} \\ \lambda_{xx}\delta + \delta'\lambda_{zz} & \lambda_{xx}(\lambda_{zz} + \lambda_{xx}) + \delta(\delta - \delta') \end{pmatrix}. \quad (4.27)$$

We use this decomposition in Sect. 6.2.4 to understand the soft deformations of nematic elastomers since the rotational component takes great physical significance when director rotation dominates the response.

## PRINCIPAL EXTENSIONS

Symmetric distortions  $\underline{\lambda}$  have no rotational component and their principal extensions and compressions are perpendicular to each other and at  $\pm 45^\circ$  to the laboratory axes (exercise 4.1) when distortions are small. We have seen that any asymmetry in  $\underline{\lambda}$  implies there is a component of pure (irrotational) shear plus a certain degree of local rotation. In nematic rubber elasticity it is useful to identify these components separately. It is also interesting to examine the principal directions of extension/compression of an arbitrary  $\underline{\lambda}$ . These are the directions in which an element of the body is extended or compressed without being realigned; in the general case they are not perpendicular to each other.

*Exercise 4.5:* Find the eigenvectors  $\mathbf{e}_\pm$  and eigenvalues  $\lambda_\pm$  of a deformation  $\underline{\lambda} = \begin{pmatrix} A & \lambda \\ \lambda' & A \end{pmatrix}$  in the  $xz$  plane, where  $A = \sqrt{1 + \lambda\lambda'}$  ensures  $\text{Det}(\underline{\lambda}) = 1$ .

*Solution:* The eigenvalues are the roots of the characteristic equation for the non-symmetric  $\underline{\lambda}$ :

$$\text{Det}(\underline{\lambda} - \lambda_\pm \underline{\delta}) = \lambda_\pm^2 - 2A\lambda_\pm + A^2 - \lambda\lambda' \equiv \lambda_\pm^2 - 2A\lambda_\pm + 1 = 0,$$

also using  $\text{Det}(\underline{\lambda}) = 1$ . This quadratic equation does not always have a solution (as not every non-symmetric matrix can be diagonalised), e.g. the case of simple shear,  $\lambda' = 0$  is degenerate. When the solution exists, the principal extensions(+) or compressions(-) are:

$$\lambda_\pm = \sqrt{1 + \lambda\lambda'} \pm \sqrt{\lambda\lambda'}$$

with the corresponding (normalised) eigenvectors and angle between them:

$$\mathbf{e}_\pm = \frac{1}{\sqrt{1 + \lambda'/\lambda}} \left( 1, \pm \sqrt{\lambda'/\lambda} \right) \quad \chi = \cos^{-1}(\mathbf{e}_+ \cdot \mathbf{e}_-) = \cos^{-1} \left( \frac{\lambda - \lambda'}{\lambda + \lambda'} \right).$$

The symmetric case  $\lambda = \lambda'$  clearly yields perpendicular directions. The limit of simple shear,  $\lambda' \rightarrow 0$ , with pure shear and rotation in equal measure in the infinitesimal case, is degenerate.

We shall describe soft distortions of nematic elastomers where rotations are important. When determining directions associated with pure extension/compression the diagonal elements of  $\underline{\lambda}$  will not be equal as here.

## SQUARE ROOTS AND POLAR DECOMPOSITION OF TENSORS

The square root of a tensor is, most simply, a tensor that when multiplied by itself returns the original tensor. Representing tensors by matrices and adopting the principal frame, tensor multiplication is achieved by multiplying the corresponding diagonal elements. It is then easy to construct the square root tensor by taking the square root of each diagonal element. One can then subsequently rotate to a general coordinate frame. This procedure is only valid for the roots of symmetric tensors. More general results are required when such tensors are used to describe soft and semi-soft rubber elasticity. By the polar decomposition theorem we discuss below, we can find a symmetric tensor followed by a rotation to represent any deformation. In fact this theorem and the roots of tensors are deeply related. We conclude with the connection between decompositions of non-singular matrices in general and a practical algorithm for finding the pure shear times rotation for general deformations.

*Exercise 4.6:* Show in a general frame, where a symmetric matrix  $\underline{\mathbf{X}}$  is not necessarily diagonal, that the product of roots is as expected:  $\underline{\mathbf{X}}^{1/2} \cdot \underline{\mathbf{X}}^{1/2} = \underline{\mathbf{X}}$ . (We shall only require the roots of symmetric tensors in these notes.)

*Solution:* Let  $\underline{\mathbf{U}}$  be the rotation that takes one from the current frame to the principal frame where

$\underline{\underline{\mathbf{X}}}$  is represented by the diagonal matrix  $\underline{\underline{\mathbf{X}}}_D = \begin{pmatrix} x_1 & 0 & 0 \\ 0 & x_2 & 0 \\ 0 & 0 & x_3 \end{pmatrix}$ . The definition of the root in the diagonal frame is:

$$\underline{\underline{\mathbf{X}}}_D = \underline{\underline{\mathbf{X}}}_D^{1/2} \cdot \underline{\underline{\mathbf{X}}}_D^{1/2}, \quad \text{with } \underline{\underline{\mathbf{X}}}_D^{1/2} = \begin{pmatrix} \sqrt{x_1} & 0 & 0 \\ 0 & \sqrt{x_2} & 0 \\ 0 & 0 & \sqrt{x_3} \end{pmatrix}.$$

Post- and pre-multiply this equation by  $\underline{\underline{\mathbf{U}}}$  and  $\underline{\underline{\mathbf{U}}}^T$  to give on the left hand side  $\underline{\underline{\mathbf{X}}} = \underline{\underline{\mathbf{U}}}^T \cdot \underline{\underline{\mathbf{X}}}_D \cdot \underline{\underline{\mathbf{U}}}$ . On the right-hand side insert between the factors of  $\underline{\underline{\mathbf{X}}}_D^{1/2}$  the unity in the form  $\underline{\underline{\boldsymbol{\delta}}} = \underline{\underline{\mathbf{U}}} \cdot \underline{\underline{\mathbf{U}}}^T$ . Judiciously inserting some brackets to guide the eye, one obtains:

$$\underline{\underline{\mathbf{U}}}^T \cdot \underline{\underline{\mathbf{X}}}_D \cdot \underline{\underline{\mathbf{U}}} = (\underline{\underline{\mathbf{U}}}^T \cdot \underline{\underline{\mathbf{X}}}_D^{1/2} \cdot \underline{\underline{\mathbf{U}}}) \cdot \underbrace{(\underline{\underline{\mathbf{U}}}^T \cdot \underline{\underline{\mathbf{X}}}_D^{1/2} \cdot \underline{\underline{\mathbf{U}}})}_{\underline{\underline{\boldsymbol{\delta}}}},$$

which can be rewritten as

$$\underline{\underline{\mathbf{X}}} = \underline{\underline{\mathbf{X}}}^{1/2} \cdot \underline{\underline{\mathbf{X}}}^{1/2}.$$

The result is evidently true in all frames.

A sketch of the proof of the polar decomposition theorem brings us into contact with the more general properties of the square roots of tensors. Take  $\underline{\underline{\mathbf{C}}} = \underline{\underline{\boldsymbol{\lambda}}}^T \cdot \underline{\underline{\boldsymbol{\lambda}}}$ , which is symmetric by construction. Since  $\text{Det}(\underline{\underline{\mathbf{C}}}) = \text{Det}(\underline{\underline{\boldsymbol{\lambda}}}^T \cdot \underline{\underline{\boldsymbol{\lambda}}}) = (\text{Det}(\underline{\underline{\boldsymbol{\lambda}}}))^2 > 0$ , the matrix  $\underline{\underline{\mathbf{C}}}$  is also non-singular. A non-singular matrix has at least  $2^\mu$  non-similar roots, where  $\mu$  is the number of distinct eigenvalues ( $\underline{\underline{\mathbf{A}}}$  and  $\underline{\underline{\mathbf{B}}}$  are non-similar if they cannot be related by  $\underline{\underline{\mathbf{A}}} = \underline{\underline{\mathbf{W}}} \cdot \underline{\underline{\mathbf{B}}} \cdot \underline{\underline{\mathbf{W}}}'$  where  $\underline{\underline{\mathbf{W}}}$  and  $\underline{\underline{\mathbf{W}}}'$  are proper, orthogonal matrices). There are also not more than  $2^\nu$  non-similar roots, with  $\nu$  the number of Jordan blocks in  $\underline{\underline{\mathbf{C}}}$ . At least one of these roots is a polynomial in  $\underline{\underline{\mathbf{C}}}$ . Since in this case  $\underline{\underline{\mathbf{C}}}$  is symmetric, then so will the polynomial roots be symmetric. Denote such a symmetric root by  $\underline{\underline{\boldsymbol{\lambda}}}^R$ . Now construct a matrix  $\underline{\underline{\mathbf{U}}} = \underline{\underline{\boldsymbol{\lambda}}} \cdot (\underline{\underline{\boldsymbol{\lambda}}}^R)^{-1}$ . Then test whether this matrix is proper orthogonal by considering  $\underline{\underline{\mathbf{U}}}^T \cdot \underline{\underline{\mathbf{U}}}$ :

$$\underline{\underline{\mathbf{U}}}^T \cdot \underline{\underline{\mathbf{U}}} = (\underline{\underline{\boldsymbol{\lambda}}}^R)^{-1} \cdot \underline{\underline{\boldsymbol{\lambda}}}^T \cdot \underline{\underline{\boldsymbol{\lambda}}} \cdot (\underline{\underline{\boldsymbol{\lambda}}}^R)^{-1} = (\underline{\underline{\boldsymbol{\lambda}}}^R)^{-1} \cdot \underline{\underline{\mathbf{C}}} \cdot (\underline{\underline{\boldsymbol{\lambda}}}^R)^{-1} \quad (4.28)$$

$$\equiv (\underline{\underline{\boldsymbol{\lambda}}}^R)^{-1} \cdot (\underline{\underline{\boldsymbol{\lambda}}}^R)^2 \cdot (\underline{\underline{\boldsymbol{\lambda}}}^R)^{-1} = \underline{\underline{\boldsymbol{\delta}}} \quad (4.29)$$

which confirms that  $\underline{\underline{\mathbf{U}}}$  is indeed orthogonal. Inverting the definition of  $\underline{\underline{\mathbf{U}}}$ , we recover the desired decomposition  $\underline{\underline{\boldsymbol{\lambda}}} = \underline{\underline{\mathbf{U}}} \cdot \underline{\underline{\boldsymbol{\lambda}}}^R$ . Thus the utility of constructing Cauchy tensors from  $\underline{\underline{\boldsymbol{\lambda}}}$  and that of roots of tensors are intimately related.

Nematic networks can be highly rubbery, that is capable of large extensions and composed of molecules with liquid-like mobility. The difference between nematic and classical elastomers is principally only that of molecular shape anisotropy induced internally by the liquid crystalline order, Fig. 5.1. The simplest description of nematic rubber elasticity is essentially an extension of classical molecular rubber elasticity, reviewed in Chapter 3. We shall accordingly call this nematic rubber elasticity theory ‘neo-classical’, referring to the identity of approach. It will be introduced in this chapter phenomena not involving rotations of the director and complex strains explored. Its further richness is explored in subsequent chapters when director rotation is considered.

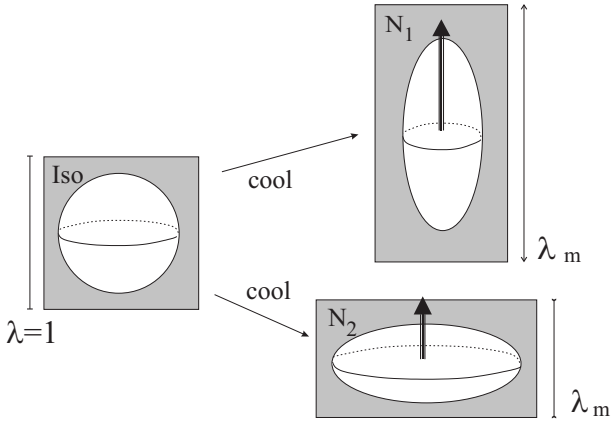


Figure 5.1: Chain shape changes drive the shape changes of the network as a whole. The detailed chains of Fig. 3.3 have been replaced by spheroids characterising their (anisotropic distribution of shapes. For example, a chain extending from on average a sphere to a prolate spheroid induces a macroscopic elongation  $\lambda_m > 1$ . For a chain that flattens to an oblate shape, the shape change would be a contraction,  $\lambda_m < 1$ , along the principal axis, that is along the nematic director  $\mathbf{n}$ .

### 5.1 NEO-CLASSICAL THEORY

The number of configurations of a test strand, connecting two crosslinks separated by a distance  $\mathbf{R}$  in a nematic network, is proportional to the anisotropic Gaussian distribution we saw in Chapter 3, eqn (3.19):

$$p(\mathbf{R}) \propto \left( \frac{1}{\text{Det}(\underline{\underline{\ell}})} \right)^{1/2} \exp \left( -\frac{3}{2L} \mathbf{R} \cdot \underline{\underline{\ell}}^{-1} \cdot \mathbf{R} \right). \quad (5.1)$$

The effective step length tensor  $\underline{\underline{\ell}}$  reflects the current nematic ordering in the network. At formation however, the span between the links was  $\mathbf{R}_f$ , say, and the shape of the chains at that time was described by a Gaussian distribution similar in form to eqn (5.1) but with a step-length tensor  $\underline{\underline{\ell}}_o$ . One reason the distributions might differ is that the temperature, and hence the nematic order, of the two states differs. If the formation condition was nematic, another reason might be the current director adopting a direction different from the director orientation at formation.

The probability of having crosslinked the current span  $\mathbf{R}$  into the network is  $p_o(\mathbf{R}_f)$ , that is the probability of finding at formation the span  $\mathbf{R}_f$  that  $\mathbf{R}$  derives from. The distribution  $p_o$  is of the same form as eqn (5.1), but instead governs  $\mathbf{R}_f$  and has the step length tensor  $\underline{\underline{\ell}}_o$ . For the moment we take the subscript  $_o$  to denote formation which we identify with the conditions before deformation is imposed. As in Chapter 3, we assume affine deformation: the total deformation tensor  $\underline{\underline{\lambda}}_t$  from the formation to the current state is what took the initial span  $\mathbf{R}_f$  to become  $\mathbf{R}$ , that is  $\mathbf{R} = \underline{\underline{\lambda}}_t \cdot \mathbf{R}_f$ . The subscript  $_t$  on  $\underline{\underline{\lambda}}$  denotes total deformation, which is needed in case there were several deformation steps between formation ( $\mathbf{R}_f$ ) and currently ( $\mathbf{R}$ ). For instance there could be a spontaneous distortion associated with changing conditions, followed then by an imposed distortion. The free

energy of a strand,  $\mathcal{F}_s$ , averaged over formation conditions, is then:

$$\begin{aligned}\mathcal{F}_s &= -k_B T \langle \ln p(\mathbf{R}) \rangle_{p_0(\mathbf{R}_f)} \\ &= \frac{3k_B T}{2L} \langle R_i \ell_{ij}^{-1} R_j \rangle + \frac{k_B T}{2} \ln \left( \frac{\text{Det}(\underline{\underline{\ell}})}{a^3} \right) \\ &\equiv \frac{3k_B T}{2L} \langle \mathbf{R} \cdot \underline{\underline{\ell}}^{-1} \cdot \mathbf{R} \rangle + \dots\end{aligned}\quad (5.2)$$

The  $\ln(\text{Det})$ -term arises from the normalisation of the probability, the prefactor in (5.1). Inserting the  $a^3$  in the normalisation logarithm gives an arbitrary, additive constant. It is done simply to make the argument of the logarithm dimensionless. The  $\ln \text{Det}$  contains the nematic order, via the step-length tensor  $\underline{\underline{\ell}}$ , but not the deformation  $\underline{\underline{\lambda}}$ . We shall generally only display it when it plays a role, that is, when the *magnitude* rather than *direction* of nematic order changes. The free energy  $\mathcal{F}_s$  can be simplified by using  $\underline{\underline{\lambda}}$  and  $\mathbf{R}_f$  for  $\mathbf{R}$ :

$$\mathcal{F}_s = \frac{3k_B T}{2L} \langle \mathbf{R}_f \cdot \underline{\underline{\lambda}}^T \cdot \underline{\underline{\ell}}^{-1} \cdot \underline{\underline{\lambda}} \cdot \mathbf{R}_f \rangle_{p_0} . \quad (5.3)$$

The average over the initial span is easy – the second moment of the Gaussian distribution is  $\langle \mathbf{R}_f \mathbf{R}_f \rangle_{p_0(\mathbf{R}_f)} = \frac{1}{3} \underline{\underline{\ell}}_0 L$  whence the free energy of a strand is finally:

$$\mathcal{F}_s = \frac{1}{2} k_B T \text{Tr} \left( \underline{\underline{\ell}}_0 \cdot \underline{\underline{\lambda}}^T \cdot \underline{\underline{\ell}}^{-1} \cdot \underline{\underline{\lambda}} \right) + \frac{1}{2} k_B T \ln \left( \frac{\text{Det}(\underline{\underline{\ell}})}{a^3} \right) . \quad (5.4)$$

This is what we call the neo-classical free energy of an average network strand since it is a simple generalisation of classical, Gaussian rubber elasticity. To convert it to a free energy density  $F$  we should simply count the number of such network strands,  $n_s$ , per unit volume:  $F = n_s \mathcal{F}_s$ . We have seen that the combination  $n_s k_B T$  is  $\mu$ , the linear shear modulus of an isotropic rubber with this density of network strands. The free energy density is then

$$F = \frac{1}{2} \mu \text{Tr} \left( \underline{\underline{\ell}}_0 \cdot \underline{\underline{\lambda}}^T \cdot \underline{\underline{\ell}}^{-1} \cdot \underline{\underline{\lambda}} \right) \quad (5.5)$$

All the nematic rubber phenomena we describe will arise from this free energy and some non-ideal deviations from it. The deviations will arise from entanglements, compositional fluctuations, crosslinks of finite size and related random field effects. We shall frequently refer to it as the *Trace formula*. Ideally, it is valid for all, including very large, deformations and is only limited by extensions sufficient to so stretch network chains that they violate Gaussian statistics. It records, via  $\underline{\underline{\ell}}_0$  and  $\underline{\underline{\ell}}$ , the initial and current directors  $\mathbf{n}_0$  and  $\mathbf{n}$  of the elastomer, unlike the free energy of a liquid nematic where  $F$  depends only on the current director. The initial and current magnitudes of the local nematic order parameter,  $Q_0$  and  $Q$ , are also contained in  $F$  through the anisotropy of  $\underline{\underline{\ell}}_0$  and  $\underline{\underline{\ell}}$ .

Smectics have an underlying nematic order and in a molecular theory of such elastomers we again employ this free energy, but heavily modified by the dominating influence of the layers.

The free energy (5.5) has a very rich structure compared with the classical result  $\text{Tr} \left( \underline{\underline{\lambda}}^T \cdot \underline{\underline{\lambda}} \right)$ . The distortions appear now not as simple forms  $\underline{\underline{\lambda}}^T \cdot \underline{\underline{\lambda}}$ , but rather in the combination  $\underline{\underline{\lambda}}^T \cdot \underline{\underline{\ell}}^{-1} \cdot \underline{\underline{\lambda}}$ . Thus the current (after deformation) nematic state of the body is encoded into the elastic energy via the sandwiched factor of  $\underline{\underline{\ell}}^{-1}$ . The main principal direction of  $\underline{\underline{\ell}}^{-1}$ , the director  $\mathbf{n}$ , is not necessarily along a principal direction of  $\underline{\underline{\lambda}}$ . Diagonal elements of  $\underline{\underline{\lambda}}$  (simple extensions and compression) can now couple with off-diagonal elements (shears), for instance giving terms like  $\lambda_{xx} \lambda_{zx}$  in the free energy. This does not occur in classical rubber elasticity. The structure  $\underline{\underline{\lambda}}^T \cdot \underline{\underline{\ell}}^{-1} \cdot \underline{\underline{\lambda}}$  also allows local torques and rotations to be applied to nematic elastomers, thereby coupling mechanical effects to the internal nematic freedom. Finally, the combination  $\underline{\underline{\lambda}}^T \cdot \underline{\underline{\ell}}^{-1} \cdot \underline{\underline{\lambda}}$  couples to  $\underline{\underline{\ell}}_0$ , that is to the original director  $\mathbf{n}_0$  of the state before deformation, thereby coupling the current strains and director to the original anisotropy of the solid matrix, see Chapter 1, page 3.

At first sight  $F$  seems rather tensorial, but it is easily dissected with a few examples where directions are unchanging (for instance that of the director and the step length tensors) and where the tensor structure is always diagonal and hence trivial. Most trivially, if the formation and current states are both isotropic, that is  $\underline{\underline{\ell}}_0 = a\underline{\underline{\delta}}$  and  $\underline{\underline{\ell}}^{-1} = a^{-1}\underline{\underline{\delta}}$ , then (5.5) collapses to the classical result  $F = \frac{1}{2}\mu \text{Tr}(\underline{\underline{\lambda}}^T \cdot \underline{\underline{\lambda}})$ . For the remainder of this chapter, we shall consider simple examples not involving director rotation: We defer until the next chapter questions of shear, of continuous rotations of the director induced by fields, and of torques in general. These lead to yet more new phenomena and in effect a new elasticity.

## 5.2 SPONTANEOUS DISTORTIONS

Consider an elastomer formed in the isotropic state, that is with  $\underline{\underline{\ell}}_0 = a\underline{\underline{\delta}}$ . It is cooled to its current, relaxed, monodomain nematic state. The chains now have a natural shape described by the tensor  $\underline{\underline{\ell}}_r$ , the subscript  $\{r\}$  denoting ‘relaxed’. No stresses or constraints have been applied to it and thus any  $\underline{\underline{\lambda}}_r$  is a *spontaneous* distortion,  $\underline{\underline{\lambda}}_m$ . From the symmetry of the phase that has developed on cooling, the distortion must be uniaxial and directed along  $\mathbf{n}$ . It must also be volume preserving. Taking the director to be along  $\mathbf{z}$ , that is  $\mathbf{n} = \mathbf{z}$ , the deformation tensor  $\underline{\underline{\lambda}}_m$  must have its principal extension element along  $\mathbf{z}$ . Call this component  $\lambda$ , whence the whole matrix  $\underline{\underline{\lambda}}_m$  can only be:

$$\underline{\underline{\lambda}}_m = \begin{pmatrix} 1/\sqrt{\lambda} & 0 & 0 \\ 0 & 1/\sqrt{\lambda} & 0 \\ 0 & 0 & \lambda \end{pmatrix} \equiv \underline{\underline{\lambda}}_m^T. \quad (5.6)$$

The inverse step length tensor  $\underline{\underline{\ell}}_r^{-1}$  in the same system of coordinate axes is:

$$\underline{\underline{\ell}}_r^{-1} = \begin{pmatrix} 1/\ell_{\perp}^r & 0 & 0 \\ 0 & 1/\ell_{\perp}^r & 0 \\ 0 & 0 & 1/\ell_{\parallel}^r \end{pmatrix}. \quad (5.7)$$

Evaluating the free energy reduces to the trivial problem of multiplying four diagonal matrices that form  $[(a\underline{\underline{\delta}}) \cdot \underline{\underline{\lambda}}_m^T \cdot \underline{\underline{\ell}}_r^{-1} \cdot \underline{\underline{\lambda}}_m]$  and then tracing the result, that is summing along the diagonal. We take

$$\text{Tr} \begin{pmatrix} a/(\lambda \ell_{\perp}^r) & 0 & 0 \\ 0 & a/(\lambda \ell_{\perp}^r) & 0 \\ 0 & 0 & a\lambda^2/\ell_{\parallel}^r \end{pmatrix} \rightarrow \frac{1}{2}\mu \left( \lambda^2 \frac{a}{\ell_{\parallel}^r} + \frac{2}{\lambda} \frac{a}{\ell_{\perp}^r} \right). \quad (5.8)$$

The free energy is close to that of a classical elastomer undergoing uniaxial extension, but there are separate factors  $a/\ell_{\parallel}^r$  and  $a/\ell_{\perp}^r$  for the parallel and the two perpendicular directions – the imbalance between the directions induces shape change.

Unconstrained, the system will adopt a spontaneous extension  $\lambda$  minimising the elastic free energy density (5.8). Taking  $\partial F/\partial \lambda = 0$ , we immediately conclude that on cooling from formation to current conditions, there must be a spontaneous uniaxial elongation  $\lambda_m$ , of (Abramchuk and Khokhlov, 1987; Warner *et al.*, 1988):

$$\lambda_m = \left( \ell_{\parallel}^r / \ell_{\perp}^r \right)^{1/3} \equiv r^{1/3}, \quad (5.9)$$

defining the anisotropy  $r$ , the ratio of the step lengths. The result offers possibilities for temperature controlled actuation. We have assumed in this example a chain elongated by its nematic order to a prolate shape. If by contrast the chain backbone were flattened by nematic order to an oblate shape, then the above elongation on leaving the nematic state would become instead a contraction.

Does the solid that the chains form allow them to become isotropic in shape on average when they leave the nematic state? One might doubt whether this is possible since the rubber is constrained to preserve volume as it reacts to changing order by deforming. De Gennes (de Gennes, 1969) posed this problem; for ideal chains it is possible — see WT Ex. 5.2 for a discussion. Ideal chains have an isotropic shape distribution after entering the

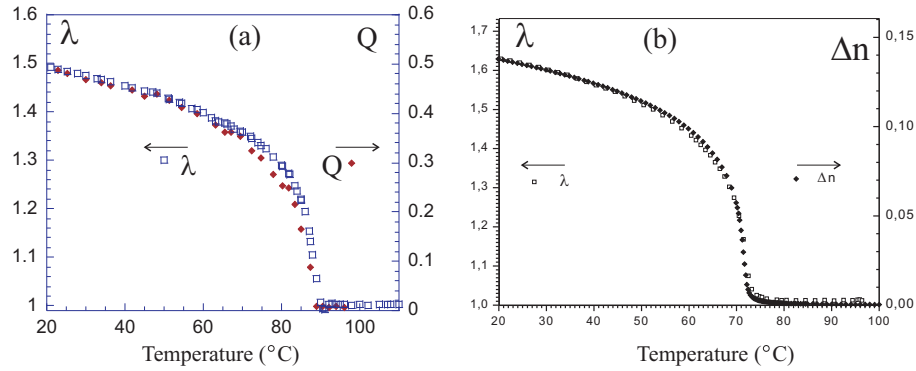


Figure 5.2: (a) Spontaneous distortion,  $\lambda$ , and nematic order parameter,  $Q$  (Clarke *et al.*, 2001), plotted against temperature  $T$ ; (b) the optical birefringence,  $\Delta n$ , against temperature (Finkelmann *et al.*, 2001a).  $Q$  is measured from X-ray scattering, mainly from the aligned pendant side-chain rods. The birefringence is also a direct measure of  $Q$ , expressing the ordering of the most polarisable component of the elastomer, the mesogenic rods.

orientationally isotropic state. There is therefore no memory of the chain shape anisotropy that pertained at the crosslinking of such chains. An important theorem due to Golubovic and Lubensky (Golubovic and Lubensky, 1989), about the attainability of deformation *without energy cost* for nematic elastomers, rests upon being able to obtain such perfectly isotropic states despite topological constraints. We explicitly construct such soft deformations for nematic elastomers.

*Exercise 5.1:* If the formation state was nematic, with an  $\underline{\ell}_0$  characterised by principal values  $\ell_{\parallel}^0$  and  $\ell_{\perp}^0$ , and the current state is also nematic (with  $\underline{\ell}$ ), show that the spontaneous distortion in going from formation to current states would be  $\lambda_m = \left( \frac{\ell_{\parallel}^0}{\ell_{\perp}^0} \frac{\ell_{\perp}}{\ell_{\parallel}} \right)^{1/3}$ . Check that for prolate elastomers there is indeed spontaneous *extension* on further cooling.

The spontaneous distortion  $\lambda_m = (\ell_{\parallel}/\ell_{\perp})^{1/3}$  from the isotropic state turns out to be central to all of nematic rubber elasticity. Indeed, after relaxation has occurred, it is the only input to neo-classical rubber elasticity. For Gaussian chains it is a direct, and indeed the only, measure of chain anisotropy at current conditions. Since chains must be Gaussian to be rubbery, and since Gaussians are entirely determined by their second moments, the ratio of these second moments,  $r = \ell_{\parallel}/\ell_{\perp}$ , is in Gaussian rubber elasticity the *only* measure of chain anisotropy. In discussing the shape anisotropy of nematic polymers, e.g. in Eq. (3.21), we denoted the ratio  $(\ell_{\parallel}/\ell_{\perp})$  by  $r$ . The step length ratio can be thus deduced from thermal expansion measurements,  $r = \lambda_m^3$ , see 5.9. It can be correlated with direct measurements from neutron scattering from labelled chains in nematic elastomers at the same conditions. This is a demanding situation for theory since there are finally no phenomenological free parameters in this theory of ideal nematic rubber elasticity.

Side chain nematic elastomers spontaneously distort, Fig. 5.2. Simple models of nematic polymers (freely jointed for instance) relate  $r$  to  $Q$ . Figure 5.2(b) shows that  $Q$  and  $\lambda_m$  can be superposed, just as such models propose they are closely related. We are interested in new mechanics and don't pursue these molecular models here; see WT§6.2 for that connection. Most anisotropic of all in shape are nematic elastomers composed purely or partly of main chain polymers. Figures 5.3 show spontaneous shape changes of 350% are easily achievable. From  $\lambda_s = 3.5 = r^{1/3}$ , we can conclude that  $R_{\parallel}/R_{\perp} = r^{1/2} = \lambda_s^{3/2}$  must give a ratio of the radii of gyration of 6.5. This large value is consistent with the values that emerge for main chain polymers from neutron scattering, Fig. 3.7(a).

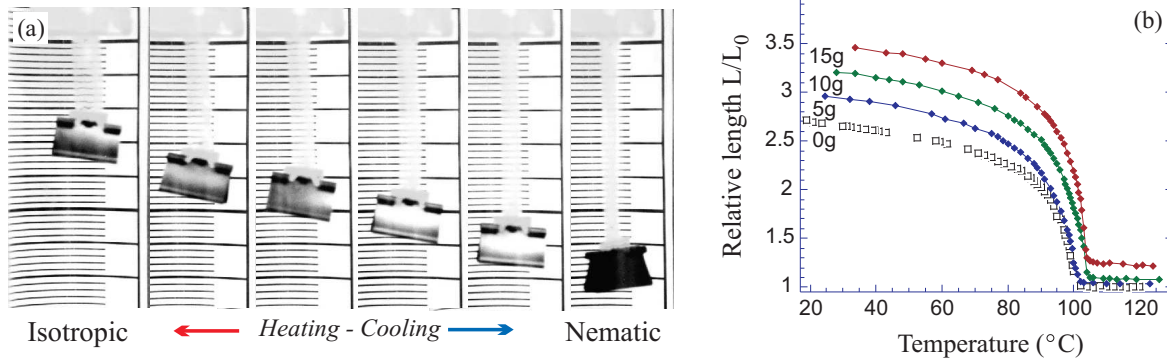


Figure 5.3: Large shape changes ( $\sim 300\%$ ) in a mixed main-chain side-chain nematic monodomain elastomer, with the director aligned along the vertical axis. (a) Contraction with temperature depicted as a series of stills. (b) Quantitative measure of changing natural length; different curves correspond to the sample lifting an increasing weight (Tajbakhsh and Terentjev, 2001), and work is done. Self-assembling thermoplastic nematic elastomers allow drawing of thin fibers with a very high nematic alignment (Ahir *et al.*, 2006), giving spontaneous length changes of 500% and more.

#### Monodomains

To obtain spontaneous distortions one requires a uniform director field, that is a monodomain elastomer. They result from several procedures: One can (Lacey *et al.*, 1998) align a nematic polymer melt with a strong magnetic field and then crosslink it. Two-step crosslinking (Küpfer and Finkelmann, 1991) first lightly crosslinks to form a weak gel which is then uniaxially stretched in either the isotropic phase at  $T > T_{ni}$  or in the nematic phase. The stretched sample is second crosslinked, which fixes the enforced uniaxial alignment. Provided the strain imposed between the two crosslinking stages is great enough, the final elastomer will be a nematic monodomain below a clearing temperature,  $T_{ni}$ . Figure 5.4 (Küpfer and Finkelmann, 1991) shows both poly- and monodomain versions of the same elastomer. The polydomain is opaque because of the strong light scattering by random director textures. The monodomain is optically clear, with its birefringence axis (nematic director  $\mathbf{n}$ ) uniform over the whole sample. This is in contrast to monodomains of ordinary nematic liquid crystals, which are cloudy and turbid, because of director fluctuations. Nematic rubber elasticity is very different from liquid nematics. Chapter 1, page 3, briefly discusses this difference between liquid and solid nematics. In elastomers, the director is anchored to the rubbery matrix and there is an energy penalty even for long wavelength (nearly uniform) director distortions. In ordinary liquid nematics these distortions are of vanishing energy and thus uncontrolled,

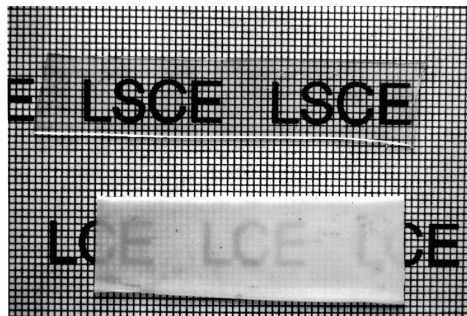
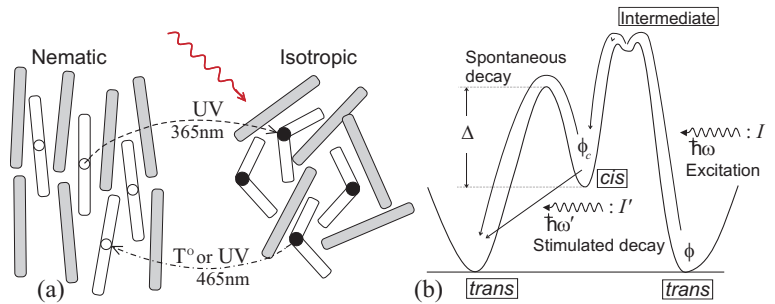


Figure 5.4: A monodomain nematic elastomer prepared by two-step crosslinking and the corresponding polydomain sample, which was not stretched before the second crosslinking stage (Küpfer and Finkelmann, 1991). The free monodomain elastomer is perfectly transparent, while the polydomain sample is opaque unless stretched.

whereupon they strongly scatter light.

### 5.3 NEMATIC PHOTOELASTOMERS

Figure 5.5: (a) The effect of *trans-cis* isomerisation on the nematic order. Bent *cis* rods dilute the straight *trans* rods and reduce the order. For azobenzenes, photon absorption is around 365 nm; reverse *cis-trans* isomerisation is either by thermal relaxation, or stimulated by light at 465 nm. (b) Potential landscape of a dye moiety with *cis* and *trans* states and an intermediate absorption state.



Photoisomerisable rod-like molecules undergo a molecular transition from the *trans* to *cis* state on absorbing an appropriate photon, Fig. 5.5. Azo benzene is the most studied. They strongly bend and no longer contribute to the nematic ordering; in fact, they act as an impurity and destabilise the nematic order. In effect illumination plays a role equivalent to temperature elevation in reducing nematic order. One might then expect UV illumination to induce contractions in nematic elastomers containing such rods analogous to those observed thermally, which is indeed observed (Finkelmann *et al.*, 2001b; Hogan *et al.*, 2002). Figure 5.6(a) shows a sizeable ( $> 20\%$ ) photo contraction and subsequent dark-state thermal recovery, while Fig. 5.6(b) shows the same photoelastomer exhibiting the usual uniaxial thermal contraction, for comparison. In this photoelastomer (Finkelmann *et al.*, 2001b), the rods that bend and thus disrupt the order are the crosslinkers. Irradiation and temperature increase play equivalent roles; the common element between photo and thermal response is the dependence of length on  $Q$ , be it changed by heat or illumination. Figure 5.7 shows stress and order parameter changing together on illuminating a clamped sample. Stress is a measure of the contraction were the sample to be free. Photo-effects can be simply modelled, for instance by mapping photo-response on to a known thermal response. Equally, the dynamics of the response is simply and accurately modelled by describing the dynamics of photo transitions in the population of dye molecules and assuming that the mechanical state follows these changes in dye population. See WT§6.4. With photo-elasticity it is easier to obtain a new element — a spatially varying response since light is necessarily

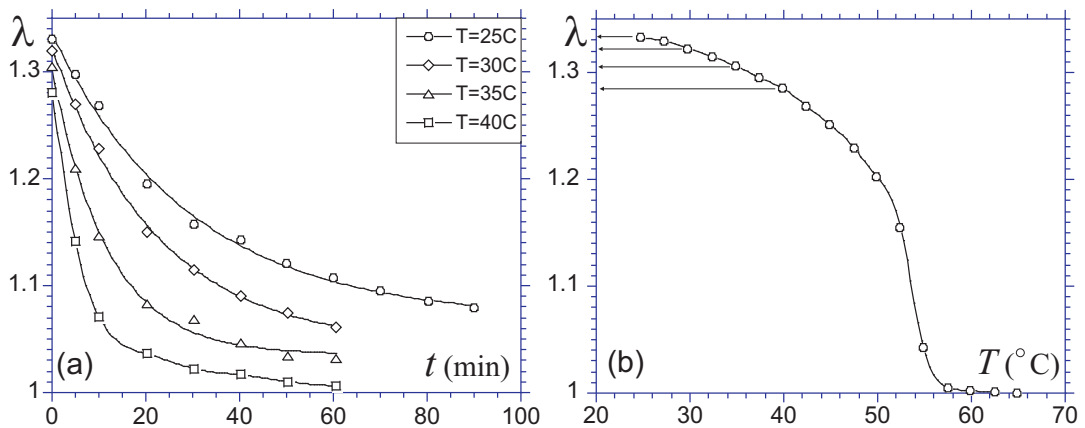


Figure 5.6: (a) The retraction  $\lambda$  against time  $t$  of a nematic photoelastomer, on exposure to UV radiation at various temperatures (Finkelmann *et al.*, 2001b). The reference state,  $\lambda = 1$ , is at high temperatures. (b) The underlying thermal  $\lambda(T)$ : arrows indicate the temperatures of the UV-experiments in (a).

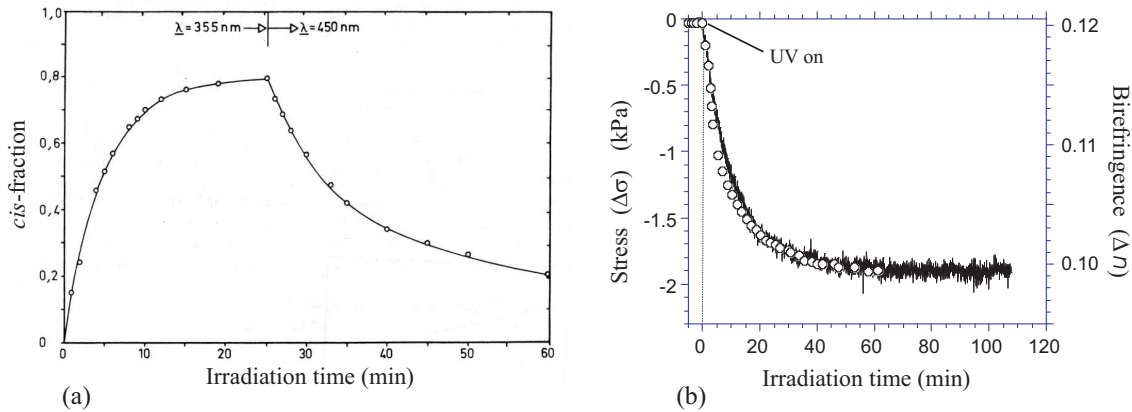


Figure 5.7: (a) The build up and decay of the fraction of *cis* monomers on illumination with appropriate UV light (Eisenbach, 1978). (b) The simultaneous plot of the exerted mechanical stress,  $\Delta\sigma$  – left axis, of a clamped irradiated sample and the material birefringence  $\Delta n$  – right axis, which is a direct measure of order parameter  $Q$  (Cviklinski *et al.*, 2002).

absorbed and hence its intensity varies with depth. There can be significant bending of photoelastomers due to the gradient of contractile strain across the sample thickness, associated with the gradient of light intensity in the sample, Fig. 5.8. It is possible if light is being converted into heat at each dye molecule that some of the response

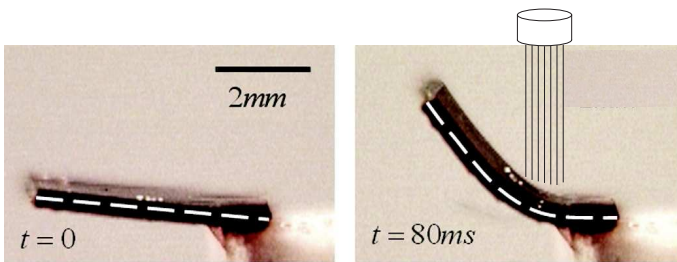


Figure 5.8: Bending of a nematic elastomer doped with a photoisomerising rod-like dye molecules. The full range of motion, on illumination, is achieved in fractions of a second (image: P. Palfy-Muhoray).

is also thermal, but temperature too clearly varies with depth, if diffusion is not too fast, and adds to the bend. How thin the absorption region must be relative to the elastomer thickness to optimise bend is an interesting question (Warner and Mahadevan, 2004). Too thin means that most of the volume is unaffected by the light and resists the contraction of the upper skin and thus also frustrates bend. Too thick, and the elastomer contracts uniformly with depth and there is overall contraction in favour of bend. Theory suggests that the absorption length optimal for bend is about 1/3 of the sample thickness, in the case of exponential decay of intensity.

So far we have considered monodomain elastomers – for instance in Fig. 5.8 the director is along the long dimension of the sample. The contraction in this direction determines the direction of bend. Polydomain nematic polymer glasses have been shown (Yu *et al.*, 2003) to bend too, the direction of bend being in the direction of the light's polarisation. The direction of bend readily changes as the plane of polarisation of the light is rotated. Such photo-actuation in the equivalent elastomer polydomains would offer a greater degree of control than in the monodomain case. The specificity of bend direction to polarisation suggests strongly that such mechanical response is indeed due to photo-response and not simply a contraction in response to optically-generated heat which would be nugatory in a polydomain. The mechanism for contraction of polydomain photo-elastomers is thought to be subtle (Corbett and Warner, 2006). Contraction cannot be monotonic with increasing light intensity since the isotropic sample achieved at very high light intensity must have the same shape as its polydomain parent state that too is effectively isotropic. Contraction by director rotation of the passive domains with director at an angle to the light polarisation to accommodate those domains affected by the light is a possibility – the following Chapter addresses the role of director rotation and it will be a recurrent theme in all of these notes.



Nematic elastomers possess a mobile internal degree of freedom, the rotations of a director. We now investigate their elasticity allowing director rotations and shears. These influences render them unlike any other solid. Director orientation allows a significant reduction in the elastic energy cost of shape change. For example a nematic-mechanical instability occurs (Mitchell *et al.*, 1993) where the director jumps discontinuously to allow a nematic network to accommodate an imposed perpendicular strain. See the cartoon of Fig. 6.1; if the chain distribution (aligned with  $\mathbf{n}$ ) rotates by  $\pi/2$  without change of character, the sample elongates perpendicular and contracts along the original director direction. But there has been no essential distortion of the polymer

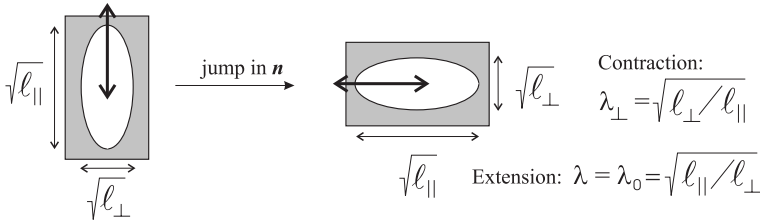


Figure 6.1: Accommodation of chains by the shape changes of the embedding solid. A solid with dimensions in proportion to chain dimensions changes by the given factors when the director jumps by  $90^\circ$ .

network and hence no energy cost associated with this shape change. This transition is reminiscent perhaps of the Freedericks transition in nematic liquid crystals where an electric field is applied perpendicular to the director and induces rotation at a critical voltage, see WT§6.7 for discussion of this mechanical analogue in elastomers. [Since the anchoring will turn out to be in the bulk and not at surfaces, and the field (stress) is applied at the surfaces and not in the bulk, this should perhaps be called an “anti-Freedericks transition”.]

In this chapter we initially illustrate the role of rotation by discussing the relative rotation coupling constant  $D_1$  (briefly mentioned in Chapter 1). The analogous coupling  $D_2$  of symmetric network strains to relative rotations is also discussed. More generally, the director rotates in a continuous fashion. We then address the observed singular nematic rotational response to strains and the apparent liquid-like mechanical response (low storage moduli) observed for some strain geometries. We call this effect ‘soft elasticity’. Experiments confirm it is indeed nematic rotations that make the new elasticity possible.

When softness occurs, its effect can extend up to 50-60% strain and much more than that ( $> 300\%$ ) in highly anisotropic main-chain nematic elastomers. Then, ideally, even an infinitesimal applied stress will induce such large strains before any elastic resistance is felt that the response to a stress is always non-linear – far beyond the validity of linear theory. The full non-linear possibilities of the Trace formula offer the simplest way forward.

## 6.1 DIRECTOR ANCHORING TO THE BULK

Non-classical elasticity arises when the director rotates continuously during distortion; as preliminaries we consider rotation either with no deformation, or with symmetric shears, the latter giving the first pointers to soft elasticity.

### 6.1.1 DIRECTOR ROTATION WITHOUT STRAIN

Let the director rotate relative to the fixed matrix by an angle  $\theta$  about the  $y$  axis. The free energy density with  $\underline{\lambda} = \underline{\delta}$  is then  $F_{el} = \frac{1}{2}\mu \text{Tr}(\underline{\ell}_0 \cdot \underline{\ell}^{-1})$ . Ignoring changes in the magnitude  $Q$ , we have the current step-length tensor  $\underline{\ell} = \underline{U}_\theta^T \cdot \underline{\ell}_0 \cdot \underline{U}_\theta$ , rotated by  $\theta$  from its original configuration before deformation. Recall that  $\underline{\ell} = \ell_\perp \underline{\delta} + (\ell_\parallel - \ell_\perp) \mathbf{nn}$ . If we take out a factor of  $\ell_\perp$ , we have  $\underline{\ell} = \ell_\perp (\underline{\delta} + (r - 1) \mathbf{nn})$  where  $r = \ell_\parallel / \ell_\perp$  measures the anisotropy of the average chain shape spheroid, that is the deviation from a sphere. Equally, the inverse is  $\underline{\ell}^{-1} = \frac{1}{\ell_\perp} \underline{\delta} + (\frac{1}{\ell_\parallel} - \frac{1}{\ell_\perp}) \mathbf{nn}$  and one can take out a factor of  $1/\ell_\perp$  to give  $\frac{1}{\ell_\perp} (\underline{\delta} - (1 - \frac{1}{r}) \mathbf{nn})$  where again there is a negative deviation from spherical  $(1 - \frac{1}{r})$  for the inverse  $\underline{\ell}^{-1}$  of a prolate ( $r > 1$ ) spheroid. Back in the Trace formula the  $\ell_\perp$  and  $1/\ell_\perp$  factors cancel and the whole result is characterised by the single parameter, the ratio  $r$ .

Using such step-length tensors reduced by  $\ell_{\perp}$  factors,

$$F_{\text{el}} = \frac{1}{2}\mu \left( 3 + \left(r + \frac{1}{r} - 2\right) (1 - (\mathbf{n}_o \cdot \mathbf{n})^2) \right) \quad (6.1)$$

$$= \frac{3}{2}\mu + \frac{1}{2}\mu \frac{(r-1)^2}{r} \sin^2 \theta \equiv \frac{3}{2}\mu + \frac{1}{2}D_1 \sin^2 \theta. \quad (6.2)$$

For small  $\theta$  we get, apart from the ground state constant value  $\frac{3}{2}\mu$ ,

$$F_{\text{el}} \sim \frac{1}{2}\mu \frac{(r-1)^2}{r} \theta^2 \equiv \frac{1}{2}D_1 \theta^2. \quad (6.3)$$

The coefficient is identified as  $D_1 = \mu(r-1)^2/r$ , giving the harmonic penalty for small rotations  $\theta$  of the director with respect to the matrix.

The distribution of chain conformations (and hence its principal axis, the director  $\mathbf{n}$ ) is rotated with respect to the background as in Fig. 6.2 and without the shape of the solid changing to accommodate the spheroid as it rotates, there is clearly an elastic penalty to be paid. When the rotation is by  $\theta = \pi$ , in the nematic sense the

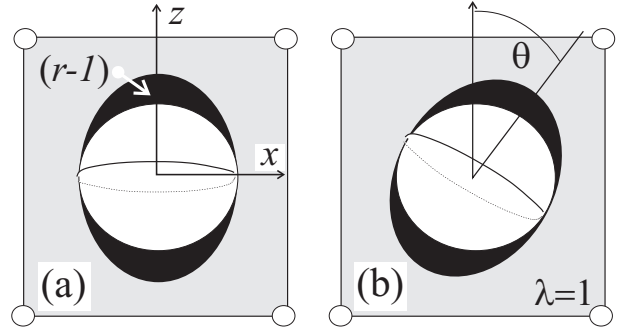


Figure 6.2: Rotation of the anisotropic part  $(r-1)$  of the step-length tensor with respect to the fixed rubber matrix; (a)  $\rightarrow$  (b) has  $\underline{\underline{\ell}}_o \rightarrow \underline{\underline{\ell}}$ . Axis  $\mathbf{y}$  is into the paper; the director is rotated about  $\mathbf{y}$  in the positive sense.

system has recovered its initial state and the energy returns to zero, as we indeed see in  $\frac{1}{2}D_1 \sin^2 \theta$ . We require the full non-linear form of the nematic rubber-elastic energy involving  $\sin^2 \theta$  rather than  $\theta^2$ .

As the rubber becomes isotropic,  $r \rightarrow 1$ , the rotation of anisotropy loses its meaning and  $D_1 \sim (r-1)^2$  vanishes, as it must. Note also that both prolate ( $r > 1$ ) and oblate ( $r < 1$ ) elastomers have a positive cost,  $D_1 > 0$ , of rotating their respective anisotropy directions  $\mathbf{n}$  with respect to the rubber matrix, Fig. 6.2.

### 6.1.2 COUPLING OF ROTATIONS TO PURE SHEAR

Apply a symmetric (rotation-free) shear,  $\underline{\underline{\lambda}}^S$ , to a nematic elastomer in a plane that includes the director  $\mathbf{n}$ . Sect. 4.3.2 and Fig. 4.4 show that such shears are represented by a local combination of extensions and compressions and induce director rotation toward the extension diagonal despite having no rotational component.

To preserve volume, the tensor of pure shear must be written as

$$\underline{\underline{\lambda}}^S = \begin{pmatrix} \sqrt{1 + \lambda_{xz}^2} & \lambda_{xz} \\ \lambda_{xz} & \sqrt{1 + \lambda_{xz}^2} \end{pmatrix},$$

diagonal elements ensuring that  $\text{Det}(\underline{\underline{\lambda}}^S) = 1$ ; nothing is assumed to happen in the third direction, out of the shear plane – see the exercises in Sect. 4.3. We take terms of  $\mathcal{O}(\lambda_{xz}^2)$  in the Trace expression for  $F_{\text{el}}$ , so retain the  $\sqrt{1 + \lambda_{xz}^2}$  contributions. Multiply the tensors  $\underline{\underline{\ell}}_o \cdot \underline{\underline{\lambda}}^S \cdot \underline{\underline{\ell}}^{-1} \cdot \underline{\underline{\lambda}}^S$  and take the trace, for instance by taking diadic forms such as  $\underline{\underline{\lambda}}^S$  is  $\sqrt{1 + \lambda_{xz}^2} (\mathbf{x}\mathbf{x} + \mathbf{z}\mathbf{z}) + \lambda_{xz} (\mathbf{x}\mathbf{z} + \mathbf{z}\mathbf{x})$ , and  $\underline{\underline{\ell}}_o = \ell_{\perp} (\underline{\underline{\delta}} + (r-1)\mathbf{n}_o\mathbf{n}_o)$  etc. One obtains:

$$F_{\text{el}} = \frac{1}{2}\mu \left[ 1 + r + 2(r+1)\lambda_{xz}^2 - \frac{r-1}{r} \left( (r - (r-1)\sin^2 \theta) (1 + \lambda_{xz}^2) + (1 + (r-1)\sin^2 \theta)\lambda_{xz}^2 + 2(1+r)\lambda_{xz}\sqrt{1 + \lambda_{xz}^2} \sin \theta \cos \theta \right) \right].$$

Expanding to take terms at harmonic order, that is  $\lambda_{xz}^2$ ,  $\theta^2$  and  $\lambda_{xz}\theta$  only, one obtains terms in the energy:

$$\frac{1}{2}\mu \frac{(r+1)^2}{r} \lambda_{xz}^2 \equiv 4C_5 \lambda_{xz}^2 \quad \frac{1}{2}\mu \frac{(r-1)^2}{r} \theta^2 \equiv \frac{1}{2}D_1 \theta^2 \quad \mu \left(r - \frac{1}{r}\right) \lambda_{xz} \theta \equiv -D_2 \lambda_{xz} \theta. \quad (6.4)$$

The imposed shear induces the director to rotate with respect to the unrotating background matrix with an energy cost  $D_1$ . There is also a purely elastic penalty,  $4C_5 \lambda_{xz}^2$  to symmetric shears in a plane encompassing  $\mathbf{n}_o$ . The shear modulus, called  $C_5$  in small strain elasticity, does not vanish as  $r \rightarrow 1$ ; in isotropic solids pure shear still costs energy  $4\mu \lambda_{xz}^2$ , as we saw in Ex. 4.2.

The new coupling  $-D_2 \lambda_{xz} \theta$  between the elastic shear and the director rotation demands a new elastic constant (de Gennes, 1982),  $D_2 = \mu(1-r^2)/r$ . As expected,  $D_2 \rightarrow 0$  as isotropy is approached,  $r \rightarrow 1$ , and there is nothing to rotate. On going from prolate ( $r > 1$ ) to oblate ( $r < 1$ ) chains, the sign of  $D_2$  reverses – in contrast to the always positive  $D_1$ . This means that the sign of a rotation  $\theta$  induced by a given  $\lambda_{xz}$  will be the opposite for prolate and oblate elastomers. Prolate elastomers have their director rotated by  $\underline{\lambda}^S$  to the extension diagonal, as is suggested by Fig. 4.4. Oblate elastomers have their director attracted to the contraction diagonal – it allows them to put a long dimension of their shape ellipsoid along the extension direction and thereby lower the elastic energy.

We see another astonishing elastic effect. The term  $-D_2 \lambda_{xz} \theta$  in the last of eqn (6.4) is bilinear which means its overall sign can always be made negative by a suitable choice of the sign of the response  $\theta$  to a given imposed  $\lambda_{xz}$ . For instance for  $D_2 > 0$ , taking both  $\theta$  and  $\lambda_{xz}$  to be positive, or both negative, lowers the energy by  $-D_2 \lambda_{xz} \theta < 0$ . Thus, although the  $C_5 \lambda_{xz}^2$  and  $D_1 \theta^2$  terms are positive, the  $D_2$  term offers a mechanism for reducing these penalties. The next section derives this effect for general geometries and large amplitudes. It is found ideally that the three terms can cancel overall to give no net energy cost to such symmetric shears encompassing the director! We call this soft elasticity and this rotation-dominated response drives most nematic and cholesteric rubber elastic phenomena.

## 6.2 SOFT ELASTICITY

A gas adopts the volume and shape of its container. A liquid adopts its container's shape but has its own volume which then costs energy to change. A solid has both its own volume and shape, both of which cost energy to change. Let us see how nematic elastomers fit into this classical categorisation of the states of matter.

Consider the deformation gradient represented by the expression (Olmsted, 1994)

$$\underline{\lambda} = \underline{\ell}^{1/2} \cdot \underline{W}_\alpha \cdot \underline{\ell}_o^{-1/2}, \quad (6.5)$$

where  $\underline{W}$  is an arbitrary rotation by an angle  $\alpha$ . The current and initial chain step-length tensors  $\underline{\ell}$  and  $\underline{\ell}_o$  specify the current state, characterised by its director  $\mathbf{n}$  and order parameter  $Q$ , and the initial state with  $\mathbf{n}_o$  and  $Q_o$ . Considering the rotations connecting  $\mathbf{n}$  and  $\mathbf{n}_o$  and those associated with  $\underline{W}_\alpha$ , this  $\underline{\lambda}$  represents a large number of potential distortions. If we insert such a deformation into the Trace formula, as well as its transpose  $\underline{\lambda}^T = \underline{\ell}_o^{-1/2} \cdot \underline{W}_\alpha^T \cdot \underline{\ell}^{1/2}$  since the  $\underline{\ell}$  are symmetric, we obtain:

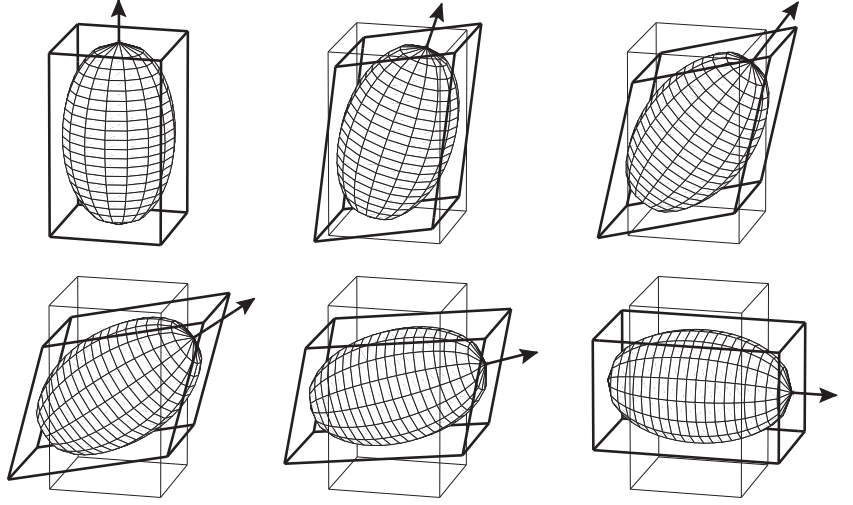
$$F_{el} = \frac{1}{2}\mu \text{Tr} \left( \underline{\ell}_o \cdot \underline{\ell}_o^{-1/2} \cdot \underline{W}_\alpha^T \cdot \underbrace{\underline{\ell}^{1/2} \cdot \underline{\ell}^{-1} \cdot \underline{\ell}^{1/2}}_{\underline{\delta}} \cdot \underline{W}_\alpha \cdot \underline{\ell}_o^{-1/2} \right) \equiv \frac{1}{2}\mu \text{Tr} \left( \underline{\delta} \right) = \frac{3}{2}\mu. \quad (6.6)$$

The middle section  $\underline{\ell}^{1/2} \cdot \underline{\ell}^{-1} \cdot \underline{\ell}^{1/2}$  gives the unit matrix  $\underline{\delta}$ , by definition. The rotation matrix  $\underline{W}$  then meets its transpose to also give unity:  $\underline{W}^T \cdot \underline{W} = \underline{\delta}$ . Likewise disposing of the  $\underline{\ell}_o$  terms, one obtains the final value  $F_{el} = \frac{3}{2}\mu$ . This is identical to the free energy of an undistorted network. The non-trivial set of distortions  $\underline{\lambda}$  of the form eqn (6.5) have not raised the energy of nematic elastomer!

We see in Fig. 6.3 snapshots of soft response as director rotation proceeds. On applying a extension perpendicular to the initial director, rotation of the chain distribution is accommodated by the very elongation we have applied, together with a shear. Two remarkable consequences of nematic elastomer response via rotation follow:

- All the distortions accompanying e.g. an imposed extension  $\lambda_{xx}$  must be in the plane of rotation, that is a transverse contraction  $\lambda_{zz}$  and a shear (only  $\lambda_{xz}$  is evident in the figure, but  $\lambda_{zx}$  would also accommodate

Figure 6.3: Soft deformations of a nematic elastomer, anisotropy  $r = 2.78$ . Director rotations  $\theta$  parametrically generate the distortions: snapshots at  $\theta = 0, \pi/6, \pi/4, \pi/3, 5\pi/12$  and  $\pi/2$ . The embedded distribution of chains, embedded in the deforming solid, can be accommodated without distortion when rotated by  $\theta$ .



the rotation of the distribution). No distortions perpendicular to this plane, that is involving the  $y$ -direction ( $\lambda_{yy}, \lambda_{yx}, \dots$  etc.), are needed. For a classical isotropic elastomer  $\lambda_{yy} = \lambda_{zz} = 1/\sqrt{\lambda_{xx}}$  is demanded by incompressibility, whereas in soft elasticity there is no shrinkage in the  $y$  direction ( $\lambda_{yy} = 1$  and the appropriate Poisson ratio is zero).

- Softness must come to an end when the rotation is complete and the  $z$  dimension has diminished in the proportion  $\lambda_{zz} = \sqrt{\ell_{\perp}/\ell_{\parallel}}$  and the  $x$  dimension extended in the proportion  $\lambda_{xx} = \sqrt{\ell_{\parallel}/\ell_{\perp}}$ . The original sizes  $\sqrt{\ell_{\parallel}}$  and  $\sqrt{\ell_{\perp}}$  have transformed to  $\sqrt{\ell_{\perp}}$  and  $\sqrt{\ell_{\parallel}}$  respectively. Thus softness would cease and director rotation be complete at  $\lambda_{xx} = r^{1/2} \equiv \lambda_m^{3/2}$ . The familiar characteristic deformation  $\lambda_m = (\ell_{\parallel}/\ell_{\perp})^{1/3}$  is the spontaneous extension suffered on cooling to the nematic phase, see Sect. 5.2. This final deformation, we denote by  $\lambda_2 = r^{1/2}$ , is that associated in Fig. 6.1 with change in extent perpendicular to the director, and for the same reason, namely that the long dimension of the chain shape distribution now points there.

Likewise one can imagine starting from one of the oblique shapes in Fig. 6.3, that is the initial director  $\mathbf{n}_0$  (the long axis of the shape ellipsoid) is not at  $90^\circ$  to the imposed strain. Then rotation and thus softness is complete at a smaller  $\lambda_{xx} < \lambda_2$ .

Shape change without energy cost suggests that nematic elastomers fit the classical category of liquid! However their non-soft deformations are rubbery, that is at least notionally solid-like.

### 6.2.1 SOFT MODES OF DEFORMATION

We now explore the general character of soft modes.

*Exercise 6.1:* What distortion does the soft mode  $\underline{\lambda}_{\text{soft}} = \underline{\underline{\ell}}_{\theta}^{1/2} \cdot \underline{\underline{\ell}}_0^{-1/2}$  represent? (The arbitrary rotation matrix  $\underline{\underline{W}}_{\alpha}$  is absent in this example.)

*Solution:* The soft mode is characterised parametrically by the angle  $\theta$  by which  $\underline{\underline{\ell}}_0$  is rotated to  $\underline{\underline{\ell}}_{\theta}$ , that is by which  $\mathbf{n}_0$  is rotated to  $\mathbf{n}$ :

$$\begin{aligned} \underline{\lambda}_{\text{soft}} &= (\underline{\underline{\delta}} + (\sqrt{r} - 1)\mathbf{nn}) \cdot (\underline{\underline{\delta}} + (\frac{1}{\sqrt{r}} - 1)\mathbf{n}_0\mathbf{n}_0) \\ &= \underline{\underline{\delta}} + (1/\sqrt{r} - 1)\mathbf{n}_0\mathbf{n}_0 + (\sqrt{r} - 1)\mathbf{nn} + (\mathbf{n} \cdot \mathbf{n}_0)(2 - \sqrt{r} - 1/\sqrt{r})\mathbf{nn}_0. \end{aligned} \quad (6.7)$$

If  $\mathbf{n}_0$  is along  $\mathbf{z}$  and is rotated by  $\theta$  toward  $\mathbf{x}$ , it becomes  $\mathbf{n} = \mathbf{z} \cos \theta + \mathbf{x} \sin \theta$ . We can write down a particular representation of  $\underline{\underline{\lambda}}_{\text{soft}}$ :

$$\begin{aligned} \underline{\underline{\lambda}}_{\text{soft}} &= (1 - (1 - \frac{1}{\sqrt{r}}) \sin^2 \theta) \mathbf{z}\mathbf{z} + (1 + (\sqrt{r} - 1) \sin^2 \theta) \mathbf{x}\mathbf{x} + \mathbf{y}\mathbf{y} \\ &\quad + (1 - \frac{1}{\sqrt{r}}) \sin \theta \cos \theta \mathbf{x}\mathbf{z} + (\sqrt{r} - 1) \sin \theta \cos \theta \mathbf{z}\mathbf{x} \\ &\equiv \begin{pmatrix} 1 + (\sqrt{r} - 1) \sin^2 \theta & 0 & (1 - 1/\sqrt{r}) \sin \theta \cos \theta \\ 0 & 1 & 0 \\ (\sqrt{r} - 1) \sin \theta \cos \theta & 0 & 1 - (1 - 1/\sqrt{r}) \sin^2 \theta \end{pmatrix} \end{aligned} \quad (6.8)$$

which is illustrated in Fig. 6.3.

The distortions are parameterised by the director rotation,  $\theta$ , which ranges between 0 and  $\pi/2$ . The  $x$ -extension is  $\lambda_{xx} = 1 + (\sqrt{r} - 1) \sin^2 \theta \geq 1$  and the perpendicular contraction is  $\lambda_{zz} = 1 - (1 - 1/\sqrt{r}) \sin^2 \theta \leq 1$ . Both are proportional to  $\sin^2 \theta$ . Thus the infinitesimal diagonal strain components  $\epsilon_{zz} = \lambda_{zz} - 1$  and  $\epsilon_{xx} = \lambda_{xx} - 1$ , at small rotations  $\theta$ , are proportional to  $\theta^2$ . By contrast the shears  $\lambda_{xz}$  and  $\lambda_{zx}$  are proportional to  $\sin \theta \cos \theta$  and hence the infinitesimal strains  $\epsilon_{xz}$  and  $\epsilon_{zx}$  are linear in small rotation angle  $\theta$  – a lower order than  $\epsilon_{xx}$  and  $\epsilon_{zz}$ . The soft mode, eqn (6.7), starts at no strain,  $\underline{\underline{\lambda}} = \underline{\underline{\delta}}$ , and as the director rotates from  $\theta = 0$  all the way to  $\pi/2$ , the soft regime eventually ends at  $\underline{\underline{\lambda}} = \text{Diag}(\sqrt{r}, 1, 1/\sqrt{r})$ , that is a  $x$ -extension  $\lambda_{xx} = \sqrt{r}$ , a  $z$ -transverse contraction  $\lambda_{zz} = 1/\sqrt{r}$  and no remaining shear.

Director rotation is taken up by shape change so that there is no entropically expensive deformation of the chain distribution as when a conventional elastomer deforms. The anisotropy of step-length tensor  $r = \ell_{\parallel}/\ell_{\perp}$  characterises the ratio of the mean square size along the director to that perpendicular to the director. The square root of this ratio,  $\sqrt{r}$ , gives the characteristic ratio of average (r.m.s.) dimensions of chains in the network. During a soft deformation, the solid must change shape such that the rotating ellipsoid  $\underline{\underline{\ell}}^{1/2}$ , characterising the physical dimensions of the distribution of chains<sup>1</sup>, is accommodated without distortion, Fig. 6.3.

In the isotropic limit ( $r = 1$ ) both chain step-length tensors,  $\underline{\underline{\ell}}_0$  and  $\underline{\underline{\ell}}_{\theta}$ , reduce to a unit matrix and the general soft deformation matrix (6.5) reduces to  $\underline{\underline{W}}_{\alpha}$ , an arbitrary body rotation. Certainly, we would expect no elastic energy rise when we turn and rotate the sample as a whole! The soft modes become real, non-trivial deformations when the material becomes a nematic elastomer.

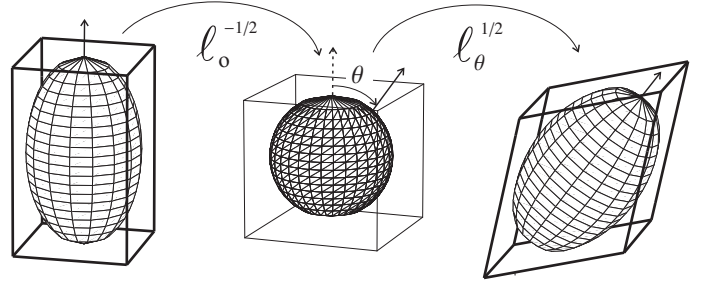
The nematic order, so crucial for the availability of internal orientational microstructure leading to soft deformations, does not change through such a distortion. At the outset the value  $Q$  minimised the nematic component of the free energy. Since the elastic component of the energy does not rise, then the initial optimal magnitude of  $Q$  remains optimal during the soft deformation. Unchanging  $Q$  implies an unchanging distribution of chain shapes, that is  $\underline{\underline{\ell}}$  is strictly a rotated form of  $\underline{\underline{\ell}}_0$ . Thus  $\underline{\underline{\ell}}_{\theta} = \underline{\underline{M}}^T \cdot \underline{\underline{\ell}}_0 \cdot \underline{\underline{M}}$  where  $\underline{\underline{M}}(\theta)$  is a rotation, represented by an orthogonal matrix with  $\text{Det}(\underline{\underline{M}}) = 1$ . Note that one cannot simply take an orthogonal matrix,  $\underline{\underline{M}}^T = \underline{\underline{M}}^{-1}$ , without  $\text{Det}(\underline{\underline{M}}) = 1$ . Even though such matrices  $\underline{\underline{M}}$  would also generate a volume-preserving deformation  $\underline{\underline{\lambda}}$  yielding  $F_{\text{el}} = \frac{3}{2}\mu$ , they would at the same time change the shape of  $\underline{\underline{\ell}}$  from that of  $\underline{\underline{\ell}}_0$  which already has the optimal aspect ratio. The consequent change in  $Q$  during such a deformation means the thermodynamic nematic part of the free energy,  $F_{\text{nem}}$ , would rise and deformation could not be soft.

Thus elastomers can be soft through a changing macroscopic shape of the elastic body by rotating the distribution of chains at constant average shape of network chains. This implies that chain entropy, normally at the root of rubber elastic response, does not drop. Equally there is no change of the nematic order; it has merely been rotated in alignment direction. The energy change is zero. The overall change in free energy density,  $\Delta F = \Delta U - T\Delta S$ , is thus also zero ( $U$  and  $S$  being the internal energy and entropy).

Alternatively, the soft deformations of the cartoon Fig. 6.3,  $\underline{\underline{\lambda}}_{\text{soft}} = \underline{\underline{\ell}}_{\theta}^{1/2} \cdot \underline{\underline{\ell}}_0^{-1/2}$ , can be viewed as two multiplicative deformations (since they may correspond to large strains); Fig. 6.4 illustrates their successive action. The first,  $\underline{\underline{\ell}}_0^{-1/2}$ , takes the original solid to a cube and the anisotropic chain distribution to the isotropic spherical

<sup>1</sup>The ellipsoid is described by the condition  $\mathbf{R} \cdot \underline{\underline{\ell}}^{-1} \cdot \mathbf{R} = 1$ , or in the initial principal frame,  $x^2 + y^2 + z^2/r = 1$ , that is, the  $xz$ -sectional ellipse has semi-major axes of 1 and  $\sqrt{r}$ .

Figure 6.4: Soft deformations  $\underline{\underline{\ell}}_\theta^{1/2} \cdot \underline{\underline{\ell}}_0^{-1/2}$  of a nematic elastomer can be broken down into two component deformations that reduce the initial anisotropic state to isotropy and then recreates it again at angle  $\theta$  with its associated deformation.



one. The intermediate distribution, being isotropic, can be rotated through an angle  $\theta$  without energy cost or physical effect. The second,  $\underline{\underline{\ell}}_\theta^{1/2}$ , then restores the current anisotropic distribution, but at the new angle  $\theta$ . The cube suffers a non-trivial distortion to the new shape which excribes the rotated ellipsoid.

In fact  $\underline{\underline{\ell}}_\theta^{1/2}$  is related to the spontaneous elongation on cooling,  $\underline{\underline{\lambda}}_m$ , by a simple constant. Likewise  $\underline{\underline{\ell}}_0^{-1/2}$  is related to the inverse spontaneous deformation on heating:

$$\begin{aligned}\underline{\underline{\ell}}_\theta^{1/2} &= \begin{pmatrix} \sqrt{r} & 0 & 0 \\ 0 & 1 & 0 \\ 0 & 0 & 1 \end{pmatrix} \equiv r^{1/6} \begin{pmatrix} r^{1/3} & 0 & 0 \\ 0 & r^{-1/6} & 0 \\ 0 & 0 & r^{-1/6} \end{pmatrix} \equiv r^{1/6} \underline{\underline{\lambda}}_m \\ \underline{\underline{\ell}}_0^{-1/2} &= \begin{pmatrix} 1/\sqrt{r} & 0 & 0 \\ 0 & 1 & 0 \\ 0 & 0 & 1 \end{pmatrix} \equiv r^{-1/6} \begin{pmatrix} r^{-1/3} & 0 & 0 \\ 0 & r^{1/6} & 0 \\ 0 & 0 & r^{1/6} \end{pmatrix} \equiv r^{-1/6} \underline{\underline{\lambda}}_m^{-1}.\end{aligned}\quad (6.9)$$

The two tensors are expressed in their principal frames, the first being rotated by  $\theta$  with respect to the second. The prefactors cancel when we take their product and we obtain:

$$\underline{\underline{\ell}}_\theta^{1/2} \cdot \underline{\underline{\ell}}_0^{-1/2} = \underline{\underline{\lambda}}_m(\theta) \cdot \underline{\underline{\lambda}}_m^{-1} = \underline{\underline{U}}^T(\theta) \cdot \underline{\underline{\lambda}}_m \cdot \underline{\underline{U}}(\theta) \cdot \underline{\underline{\lambda}}_m^{-1}.\quad (6.10)$$

The notation  $\underline{\underline{\lambda}}_m(\theta)$  means we take the spontaneous distortion along a director that has been rotated by  $\theta$ . The final form of eqn (6.10) explicitly displays the rotation matrices. The existence of a (virtual) intermediate isotropic state, as in Fig. 6.4, is the basis of symmetry arguments that prove the soft response associated with Fig. 6.3 is universal. This state is often taken as the reference state, although it is far from the physical reference state associated with experiment.

### 6.2.2 SYMMETRY ARGUMENTS FOR SOFT RESPONSE

Golubovic and Lubensky (1989) first demonstrated that some solids must, on general symmetry grounds, possess soft elastic modes. Imagine an initially isotropic elastic body, where all material points are labelled by a vector  $\mathbf{X}$  in the laboratory frame. The reference state possesses full rotational symmetry, that is, the state described by the set of points  $\mathbf{X}$  is completely equivalent to the set  $\underline{\underline{U}}_\phi \cdot \mathbf{X}$  which have been rotated by  $\phi$  (with  $\underline{\underline{U}}_\phi$  a rotation matrix). On transition into a uniform single-domain nematic these material points undergo a spontaneous deformation, see Sect. 5.2. They are now  $\mathbf{R} = \underline{\underline{\lambda}}_m \cdot \underline{\underline{U}}_\phi \cdot \mathbf{X}$ . Another nematic state may be obtained from the isotropic reference state without such a rotation,  $\mathbf{R}^0 = \underline{\underline{\lambda}}_m \cdot \mathbf{X}$ . Inverting this we find an expression for the reference point,  $\mathbf{X} = \underline{\underline{\lambda}}_m^{-1} \cdot \mathbf{R}^0$ , which we insert in the expression for  $\mathbf{R}$ . The latter now gives a matrix relation between the states,  $\mathbf{R}$  and  $\mathbf{R}^0$ , that is:  $\mathbf{R} = \underline{\underline{\lambda}}_m \cdot \underline{\underline{U}}_\phi \cdot \underline{\underline{\lambda}}_m^{-1} \cdot \mathbf{R}^0$ . The deformation gradient tensor that connects these two states is therefore

$$\underline{\underline{\lambda}} = \partial \mathbf{R} / \partial \mathbf{R}^0 = \underline{\underline{\lambda}}_m \cdot \underline{\underline{U}}_\phi \cdot \underline{\underline{\lambda}}_m^{-1}.\quad (6.11)$$

When the intermediate state is truly isotropic, then the two nematic states must be physically equivalent and the deformation  $\underline{\underline{\lambda}}$  between them costs no energy. Figure 6.5 shows the routes to these equivalent deformations and a picture of  $\underline{\underline{\lambda}}$  (Warner, 1999; Lubensky *et al.*, 2002). Equations (6.11) and (6.10) are of the same form. Thus this symmetry argument yields the detailed soft modes as before and explains thereby their universality.

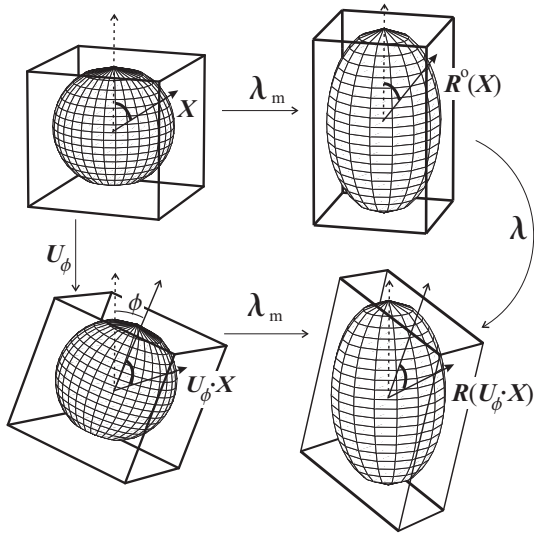


Figure 6.5: The paths to two nematic states differ only by a body rotation,  $\phi$ , of the isotropic reference state from which a spontaneous distortion has occurred. The nematic states, although equivalent in energy, differ in shape (see the cartoon Fig. 6.3) and are connected by a soft  $\underline{\underline{\lambda}}$  parameterised by rotations of the isotropic reference state.

### 6.2.3 FORMS OF THE FREE ENERGY ALLOWING SOFTNESS

Symmetry arguments show softness exists in solids with an internal degree of freedom and where an isotropic reference state is accessible. The underlying reason is the invariance of the free energy under both rotations  $\underline{\underline{V}}$  of the reference state  $\mathbf{R}_0$  and  $\underline{\underline{U}}$  of the target state  $\mathbf{R}$ . Recall, eqn (4.3), that the deformation tensor transforms like:

$$\underline{\underline{\lambda}}' = \underline{\underline{U}} \cdot \underline{\underline{\lambda}} \cdot \underline{\underline{V}}^T.$$

The first index, see eqn (4.2), of  $\underline{\underline{\lambda}}$  refers to target space  $\mathbf{R}$ s which transform by  $\underline{\underline{U}}$  and the second index refers to reference space  $\mathbf{R}_0$ s which transform by  $\underline{\underline{V}}$ . There are thus *two* sets of symmetry operations, referring to the reference and final states independently. One route to elasticity theory we saw in Sect. 4.1 was to construct the Cauchy Green tensors  $\underline{\underline{C}} = \underline{\underline{\lambda}}^T \cdot \underline{\underline{\lambda}}$  and  $\underline{\underline{B}} = \underline{\underline{\lambda}} \cdot \underline{\underline{\lambda}}^T$  which transform as second rank tensors under reference state rotations as  $\underline{\underline{C}}' = \underline{\underline{V}} \cdot \underline{\underline{C}} \cdot \underline{\underline{V}}^T$  or under target state rotations as  $\underline{\underline{B}}' = \underline{\underline{U}} \cdot \underline{\underline{B}} \cdot \underline{\underline{U}}^T$ . They can be used to form suitable, scalar expressions for the energy. In nematic elastomers there are now other tensors to draw upon, namely  $\underline{\underline{\ell}}^o$  and  $\underline{\underline{\ell}}$  with the character  $\{\mathbf{R}_0\mathbf{R}_0\}$  and  $\{\mathbf{R}\mathbf{R}\}$ .

Invariant expressions now include  $\text{Tr}(\underline{\underline{\lambda}}^T \cdot \underline{\underline{\lambda}} \cdot \underline{\underline{\ell}}_o)$  and  $\text{Tr}(\underline{\underline{\lambda}} \cdot \underline{\underline{\lambda}}^T \cdot \underline{\underline{\ell}})$ . The first non-trivial expression that records the structure of both initial and current states is our fundamental Trace formula,  $\text{Tr}(\underline{\underline{\ell}}_o \cdot \underline{\underline{\lambda}}^T \cdot \underline{\underline{\ell}}^{-1} \cdot \underline{\underline{\lambda}})$ . More complex possibilities exist that have the correct invariance properties under  $\underline{\underline{U}}$  and  $\underline{\underline{V}}$ , for instance the trace of a product  $\text{Tr}[(\underline{\underline{\lambda}} \cdot \underline{\underline{\ell}}_o \cdot \underline{\underline{\lambda}}^T)^m \cdot (\underline{\underline{\ell}}^{-1})^n \dots]$  and other scalar functions constructed from combinations of powers of the tensor expressions  $\underline{\underline{\lambda}} \cdot \underline{\underline{\ell}}_o \cdot \underline{\underline{\lambda}}^T$  and  $\underline{\underline{\lambda}}^T \cdot \underline{\underline{\ell}} \cdot \underline{\underline{\lambda}}$ . These all have the capacity to possess soft elasticity. Such more complicated forms arise when one considers deviations from the concept of an ideal Gaussian network – for example the effect of finite chain extensibility, that is where chains are sufficiently short and extensions sufficiently large that they no longer behave as Gaussians. Other even more more complex forms arise when considering the effect of entanglements in nematic elastomers, see WT§6.8. The above symmetry considerations show these elastomers must remain soft despite these new constraints. Indeed the precise form of the soft response, eqn (6.19)-(6.22), emerges independently of the form of the free energy adopted, see Sect. 6.2.2.

### 6.2.4 PRINCIPAL SYMMETRIC STRAINS AND BODY ROTATIONS

The soft deformations in Fig. 6.3 and eqns (6.7) and (6.8) of the body are in general non-symmetric;  $\underline{\underline{\lambda}}_{\text{soft}}$  is neither simple nor pure, but a mixture of pure shear times rotation. The element of body rotation, irrelevant for conventional solids, is vital for nematic elastomers. Results (4.26) and (4.27) of exercise 4.4 break the soft modes down into a symmetric shear  $\underline{\underline{\lambda}}^S$  followed by a body rotation  $\underline{\underline{U}}_\Omega$  through an angle  $\Omega$  about the axis

perpendicular to the shear. Thus,  $\underline{\lambda}_{\text{soft}} = \underline{U}_{\Omega} \cdot \underline{\lambda}^S$ . Parameterising the soft modes by the director rotation  $\theta$ , the body rotation is through  $\Omega = \tan^{-1} \left[ \frac{(\sqrt{r}-1)^2 \tan \theta}{2\sqrt{r} + (r+1) \tan^2 \theta} \right]$ . For small director rotation, body rotation is also small,  $\Omega \sim \theta \frac{(\sqrt{r}-1)^2}{2\sqrt{r}}$ . For large rotations,  $\theta \rightarrow \pi/2$ , the rotation  $\Omega$  vanishes as we have seen in Fig. 6.3. Inbetween, body rotation helps to accommodate the rotating chain distribution. The corresponding symmetric shear strain, the off-diagonal component of  $\underline{\lambda}^S$ , is

$$\lambda_{xz} \equiv \lambda^S = \frac{\sin \theta \cos \theta (r-1)}{\sqrt{r} (4 + \sin^2 \theta (r-1)^2 / r)^{1/2}} \sim \theta \frac{(r-1)}{2\sqrt{r}} \text{ for small distortions .}$$

Symmetric shear also vanishes at the end of the soft regime, Fig. 6.3 ( $\theta = \pi/2$ ), where no further accommodation of the shape tensor by body rotation and shear is possible.

More general soft deformations have the arbitrary rotation,  $\underline{W}_{\alpha}$ , embedded in the form of soft deformation eqn (6.5). Its effect is trivial if its rotation axis is along  $\mathbf{y}$  or  $\mathbf{n}_o$ . If the axis vector has components not along either of these directions, then it gives shears involving the  $y$  direction.

### 6.3 OPTIMAL DEFORMATIONS

Having seen soft deformations generally and a little of their shear and rotational character, we now look at two methods for calculating their form in more practical situations. The first is more general and offers insight into how the director angle follows the best direction set by imposed and relaxational strains. The second is a concrete example of how the best deformations are found for the practically important geometry of extension imposed perpendicular to the director.

#### 6.3.1 A PRACTICAL METHOD OF CALCULATING DEFORMATIONS

In some situations the nematic elastic free energy is straightforward to calculate and to optimise. For instance, the Freedericks transition of Fig. 7.1 has only a single (simple shear) distortion and a director rotation. Others we have seen to be more complex. Section 6.3.2 calculates soft modes by a direct attack in a practical geometry, but seems quite involved since one minimises over a large number of components of  $\underline{\lambda}$  and the director rotation. A more elegant way is to describe the distortion  $\underline{\lambda}$  parametrically by the associated director rotation, the method of Olmsted in Sect. 6.2, but then one does not have control over aspects of the distortion that may be constrained. A more straightforward way exists to evaluate the optimal free energy and this offers insight as to how the final director rotation is achieved. Moreover, for planar distortions (with, in general, relaxation in the third direction) finding the free energy only involves solving a quadratic equation.

Consider the Trace free energy density, with its tensor components conveniently cyclically permuted:

$$F = \frac{1}{2} \mu \text{ Tr} \left( \underline{\lambda} \cdot \underline{\ell}_o \cdot \underline{\lambda}^T \cdot \underline{\ell}^{-1} \right) . \quad (6.12)$$

The first three tensors can be combined to form a tensor,  $\underline{\mathcal{S}}$ , that is symmetric by construction and thus also has a frame in which it is diagonal:

$$\underline{\mathcal{S}} = \underline{\lambda} \cdot \underline{\ell}_o \cdot \underline{\lambda}^T \rightarrow \begin{pmatrix} s_1 & 0 & 0 \\ 0 & s_2 & 0 \\ 0 & 0 & s_3 \end{pmatrix} , \quad (6.13)$$

the latter form displaying the three eigenvalues  $s_i$  of  $\underline{\mathcal{S}}$  which have been ordered so that  $s_1 \geq s_2 \geq s_3$ . The principal frame of  $\underline{\mathcal{S}}$  is in general rotated a reference frame aligned with the nematic order in which  $\underline{\ell}_o$  is then diagonal and in which we conveniently define  $\underline{\lambda}$ . We now have to multiply  $\underline{\mathcal{S}}$  by  $\underline{\ell}^{-1}$  and take the trace in order to find the free energy. The trace will be minimised by aligning  $\underline{\ell}^{-1} = \begin{pmatrix} 1/r & 0 & 0 \\ 0 & 1 & 0 \\ 0 & 0 & 1 \end{pmatrix}$  (as it appears in its own principal frame) with the principal frame of  $\underline{\mathcal{S}}$  such that the smallest element of  $\underline{\ell}^{-1}$  (that is  $1/r$ ) meets the largest element of  $\underline{\mathcal{S}}$

(i.e.  $s_1$ ). This is equivalent to demanding that the final director  $\mathbf{n}$  (which describes the orientation of  $\underline{\underline{\ell}}$  and hence  $\underline{\underline{\ell}}^{-1}$ ) is aligned with the eigenvector of  $\underline{\underline{\mathbf{S}}}$  corresponding to  $s_1$ . The free energy is

$$F = \frac{1}{2}\mu (s_1/r + s_2 + s_3). \quad (6.14)$$

The difference between this approach and others is that  $\mathbf{n}$  simply follows the direction established by  $\underline{\underline{\mathbf{S}}}$ , that is by the distortions combined with the original director. It is a slave to these and is not minimised over. Now  $F$  can be minimised over the elements of  $\underline{\underline{\lambda}}$  that were not imposed or clamped, but which are allowed to relax. Only after this should the eigenvectors of  $\underline{\underline{\mathbf{S}}}$  be explicitly determined in order to determine  $\mathbf{n}$ . This is best illustrated by an example:

*Exercise 6.2:* Find the relaxations and director rotation associated with an extension  $\lambda$  imposed perpendicular to the initial director. Only shears consistent with displacements along the extension direction are allowed.

*Solution:* As before, take the general strain and initial (reduced) step-length tensors:

$$\underline{\underline{\lambda}} = \begin{pmatrix} \lambda & 0 & \lambda_{xz} \\ 0 & 1/(\lambda\lambda_{zz}) & 0 \\ 0 & 0 & \lambda_{zz} \end{pmatrix}; \quad \underline{\underline{\ell}}_0 = \begin{pmatrix} 1 & 0 & 0 \\ 0 & 1 & 0 \\ 0 & 0 & r \end{pmatrix}.$$

From these we construct  $\underline{\underline{\mathbf{S}}}$ :

$$\begin{aligned} \underline{\underline{\mathbf{S}}} &= \begin{pmatrix} \lambda & 0 & \lambda_{xz} \\ 0 & 1/(\lambda\lambda_{zz}) & 0 \\ 0 & 0 & \lambda_{zz} \end{pmatrix} \begin{pmatrix} 1 & 0 & 0 \\ 0 & 1 & 0 \\ 0 & 0 & r \end{pmatrix} \begin{pmatrix} \lambda & 0 & 0 \\ 0 & 1/(\lambda\lambda_{zz}) & 0 \\ \lambda_{xz} & 0 & \lambda_{zz} \end{pmatrix} \\ &= \begin{pmatrix} \lambda^2 + r\lambda_{xz}^2 & 0 & r\lambda_{xz}\lambda_{zz} \\ 0 & 1/(\lambda^2\lambda_{zz}^2) & 0 \\ r\lambda_{xz}\lambda_{zz} & 0 & r\lambda_{zz}^2 \end{pmatrix} \end{aligned}$$

and the determinant condition for its eigenvalues:

$$\text{Det}(\underline{\underline{\mathbf{S}}} - s\underline{\underline{\delta}}) = 0 = (1/(\lambda^2\lambda_{zz}^2) - s) [s^2 - (\lambda^2 + r\lambda_{xz}^2 + r\lambda_{zz}^2)s + r\lambda^2\lambda_{zz}^2]$$

where we have gathered terms in and simplified the final factor somewhat. Because shears were limited to the  $xz$ -plane, the matrix is blocked and one eigenvalue emerges trivially and the other two can only come from the roots of a quadratic. They are

$$s_{1,2} = \frac{1}{2} \left[ \lambda^2 + r\lambda_{xz}^2 + r\lambda_{zz}^2 \pm \sqrt{(\lambda^2 + r\lambda_{xz}^2 + r\lambda_{zz}^2)^2 - 4r\lambda^2\lambda_{zz}^2} \right] \quad \text{and} \quad s_3 = 1/(\lambda\lambda_{zz})^2 \quad (6.15)$$

whence the free energy density is:

$$F = \frac{1}{2}\mu \left[ \frac{r+1}{r} (\lambda^2 + r\lambda_{xz}^2 + r\lambda_{zz}^2) - \frac{r-1}{r} \sqrt{\dots} \right] + \frac{1}{\lambda^2\lambda_{zz}^2}.$$

This is most easily first minimised with respect to  $\lambda_{xz}^2$ , yielding:

$$(r+1) - (r-1) \frac{\lambda^2 + r\lambda_{xz}^2 + r\lambda_{zz}^2}{\sqrt{\dots}} = 0$$

which on squaring and simplifying gives:

$$\lambda^2 + r\lambda_{xz}^2 + r\lambda_{zz}^2 = (r+1)\lambda_{zz}\lambda \quad (6.16)$$

the left hand side of which pervades  $F$  and can clearly be used to advantage. Returning this combination to  $F$  then gives  $F = \frac{1}{2}\mu [2\lambda_{zz}\lambda + 1/(\lambda^2\lambda_{zz}^2)]$ . The optimal  $\lambda_{zz}$  is then trivially  $\lambda_{zz} = 1/\lambda$ . Returning this  $\lambda_{zz}$  to eqn (6.16) for  $\lambda_{xz}$  gives  $\lambda_{xz}^2 = \frac{1}{r\lambda^2}(\lambda^2 - 1)(r - \lambda^2)$ ; compare with eqn (6.20) below for the shear generated during the soft response to simple stretch imposed perpendicular to the initial director. The matrix  $\underline{\underline{S}}$  is now:

$$\underline{\underline{S}} = \begin{pmatrix} \lambda^2 + r\lambda_{xz}^2 & 0 & r\lambda_{xz}/\lambda \\ 0 & 1 & 0 \\ r\lambda_{xz}/\lambda & 0 & r/\lambda^2 \end{pmatrix}$$

and its eigenvalues are:

$$s_{1,2} = \frac{1}{2} \left[ (r+1) \pm \sqrt{(r-1)^2} \right] = r \text{ or } 1 \quad \text{and } s_3 = 1$$

on returning the left hand side of eqn (6.16) and  $\lambda_{zz} = 1/\lambda$  to eqn (6.15).

The eigenvectors  $\mathbf{e}_i$  can now be trivially found. That corresponding to  $s_1 = r$ , and thus to  $\mathbf{n}$ , is  $(x, 0, z)$  where  $x$  and  $z$  are related by  $z(r/\lambda^2 - s_1) + xr\lambda_{xz}/\lambda = 0$  using the bottom line of the matrix equation  $\underline{\underline{S}} \cdot \mathbf{e}_1 = s_1 \mathbf{e}_1$ . Each of the three equations in  $\underline{\underline{S}} \cdot \mathbf{e} = s \mathbf{e}$  is equivalent when  $s$  is set equal to a particular  $s_i$ . The simplest can be chosen to find the connection between the  $x$  and  $z$  components of the associated  $\mathbf{e}_i$ .

Since  $x/z = \tan \theta = (\lambda - \frac{1}{\lambda})/\lambda_{xz}$ , it is straightforward to find eqn (6.19) for the director rotation angle  $\theta$ , that is

$$\sin^2 \theta = \frac{r}{r-1} \frac{\lambda^2 - 1}{\lambda^2}.$$

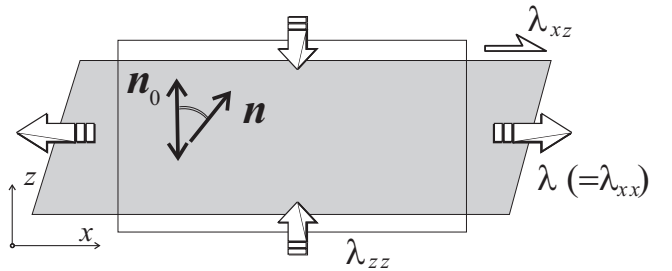
This method offers the advantage that  $\theta$ , the director rotation angle, is not a variable to be optimised over. It emerges naturally as the director rotates towards the direction of biggest extension.

### 6.3.2 STRETCHING PERPENDICULAR TO THE DIRECTOR

Although it has been easy to construct soft deformations parametrically through  $\theta$ , it is not easy this way to visualise strains imposed in practical experiments. Usually one component is directly imposed by clamping and stretching the sample. The other strains, plus  $\mathbf{n}$ , relax to their optimal values.

To the long rectangular strip of nematic elastomer of Fig. 6.6 we impose an  $x$ -extension  $\lambda_{xx} = \lambda$  perpendicular to the initial director,  $\mathbf{n}_0$ , which is along  $z$  (Verwey *et al.*, 1996). The cartoon of Fig. 6.3 suggests that soft

Figure 6.6: The extension of a long strip of nematic elastomer perpendicular to its initial director. One shear component,  $\lambda_{xz}$ , develops. The other,  $\lambda_{zx}$ , is suppressed by the counter torque that would develop from such a distortion in the field of a force applied along the  $x$  axis.



deformation requires rotation of  $\mathbf{n}_0$  toward  $x$  and that shears  $\lambda_{zx}$  and  $\lambda_{xz}$  accompany the imposed  $\lambda$ . We limit ourselves to  $\lambda_{xz}$  which derives from  $x$ -displacements,  $u_x$ . Shear  $\lambda_{zx}$  is suppressed by the turning moment,  $f_x u_z$ , generated by any  $z$ -displacement,  $u_z$ , in the presence of an  $x$  force,  $f_x$  (should it arise on extension in the  $x$ -direction). Equally, the large length to width ratio of the strip in Fig. 6.6 allows us to defer to Chapter 7 the effect on shear of the clamps gripping the sample when imposing  $\lambda$ . Assume there are no impediments to any simple shear  $\lambda_{xz}$  necessary for optimising deformations. The vanishing of the shear  $\lambda_{zx}$  (and also the shears involving  $yx, yz$  etc.) means the incompressibility,  $\text{Det}(\underline{\underline{\lambda}}) = 1$ , is ensured by taking  $\lambda_{yy} = 1/(\lambda\lambda_{zz})$ . The reduced inverse

step-length tensor, on director rotation about  $\mathbf{y}$  of  $\theta$  from the  $z$  axis, is  $\underline{\underline{\ell}}^{-1} = \begin{pmatrix} 1+(\frac{1}{r}-1)\sin^2\theta & (\frac{1}{r}-1)\sin\theta\cos\theta \\ (\frac{1}{r}-1)\sin\theta\cos\theta & 1+(\frac{1}{r}-1)\cos^2\theta \end{pmatrix}$ .

Consider  $\underline{\underline{\ell}}^{-1}$  and  $\underline{\underline{\ell}}_0$  as  $2 \times 2$  matrices spanning  $(x, z)$  since only their  $x-z$  components mix during rotations about the  $y$ -axis;  $\ell_{yy} = \ell_{yy}^{-1} = 1$  (since  $\underline{\underline{\ell}}$  is reduced by  $\ell_{\perp}$ ).

The free energy density, putting  $\underline{\underline{\ell}}^{-1}$  and  $\underline{\underline{\lambda}}$  in the Trace, becomes (in units of  $\frac{1}{2}\mu$ ):

$$\frac{F_{\text{el}}}{\frac{1}{2}\mu} = \lambda^2 + \lambda_{zz}^2 + \left(\frac{1}{\lambda\lambda_{zz}}\right)^2 + r\lambda_{xz}^2 - (r-1) \left[ 2\lambda_{zz}\lambda_{xz}\sin\theta\cos\theta + \left(\frac{1}{r}\lambda^2 - \lambda_{zz}^2 + \lambda_{xz}^2\right)\sin^2\theta \right]. \quad (6.17)$$

The first group is the energy of deforming an isotropic rubber ( $r = 1$ ). The second group represents additional effects due to rotating the anisotropy ( $r - 1$ ). The elastomer relaxes its transverse dimension,  $\lambda_{zz}$ , and its shear,  $\lambda_{xz}$ , to minimise this elastic energy. See WT§7.3.2 for the straightforward algebra leading to the free energy, at a fixed imposed extension  $\lambda$ , now a function only of the director rotation angle (through  $\sin^2\theta$ ):

$$F_{\text{el}}(\lambda, \theta) = \frac{1}{2}\mu \left( \lambda^2 \left(1 - \frac{r-1}{r}\sin^2\theta\right) + \frac{2}{\lambda} \frac{1}{\sqrt{1 - \frac{r-1}{r}\sin^2\theta}} \right). \quad (6.18)$$

On symmetry grounds rotations,  $\pm\theta$  are not distinguished - the extension  $\lambda$  is imposed at  $90^\circ$  to the initial director and it does not matter which way it rotates. Being a nematic,  $\theta = 0$  and  $\theta = \pi$  states are also identical.

The optimal angle condition, best examined as the derivative with respect to  $\sin^2\theta$  rather than  $\theta$  itself, yields the director rotation angle,  $\theta(\lambda)$  and the accompanying shear and transverse relaxations on using this  $\theta$ :

$$\theta = \sin^{-1} \sqrt{\frac{r}{r-1} \frac{\lambda^2 - 1}{\lambda^2}} \quad (6.19) \quad \lambda_{zz} = \frac{1}{\lambda}; \quad (6.21)$$

$$\lambda_{xz}^2 = \frac{(\lambda^2 - 1)(r - \lambda^2)}{r\lambda^2} \quad (6.20) \quad \lambda_{yy} = 1. \quad (6.22)$$

These results give  $F_{\text{el}} = \frac{3}{2}\mu$  for the free energy density, which is also the value in the relaxed state ( $\underline{\underline{\lambda}} = \underline{\underline{\delta}}$ ), even though the mechanical shape of the elastomer has manifestly changed.

The shear  $\lambda_{xz}$  and the angle  $\theta$  both start at zero in a singular fashion when  $\lambda = 1$ . When the extension reaches  $\lambda = \sqrt{r}$ , the rotation is complete:  $\theta \rightarrow \pi/2$ . The shear  $\lambda_{xz}$  returns to zero since off-axis shape accommodation associated with oblique director angles is no longer required. Director rotation,  $\theta(\lambda)$ , is central to the new effects

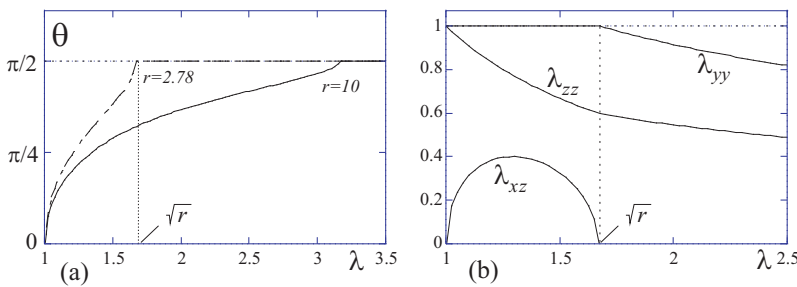
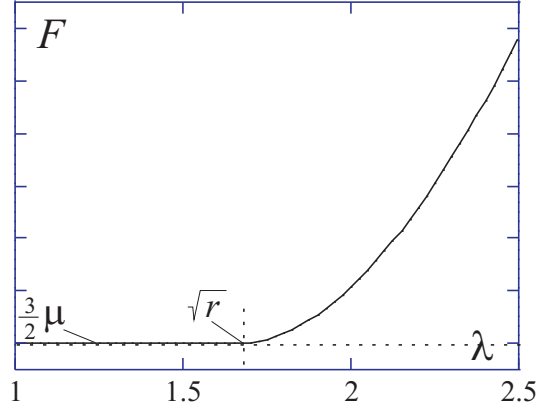


Figure 6.7: (a) Director rotation  $\theta$  against the imposed extension, for anisotropies  $r = 2.78$  and  $r = 10$ , see eqn (6.20). (b) The shear  $\lambda_{xz}$  and transverse relaxations  $\lambda_{zz}$  and  $\lambda_{yy}$ , for  $r = 2.78$ . The soft region is  $\lambda = 1$  to  $\lambda = \sqrt{r} = 1.67$ , beyond which the response is conventional.

and is of a distinctive form. Its singular form at  $\lambda = 1$  arises from the square root. The singular form at  $\lambda = \sqrt{r}$  and the saturation level  $\theta = \pi/2$  arises from the  $\sin^{-1}$  function. This reflects  $\sin\theta$ , rather than the angle itself, being the natural variable of the elastic free energy (6.18). The accompanying shear is also singular at  $\lambda = 1$  and  $\lambda = \sqrt{r}$ . The  $\theta$  response, Fig. 6.7(a), is seen in experiments which we discuss in Sect. 6.4.

In the soft interval, the  $z$ -transverse relaxation is  $\lambda_{zz} = 1/\lambda$  and the  $y$ -dimension is unchanged,  $\lambda_{yy} = 1$ , see Fig. 6.7(b). As in the cartoon, Fig. 6.3, the shape spheroid rotates in the  $xz$ -plane. No  $y$ -dimensional change is needed since no  $y$  molecular shape change has to be accommodated. The free energy is constant and thus the stress is zero - 'soft deformation', see Fig. 6.8.

Figure 6.8: Deformation  $\lambda$  applied perpendicular to the initial director, that is along the  $x$  direction, does not cause the free energy density,  $F$ , to rise until  $\lambda = \sqrt{r}$ . Thereafter the energy density rises as for a classical elastomer, of apparent natural elongation along  $x$  of  $\sqrt{r}$ , see eqn (6.23).



When  $\lambda > \sqrt{r}$  the rotation is complete ( $\theta = \pi/2$ ) and the imposed shape change cannot be further accommodated by directing the long dimension of the molecules toward  $x$ . In eqn (6.18) set  $\sin \theta = 1$ , whence

$$F_{\text{el}} = \frac{1}{2}\mu \left( \frac{\lambda^2}{r} + 2\frac{\sqrt{r}}{\lambda} \right). \quad (6.23)$$

The free energy now rises with  $\lambda$  and the stress is non-zero. The rubber responds as a normal elastomer, but with an apparent natural length of  $\sqrt{r}$ . If the strain along the  $x$  axis is measured as  $\lambda'$  with respect to this state, that is if we apply an extension  $\sqrt{r}$  first followed by  $\lambda'$ , then overall  $\lambda = \lambda'\sqrt{r}$ . We can rewrite the free energy density as  $F_{\text{el}}(\lambda') = \frac{1}{2}\mu(\lambda'^2 + 2/\lambda')$ , which appears entirely conventional.

#### 6.4 SEMI-SOFT ELASTICITY AND EXPERIMENT

Softness is a delicate phenomenon. It depends on being able to rotate a chain distribution at constant entropy by accommodating anisotropic chains with suitable extensions and shears of the body the chains comprise. We would partially lose softness if for instance we had a mixture of chains in the network with differing anisotropies. An optimal soft  $\underline{\lambda}$  for one population might not be optimal for another and such chains would then cost energy to deform along the trajectory selected for the first population — compositional fluctuations (Verwey and Warner, 1997a). Other causes of semi-softness could for instance be crosslinks being themselves rod-like and therefore able to record orientational order (Verwey and Warner, 1997b; Popov and Semenov, 1998). See WT§7.4 for a discussion of more general aspects of semisoftness and its causes.

The general soft modes  $\underline{\lambda}_{\text{soft}} = \underline{\ell}^{1/2} \cdot \underline{\mathbf{W}}_{\alpha} \cdot \underline{\ell}_{\alpha}^{-1/2}$  are intimately related to the structure of the Trace formula for the elastic free energy density. Some additions or modifications to the Trace formula preserve softness, others (see Sect. 6.2.3) lead to deviations from ideality, while still preserving the lower-energy path of deformations — which we call semi-softness.

The requirement for softness is that an isotropic reference state be in principle achievable. If there is always a residual anisotropy, even at high temperatures, then the nematic phase cannot be truly soft. We will see that chemically identical networks with differing thermomechanical histories can have drastically different stress-strain characters; the softest networks were formed in the isotropic state, the least soft were prepared in the nematic state and had more anisotropy permanently imprinted into them. Imprinting means only the gradual loss of nematic order at  $T_{\text{ni}}$  for some nematic elastomers compared with the discontinuous jump to zero order for the melt at this point.

The phenomenon of a threshold strain is related. Nematic rotation induced by an imposed extension and with it a nearly completely flat soft stress plateau do not onset directly at  $\lambda = 1$ , as the stretch starts, but instead at a small but noticeable threshold  $\lambda_1 > 1$ . It is as if the matrix first holds back the rotation of chains: the memory of an intrinsic or imprinted anisotropy must first be overcome. However, despite any non-ideality and partial loss of softness, elastomers nevertheless retain the qualitative aspects of soft elasticity, namely the same universal form of the director rotation  $\theta(\lambda)$  and the non-classical transverse contraction characteristic of the soft state:  $\lambda_{zz} \propto 1/\lambda$  and  $\lambda_{yy} = \text{const}$ .

One can derive from models (WT§7.4) additional terms, weighted by non-ideality  $\alpha$ , that cause the  $\text{Tr}(\text{---})$  result to be non-ideal:

$$F_{\text{ss}} = \frac{1}{2}\mu \text{Tr}\left(\underline{\underline{\ell}}_0 \cdot \underline{\underline{\lambda}}^{\text{T}} \cdot \underline{\underline{\ell}}^{-1} \cdot \underline{\underline{\lambda}}\right) + \frac{1}{2}\mu \alpha \text{Tr}\left(\underline{\underline{\delta}}^{(\text{tr})} \cdot \underline{\underline{\lambda}}^{\text{T}} \cdot \underline{\underline{nn}} \cdot \underline{\underline{\lambda}}\right) \quad (6.24)$$

where  $\underline{\underline{\delta}}^{(\text{tr})} = \underline{\underline{\delta}} - \underline{\underline{n}}_0 \underline{\underline{n}}_0$  is a perpendicular projector and inhabits the plane perpendicular to  $\underline{\underline{n}}_0 \underline{\underline{n}}_0$ . The form of the additional term is in fact the most general possible (Biggins *et al.*, 2008) at second order in  $\underline{\underline{\lambda}}$ : consider a non-ideal nematic elastomer subject to a deformation  $\Lambda_{ij}$  from a reference to a target state. We use  $\underline{\underline{\Lambda}}$  because we reserve  $\underline{\underline{\lambda}}$  for deformations from relaxed states, and this reference state may not be relaxed. If it is not relaxed, there is first relaxing deformation,  $\underline{\underline{\Lambda}}_r$ . Functions of  $\underline{\underline{\Lambda}}$  can be recast in terms of deformations from the relaxed state ( $\underline{\underline{\lambda}}$ ) by substituting  $\underline{\underline{\Lambda}} = \underline{\underline{\lambda}} \cdot \underline{\underline{\Lambda}}_r$ . The first subscript on  $\Lambda_{ij}$  ( $i$ ) lives in the target state and can only be contracted with subscripts from other target state variables. The second ( $j$ ) lives in the reference state and must be contracted only with reference state subscripts if rotational invariance is to be observed. Therefore the most general free energy we can write down that is quadratic in  $\Lambda$  is, if we assume that the reference state is characterised by a single direction  $\underline{\underline{n}}_0$  and the final state by a single direction  $\underline{\underline{n}}$  (so both states are uniaxial),

$$F = \text{Tr}(H\underline{\underline{\Lambda}}^{\text{T}}\underline{\underline{\Lambda}} + J\underline{\underline{n}}_0 \underline{\underline{n}}_0 \underline{\underline{\Lambda}}^{\text{T}}\underline{\underline{\Lambda}} + K\underline{\underline{n}}_0 \underline{\underline{n}}_0 \underline{\underline{\Lambda}}^{\text{T}}\underline{\underline{nn}}\underline{\underline{\Lambda}} + L\underline{\underline{\Lambda}}^{\text{T}}\underline{\underline{nn}}\underline{\underline{\Lambda}}). \quad (6.25)$$

Relaxation at constant volume over the  $\underline{\underline{\Lambda}}_r$  component of  $\underline{\underline{\Lambda}}$  reduces the number of coefficients to 3 which can then be re-caste to give Eq. (6.24) which also has 3 parameters,  $\mu$ ,  $r$  and  $\alpha$ .

The symmetry of deformations relevant to the additional,  $\alpha$  term is determined by  $\underline{\underline{\delta}}^{(\text{tr})}$ . For instance the  $xy$ -plane is perpendicular to  $\underline{\underline{n}}_0$  and the projector takes the form  $\underline{\underline{\delta}}^{(\text{tr})} = \underline{\underline{xx}} + \underline{\underline{yy}}$ . It selects out the  $x$  and  $y$  components of objects it encounters, see Ex. 6.3 for shears important to semi-softness.

*Exercise 6.3:* What shears are vital to the semi-soft fluctuation term? Assume for concreteness that  $\underline{\underline{n}}$  rotates in the  $xz$ -plane.

*Solution:* As  $\underline{\underline{n}}$  rotates in the  $xz$ -plane starting from  $\underline{\underline{n}}_0 = \underline{\underline{z}}$ , it becomes  $\cos\theta \underline{\underline{z}} + \sin\theta \underline{\underline{x}}$ . Since  $\underline{\underline{nn}}$  is sandwiched between  $\underline{\underline{\lambda}}^{\text{T}}$  and  $\underline{\underline{\lambda}}$  in the new semi-soft term of eqn (6.24), the  $\cdot \underline{\underline{n}}$  and  $\underline{\underline{n}} \cdot$  operations bind it to the  $z$  or  $x$  legs of  $\underline{\underline{\lambda}}^{\text{T}}$  and  $\underline{\underline{\lambda}}$ . There are no  $\lambda_{xy}$ ,  $\lambda_{zy}$ ,  $\lambda_{yx}$  and  $\lambda_{yz}$  elements of  $\underline{\underline{\lambda}}$ . But  $\underline{\underline{\delta}}^{(\text{tr})}$  lives in the  $xy$ -plane and thus the only part of  $\underline{\underline{\delta}}^{(\text{tr})}$  that can be active is  $\underline{\underline{xx}}$ . Recall that the diadic form of  $\underline{\underline{\lambda}}$  is  $\underline{\underline{\lambda}} = \underline{\underline{xx}}\lambda_{xx} + \underline{\underline{xz}}\lambda_{xz} + \dots$ . The vector  $\underline{\underline{n}} \cdot \underline{\underline{\lambda}} = (\lambda_{xx} \sin\theta + \lambda_{zx} \cos\theta)\underline{\underline{x}} + (\lambda_{xz} \sin\theta + \lambda_{zz} \cos\theta)\underline{\underline{z}}$  contracts with  $\underline{\underline{xx}}$ , selecting out the shear  $\lambda_{zx}$  and the imposed extension  $\lambda_{xx}$ . The non-ideal term in  $F_{\text{ss}}$ , eqn (6.24), is then:

$$\frac{1}{2}\mu\alpha(\lambda_{xx}^2 \sin^2\theta + \lambda_{zx}^2 \cos^2\theta + \lambda_{xx}\lambda_{zx}2\sin\theta\cos\theta). \quad (6.26)$$

The extension  $\lambda_{xx}$  perpendicular to  $\underline{\underline{n}}_0$  and the shearing displacements along  $\underline{\underline{n}}_0$  generate semi-softness.

#### 6.4.1 A PRACTICAL GEOMETRY OF SEMI-SOFT DEFORMATION

Reconsider the long strip of Fig. 6.6 with an  $x$ -extension  $\lambda = \lambda_{xx}$  imposed (Verwey *et al.*, 1996). Shears  $\lambda_{zx}$  are suppressed. In this case the non-ideal correction of eqn (6.26) is simply  $\alpha \sin^2\theta \lambda^2$ . It does not change the minimisation over  $\lambda_{zz}$  and  $\lambda_{xz}$  and simply adds to the soft free energy eqn (6.18):

$$F_{\text{ss}} = \frac{1}{2}\mu \left( \lambda^2 \left(1 - \frac{r-1}{r} \sin^2\theta\right) + \frac{2}{\lambda} \frac{1}{\sqrt{1 - \frac{r-1}{r} \sin^2\theta}} + \alpha \lambda^2 \sin^2\theta \right). \quad (6.27)$$

Optimising over  $\sin^2\theta$  gives

$$\frac{r-1}{r} \sin^2\theta = 1 - \frac{1}{\lambda^2} \left( \frac{r-1}{r-1-\alpha r} \right)^{2/3} \equiv 1 - \left( \frac{\lambda_1}{\lambda} \right)^2. \quad (6.28)$$

The solution for  $\sin^2 \theta$  is exactly as before, but as a function of the reduced extension,  $(\lambda/\lambda_1)$ , instead of  $\lambda$ . Accordingly, the onset of director rotation and all other features of soft regime will now take place not at  $\lambda = 1$  but at a threshold  $\lambda = \lambda_1$ , with

$$\lambda_1 = \left( \frac{r-1}{r-1-\alpha r} \right)^{1/3} \geq 1.$$

The threshold is the measure of the non-ideality. Below it a semi-soft nematic elastomer responds exactly as a conventional rubber. The transverse contraction is the usual  $1/\sqrt{\lambda}$  for both  $y$ - and  $z$ -directions and neither shear  $\lambda_{xz}$  nor director rotation arise. The semi-soft regime starts at  $\lambda = \lambda_1$  and is complete at  $\lambda = \sqrt{r}\lambda_1$ . The strains and the director rotation take forms very similar to those in eqns (6.22):

$$\begin{aligned} \theta &= \sin^{-1} \sqrt{\frac{r}{r-1} \frac{\lambda^2 - \lambda_1^2}{\lambda^2}}; & \lambda_{zz} &= \frac{\lambda_1^{1/2}}{\lambda}; \\ \lambda_{xz}^2 &= \frac{(\lambda^2 - \lambda_1^2)(r\lambda_1^2 - \lambda^2)}{r\lambda^2\lambda_1^3}; & \lambda_{yy} &= \frac{1}{\lambda_1^{1/2}}. \end{aligned} \quad (6.29)$$

Both  $\theta$  and  $\lambda_{xz}$  have exactly the same singular response as in the ideally soft case. All the strains and rotations are thus as in Fig. 6.7, if  $\lambda$  is scaled by  $\lambda_1$ . Soft and semi-soft response are qualitatively the same, except that the elastic energy rises slightly in the latter case (see below).

The threshold strain depends generally on the form of correction to the ideal free energy of the type  $\alpha$  in eqn (6.24). For the particular model of compositional fluctuations that we have chosen as an illustration,  $\alpha$  and  $r$  are connected with  $\lambda_1$  as:

$$\alpha = \frac{r-1}{r} \frac{\lambda_1^3 - 1}{\lambda_1^3} \quad (6.30)$$

where  $r$  is a mean anisotropy  $\langle r \rangle = \langle \ell_{\parallel} / \ell_{\perp} \rangle$ . It is extracted experimentally from the reduced width of the semi-soft interval, the ratio between the final and the initial threshold strain of the semi-soft regime  $\equiv (\sqrt{r}\lambda_1)/\lambda_1$ . More anisotropic chains compel greater shape change of the rubber before their rotations are complete.

#### ELASTIC FREE ENERGY

Before there is nematic rotation,  $\lambda < \lambda_1$  (region A of Figs. 6.10), the response must be classical, that is  $\theta = 0, \lambda_{xz} = 0, \lambda_{zz} = \lambda_{yy} = 1/\sqrt{\lambda}$ , with  $F_A = \frac{1}{2}\mu(\lambda^2 + 2/\lambda)$ . Between the semi-soft threshold  $\lambda_1$  and the end of semi-softness,  $\sqrt{r}\lambda_1$ , we express the elastic free energy density  $F_{el}(\lambda, \theta)$  in terms of  $\lambda_1^3$  rather than  $\alpha$ , as these two parameters measuring the degree of semi-softness are directly related in a fluctuations model by eqn (6.30). Thus re-expressing eqn (6.27) one has instead

$$F_{ss} = \frac{\mu}{2} \left( \lambda^2 \left( 1 - \frac{r-1}{r\lambda_1^3} \sin^2 \theta \right) + \frac{2}{\lambda} \frac{1}{\sqrt{1 - \frac{r-1}{r} \sin^2 \theta}} \right).$$

Using the optimal director rotation from eqn (6.29), the semi-soft free energy density in the region B of Fig. 6.10 takes the form:

$$F_B = \frac{1}{2}\mu \left( \lambda^2 \left( 1 - \frac{1}{\lambda_1^3} \right) + \frac{3}{\lambda_1} \right). \quad (6.31)$$

For  $\lambda_1 = 1$ , the case of ideally soft rubber, one recovers the unchanging  $F = \frac{3}{2}\mu$  as in Sect. 6.2. The larger the threshold  $\lambda_1$ , the harder  $F_B$  becomes; the modulus, the coefficient of  $\frac{1}{2}\lambda^2$ , is  $\mu(1 - 1/\lambda_1^3)$ .

*Exercise 6.4:* What is the free energy for  $\lambda > \lambda_1\sqrt{r}$ , that is when the director rotation is complete?

*Solution:* Recall that the free energy is (Ideal Trace) +  $\alpha\lambda^2\sin^2\theta$ . The rotation of  $\mathbf{n}$  by  $90^\circ$  to align along the stretching direction  $x$  interchanges the non-trivial diagonal element entry  $1/r$  in  $\underline{\underline{\ell}}^{-1}$  from the  $zz$  to the  $xx$  position. The  $\underline{\underline{\lambda}}$  matrices in the ideal trace formula are diagonal as well; after a rotation of  $\pi/2$  in  $\underline{\underline{\ell}}$  there are no remaining shears. Adding on the semi-soft  $\alpha$ -term with  $\theta = \pi/2$  yields overall:

$$\begin{aligned} F_C &= \frac{1}{2}\mu \left( \frac{1}{r}\lambda^2 + r\lambda_{zz}^2 + \frac{1}{\lambda^2\lambda_{zz}^2} \right) + \frac{1}{2}\mu\alpha\lambda^2 \\ &\equiv \frac{1}{2}\mu \left( \frac{\lambda^2}{r} \left( r - \frac{r-1}{\lambda_1^3} \right) + \frac{2\sqrt{r}}{\lambda} \right). \end{aligned} \quad (6.32)$$

To obtain the last formula one needs to minimise over  $\lambda_{zz}$  to give  $\lambda_{zz}^2 = 1/(\sqrt{r}\lambda)$  and then return this strain to the  $F_C$  expression.  $F_C$  looks almost classical, with  $\lambda^2$  and  $1/\lambda$  terms but with modified factors, as does the ideal  $F_{el}$  in eqn (6.23).

#### ELASTIC STRESS

We imposed an extension  $\lambda_{xx} = \lambda$  in the  $x$  direction, with other strains and rotations being a natural optimal response of the nematic elastomer under a uniaxial extension. What is the stress needed to make this imposition? Taking a sample of initially unit dimensions (and hence also unit volume), the work done by a force normal to the  $x$  surface in extending the sample by  $d\lambda$  is  $-\sigma_{xx}\lambda_{zz}\lambda_{yy}d\lambda$ . The  $(\lambda_{zz}\lambda_{yy})$ -factor is the cross-section area reduction which, when multiplying the force per unit area  $\sigma_{xx}$  (the stress), yields an actual force which does the work. The  $(-)$  sign indicates the reduction in energy when the system extends ( $d\lambda > 0$ ) in the direction of the force. If this work is added to the change in free energy per unit volume  $dF$ , then  $dF - \sigma_{xx}d\lambda/\lambda$  must vanish in equilibrium for the body (volume conservation gives  $\lambda_{zz}\lambda_{yy} = 1/\lambda$ ). Thus the true stress is:

$$\begin{aligned} \sigma_{xx} &= \lambda \left( \frac{\partial F}{\partial \lambda} \right) & (6.33) \\ \sigma_{xx}^A &= \mu \left( \lambda^2 - \frac{1}{\lambda} \right) & \rightarrow \mu \left( \lambda - \frac{1}{\lambda^2} \right) \\ \sigma_{xx}^B &= \mu\lambda^2 \left( 1 - \frac{1}{\lambda_1^3} \right) & \rightarrow \mu\lambda \left( 1 - \frac{1}{\lambda_1^3} \right) \\ \sigma_{xx}^C &= \mu \left( \lambda^2 \left( 1 - \frac{r-1}{\lambda_1^3 r} \right) - \frac{\sqrt{r}}{\lambda} \right) & \rightarrow \mu \left( \lambda \left( 1 - \frac{r-1}{\lambda_1^3 r} \right) - \frac{\sqrt{r}}{\lambda^2} \right). \end{aligned} \quad (6.34)$$

where the latter in each case are the nominal or engineering stresses, that is, the force per unit initial area. Without correcting for transverse shrinkage as strain proceeds, the nominal stress from eqn (6.33) is  $\sigma_{xx}^e = \partial F/\partial \lambda \equiv \sigma_{xx}/\lambda$  for our deformation.

One can easily confirm that the true stress is continuous on deforming between regions A, B, C, that is  $\sigma_{xx}^A(\lambda_1) = \sigma_{xx}^B(\lambda_1)$  and  $\sigma_{xx}^B(\sqrt{r}\lambda_1) = \sigma_{xx}^C(\sqrt{r}\lambda_1)$ .

Equally important is that the free energy is everywhere convex, especially in the semi-soft region B. Here the curvature is  $\partial^2 F_B/\partial \lambda^2 = \mu(1 - 1/\lambda_1^3) \geq 0$ . Convexity rules out strain-necking and related classical instabilities known in the polymer physics that might otherwise be invoked to explain the semi-soft constitutive relation in region B.

#### STRESS EXPERIMENTS

Nominal stress-strain data (Küpfer and Finkelmann, 1994; Clarke *et al.*, 2001), Fig. 6.9, is qualitatively as in Eqs. (6.34), that is essentially piecewise linear. On extension perpendicular to the initial nematic director, the measured nominal stress initially rises with  $\lambda$ . Then at a certain threshold it reaches a plateau or a region of lower slope. Finally, after the plateau, the stress increases again. Such experimental data unambiguously illustrates the effect of soft elasticity and allows extraction of the two key material parameters. The value of semi-soft threshold strain  $\lambda_1$  is directly related to the residual non-zero slope on the stress plateau, Eq. (6.34), while the

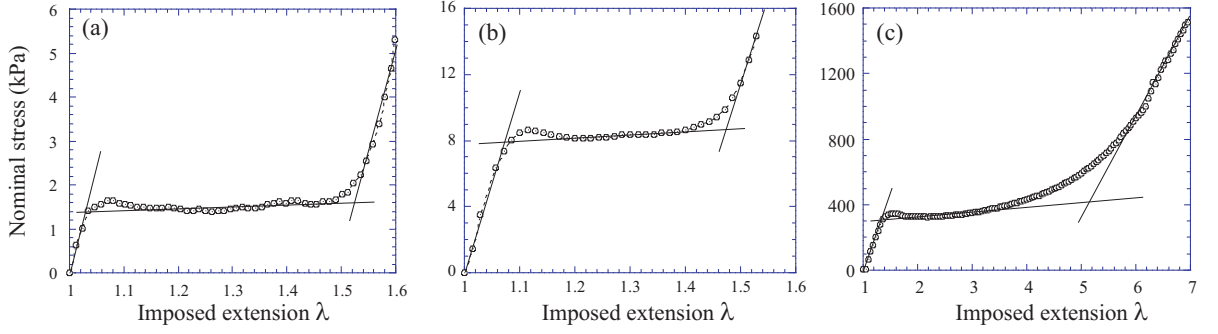


Figure 6.9: Nominal stress (in units of kPa for all three graphs) is plotted against deformation for three different nematic elastomers (experimental data from Freiburg and Cambridge groups). The composition of side-chain polysiloxane rubbers in (a) and (b) is very similar, but the materials differ in thermal history of crosslinking, i.e. residual order, resulting in different threshold and stress plateaux, while the chain anisotropy  $r$  is similar. The main chain sample in (c) has a much higher chain anisotropy  $r \sim 25$ -30, and hence a plateau end  $\lambda_2 = \sqrt{r} \sim 5$ . The straight lines are fits to the nematic elastomer constitutive relations, eqn (6.34).

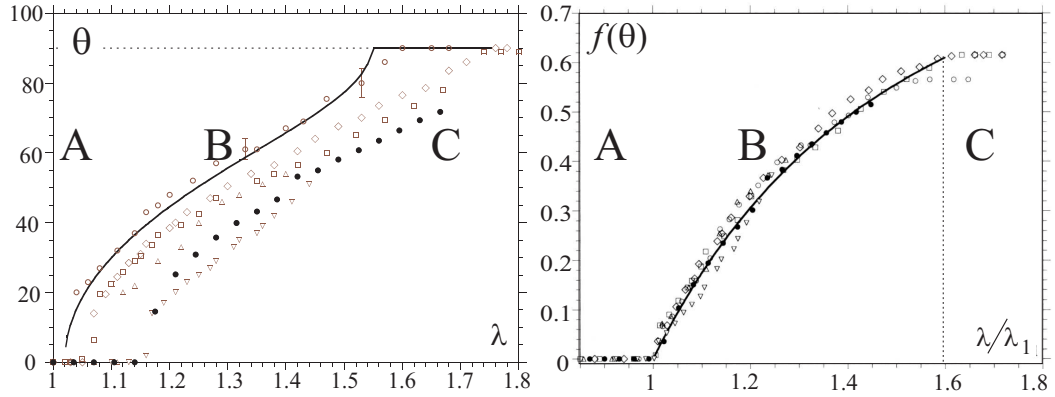


Figure 6.10: (a) Director rotation  $\theta$  after a strain  $\lambda$  applied perpendicular to the original director  $\mathbf{n}_0$ , see Fig. 6.6. Curves correspond to different crosslinking densities of the same polymer, and therefore also to different thermo-mechanical histories, or to elastomers of differing chemical composition (Kundler and Finkelmann, 1995). (b) The function  $f(\theta) = [(r-1)/r] \sin^2 \theta$  of the director rotation plotted against the reduced deformation  $\lambda/\lambda_1$ . Data from the wide range of samples in (a) collapse onto a master curve when plotted according to eqn (6.22).

average chain anisotropy  $r = \ell_{\parallel}/\ell_{\perp}$  can be estimated from the plateau end position. Three quantities (threshold, plateau slope and plateau extent) are determined by two parameters,  $\alpha$  and  $r$ , and the latter actually relates also to the separate experiment of spontaneous elongation on cooling. Thus the match of theory to experiment is vastly over-constrained, and the agreement therefore remarkable.

#### ROTATION EXPERIMENTS

The director rotation expected after the threshold is indeed found, see Fig. 6.10(a) (Kundler and Finkelmann, 1995). Different samples have different thermo-chemical histories and hence  $\lambda_1$  thresholds, and different molecular anisotropies and hence differing lengths of plateau. Each  $\theta(\lambda)$  curve however has initial and final singular behaviour ( $\sqrt{\lambda}$ ) and an inverse sine shape. Then plotted according to Eqs. (6.29),  $\theta(\lambda/\lambda_1)$  adopts its universal form — all elastomers behave in essentially the same way. Fig. 6.10(b) instead plots the function of the rotation angle given in eqn (6.28). The threshold  $\lambda_1$  is taken out via  $\lambda$  scaling, the anisotropy by the  $(r-1)/r$  factor, the  $\sin^{-1}$  and the  $\sqrt{\lambda}$  by the  $\sin^2 \theta$  factor.

Soft or semi-soft deformations are energetically the best response to shape changes imposed on a nematic elastomer. When the director can be rotated, for instance when elongations are not simply along the director, then an elastomer will always deform softly if the necessary accompanying relaxations can be reconciled with the boundary conditions. We examine distortions of nematic elastomers where the imperative to deform softly is in conflict with the external constraints imposed on them. There are generically two ways to resolve this conflict.

*Nearly soft deformation* A sample may deform almost but not quite softly because of constraints, for instance with an energy cost quartic in the deformation or the director rotation (and not quadratic, as usual). For small distortions, the rubber is thus essentially soft or semi-soft, the anchoring effect of the matrix being first felt at large amplitudes. The Fredericks effect for nematic elastomers is an example, see experiments (Chang *et al.*, 1997), the analysis of WT§8.3, and simulations (Skačej and Zannoni, 2006). See Fig. 7.1 for the set up and the contrast with the liquid case. Some deformation, limited by the need for the boundary plates not to move in their own

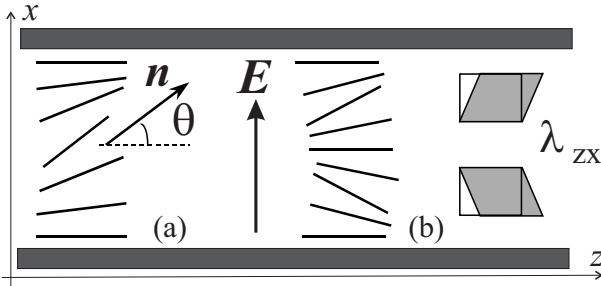


Figure 7.1: Field-induced director rotation in a conventional, liquid nematic (a) and in a nematic elastomer (b). The liquid has its director anchored at the surfaces  $x = 0$  and  $x = d$  to be along  $z$ . The solid has its initial director everywhere aligned along  $z$ . The electric field  $E$  is applied across the cell. The shear strain  $\lambda_{zx}$  accompanying the director rotation in nematic elastomers is shown on the right. The conventional Fredericks effect has one half wavelength of director rotation between the plates, while the solid nematic Fredericks effect has the full wavelength. The shear has to pass through a full cycle of variation — otherwise there is a net  $z$ -displacement of the upper boundary with respect to the lower.

plane and relative to each other, still has to occur otherwise the rubber-elastic penalty, giving bulk anchoring of the director, leads to prohibitively high electric fields to induce dielectric response: equating the elastic and electric field energy densities,  $\epsilon_0 \Delta \epsilon E^2 \sim D_1$  gives  $E \sim (r - 1)(\mu / \epsilon_0 \Delta \epsilon)^{1/2} \sim 10^7 \text{ V/m}$ , for typical values of rubber moduli, of chain anisotropy and of dielectric anisotropy  $\Delta \epsilon$ . It is as if there were effectively a very strong aligning field  $\mu$  acting along the axis  $\mathbf{n}_o$ , unless the sample is mechanically unconstrained and an appropriate soft deformation can be found (Terentjev *et al.*, 1994). The Fredericks effect is different from classical liquid crystals since the transition occurs at a critical field rather than critical voltage since the anchoring is in the bulk.

*Soft or semi-soft deformation* A sample deforms softly, but with a local strain  $\underline{\lambda}_{\text{soft}}$  that differs from region to region. For example a given soft extension,  $\lambda$  of Sect. 6.3.2, comes with simple shears of either  $\delta(\lambda)$  or  $-\delta(\lambda)$ , and director rotations  $\pm\theta(\lambda)$ . By judiciously putting together neighbouring regions with shear deformations of opposite sense, one can obtain an extension that overall has no net shear and hence may satisfy zero-shear boundary conditions in some gross sense. Fine microstructures are required in mechanical experiments to achieve global softness. We examine such microstructures in a refined treatment of a clamped version of the simple extension of Sect. 6.3.2 which produces the stripes first seen by Finkelmann and coworkers.

Coexisting neighbouring regions of differing  $\underline{\lambda}_{\text{soft}}$  create inhomogeneous interfaces in the nematic elastomer. Their energetic cost turns out to be extremely small and does not hinder elastomers resorting to microstructures to eliminate the otherwise considerable elastic costs of deformation. Ignoring interfacial energies and reducing elastic energy by judicious choices of sets of coexisting strains is called ‘quasi-convexification of the free energy’. It was invented in a more difficult problem of discrete sets of low energy crystallographic distortions in martensite, a shape-memory alloy (Ball and James, 1992).

The same geometric and physical ideas were independently applied (Verwey *et al.*, 1996) to the very much simpler problem of a nematic elastomer with an ideal form of clamping. We shall examine this problem in this chapter, including the details of the interfaces. We then review the formal quasi-convexification of the nematic elastomer free energy and describe the general microstructures that arise (DeSimone, 1999). The method has been applied to give a full numerical solution of the extension of a nematic elastomer strip and the evolution of its complex microstructures (Conti *et al.*, 2002), in effect a multi-scale analysis.

We conclude with a modern application of the ideas of DeSimone to extreme softness found in isotropic genesis polydomain nematic elastomers.

### 7.1 STRAIN-INDUCED MICROSTRUCTURE: STRIPE DOMAINS

Elastomers elongated perpendicularly to their director deform (semi) softly if they shear. The cartoon in Fig. 6.3 shows graphically how elongation must be accompanied by shear if energy cost is to be eliminated. However clamps, through which stretch is imposed, prohibit shear in their vicinity. Then microstructure, in the form of stripe domains, offers the best compromise between the drive for soft deformation and the constraining boundary conditions. Figure 7.1 in the Freedericks case illustrates the solution to the problem when the shears are less complicated: the upper plate is fixed with respect to the lower plate. If shear is required to soften the response (to make it quartic in that case), there must be two compensating shears in order that they create no net displacement.

For imposed mechanical fields, such as uniaxial extension, semi-soft simple shear is a good example with which to illustrate the emerging microstructure. See Fig. 7.2 where a strip is extended beyond the semi-soft threshold for director rotation  $\lambda = \lambda_1$ . In the bulk of the strip, the local shear and director rotation follow the optimal, semi-soft values consistent with the extension  $\lambda$ . A compensating pair of stripes is shown magnified; on traversing the pair (in the  $z$ -direction, along the initial  $\mathbf{n}_0$ ) the total  $x$ -displacement averages out. Real systems have a collection of many stripes stretching along the elongated elastomer strip, see Fig. 7.3. The elastic softness is unattainable only at the ends and in the sharp interfaces between stripes. The bulk of the elastomer deforms softly, at least until the director rotation is complete at the extension  $\lambda_2$ . This is seen macroscopically in the stress-strain and opto-mechanical relations.

The precise details of the clamp constraints will determine how the stripe domains evolve. In general the problem with simple, realistic constraints is extremely complex, see Sect. 7.2.3. A simplification is to consider rigid but sliding/rolling constraints or clamps that themselves deform at a compensating rate. Shear is suppressed at the end while allowing any necessary transverse  $\lambda_{zz}$  relaxation required to conserve volume while extension  $\lambda_{xx}$  proceeds, see Fig. 7.4. Some residual curvature at the ends of the rubber strip may still occur even if  $z$ -motion in the clamp is free: in the bulk the relaxation is  $\lambda_{zz} \sim 1/\lambda_{xx}$ , as with all soft modes, whereas at the ends it is only  $\lambda_{zz} \sim 1/\sqrt{\lambda_{xx}}$ , since the response is hard in the absence of shear. Additionally, the extension  $\lambda_{xx}$  is itself smaller at the ends than in the bulk because the nominal stress has to be conserved. We ignore curvature in the clamp

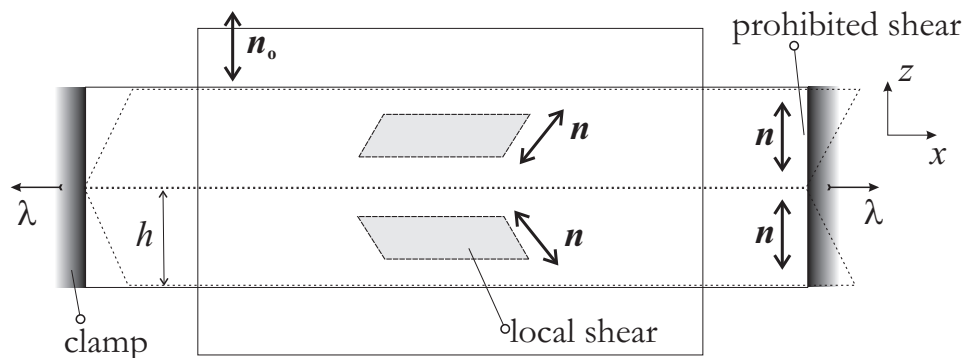


Figure 7.2: Microstructure in a nematic elastomer strip being extended perpendicular to its initial director  $\mathbf{n}_0$ , assumed along the  $z$ -axis. A section with only two neighbouring stripes of width  $h$  and opposing shear,  $\lambda_{xz}$ , and rotation is shown. At the ends the displacement associated with soft shear is shown suppressed by the clamps.

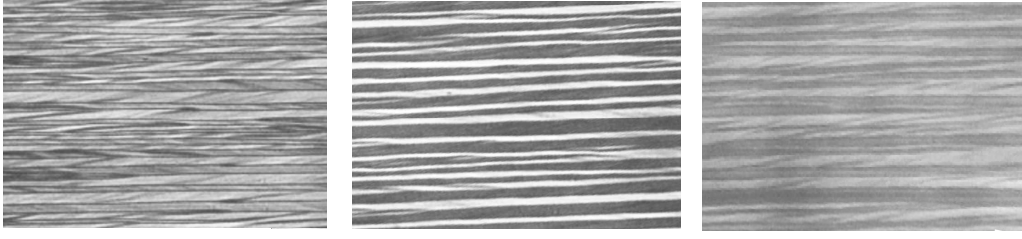


Figure 7.3: Stripe domains in a nematic elastomer extended as in the schematic Fig. 7.2. All three images are the same stripe system at a fixed extension but viewed at different angles ( $0^\circ$ ,  $15^\circ$  and  $77^\circ$ ) with respect to a crossed polariser-analyser pair. Different details of the stripe substructures then emerge (images: I. Kundler).

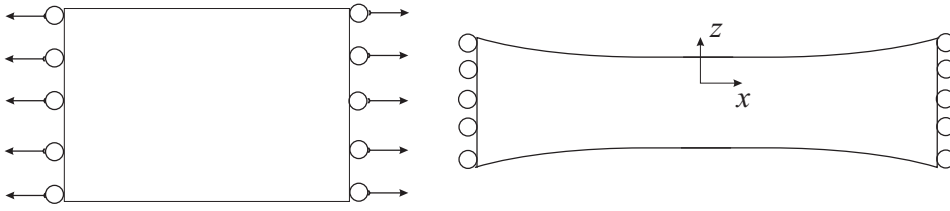


Figure 7.4: Ends of a strip are rigidly constrained, forbidding shear but allowing for transverse relaxation  $\lambda_{xz}$ .

region and use the idealisation of Fig. 7.4 as a model for how the uniform texture of Fig. 7.2 is finally terminated far enough from the ends that the complications of static clamps can be ignored. The problem is examined in more detail in Sect. 7.2.3.

If the imposed elongational deformation in the  $x$ -direction is  $\lambda$  (greater than the rotation threshold  $\lambda_1$ ), the optimal semi-soft shear and director rotation within the individual alternating stripes are  $\pm\lambda_{xz}$  and  $\theta_{\pm} = \pm\theta_o(\lambda)$ , with

$$\lambda_{xz}^2 = \frac{(\lambda^2 - \lambda_1^2)(r\lambda_1^2 - \lambda^2)}{r\lambda^2\lambda_1^3} \quad \theta_o = \sin^{-1} \sqrt{\frac{r}{r-1} \frac{\lambda^2 - \lambda_1^2}{\lambda^2}}, \quad (7.1)$$

see Sect. 6.4.1, eqn (6.29). We now see how alternating stripes can be fitted together.

#### STRIPE STRUCTURE AND ENERGY

The director generally responds to an imposed strain. Non-uniform mechanical distortions such as in the coarsened stripe structure of Fig. 7.2 generate regions of non-uniform directors which in turn cost a Frank nematic elastic penalty. We therefore, indirectly, have an energetic cost to non-uniform elastic strain. As usual in elasticity, we ignore the direct elastic cost of gradients of strain ( $\partial\lambda_{ij}/\partial x_k$ ). Since the elastic cost of not deforming softly is so high compared with Frank effects, the a rather sharp interface region must separate two domains of optimal deformations obtaining in one sense (+) and in the opposite sense (-). An area  $A$  of interface has an energy  $\Delta F \sim \gamma A$  where  $\gamma$  is an effective interfacial tension, which we now estimate. A full treatment combines Frank elasticity with nematic rubber elasticity. Strains that can relax are set equal to their minimal value, subject to a given  $\theta$  and to the strain components that are imposed. The total elastic energy, depending on  $\theta$  for the elastic part and on  $\nabla\theta$  for the Frank part, must be minimised; see WT§8.3 for a full analysis.

Take strains and director rotations to vary in the  $z$ -direction, but to be basically of the simple shear type we have already considered in Sect. 6.4.1 The director varies with  $z$  in going between stripes. It rotates in the  $xz$ -plane, making a local angle  $\theta$  with the  $z$ -direction,  $\mathbf{n} = (\sin\theta, 0, \cos\theta)$ . The Frank energy density involves only splay ( $K_1$ ) and bend ( $K_3$ ) in this geometry, see Sect. 2.4. It is:

$$F_F = \frac{1}{2} (K_1 \sin^2 \theta + K_3 \cos^2 \theta) \left( \frac{d\theta}{dz} \right)^2 \rightarrow \frac{1}{2} K \left( \frac{d\theta}{dz} \right)^2.$$

The latter simplification arises in the single constant approximation  $K_1 = K_3 = K$ .

Consider the interfacial width to be  $\xi$  where all the  $\theta$ -variation occurs and thus is also where the elastic energy density is  $\sim \mu$  since there the soft deformations of the bulk of each stripe are not achieved. The cost of an area  $A$  of interface is  $\gamma A \sim A\xi\mu + A\xi K/\xi^2$  since  $d^2\theta/dx^2 \sim \pi/\xi^2$ . Optimising over  $\xi$ , then  $\gamma/d\xi = 0$  gives  $\xi = \sqrt{K/\mu} \sim 10^{-8}\text{m}$  and  $\gamma = \sqrt{K\mu} \sim 10^{-3}\text{N/m}$  if we take some typical values,  $\mu \sim 10^5\text{Pa}$  and  $K \sim 10^{-11}\text{N}$ . The interfacial energy scale  $\gamma$  is relatively small. The surface tensions of liquids, by comparison, are in the range  $40 \times 10^{-3}\text{N/m}$  (benzene) and  $72 \times 10^{-3}\text{N/m}$  (water), at least an order of magnitude higher. We call  $\xi$  the nematic penetration depth — director variation is confined to length  $\lesssim \xi$  if there is an appreciable rubber elastic penalty  $\sim \mu$  otherwise being paid for not having an optimal (soft or semi-soft) distortion. This is why stripes are always coarsened and their interfaces play no role in macroscopic elastic response.

Experimentally it is indeed found that in stretched nematic elastomer the stripes are immediately coarse when they form (Kundler and Finkelmann, 1998; Zubarev *et al.*, 1999), that is the majority of the sample is taken by the regions of relatively uniform director rotation, alternating in neighbouring stripes, with interfaces narrow ( $\sim \xi$ ) compared with stripe width.

## 7.2 GENERAL DISTORTIONS OF NEMATIC ELASTOMERS

The Freedericks and stripes examples have shown nematic elastomers deforming softly (or with energy quartic in strain) even when soft modes are in conflict with boundary conditions. The answer is to satisfy boundary conditions on average, by the establishment of inhomogeneous microstructure. The ideal clamps of the above example allowed the whole sample, except in a small volume near the clamps, to deform softly – for instance the elongations  $\lambda$  and the transverse relaxations  $\lambda_{zz}$  were uniform. Shears differed between stripes, but averaged to zero, as demanded by the clamps.

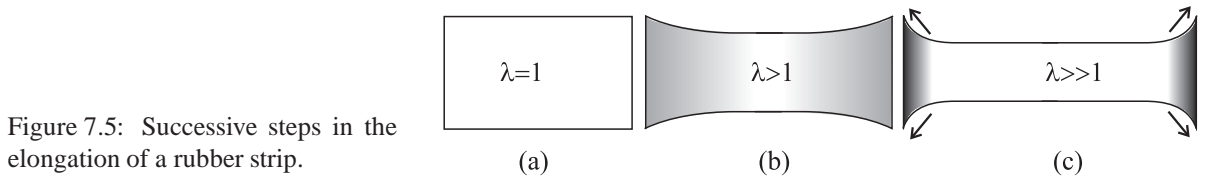


Figure 7.5: Successive steps in the elongation of a rubber strip.

A more realistic clamping and extension scenario is sketched in Fig. 7.5. The clamps do not permit transverse relaxation in their vicinity. The sample develops curved edges and a complicated shear pattern as a result. Combinations of soft shears to give a soft, non-uniform response are now more complex than in our example above. Moreover we have spatial non-uniformity both at the scale of the stripes and on the scale of the whole sample strip – it now becomes a problem of multiscale compatibility. We discuss the general problem of constructing the appropriate  $\underline{\lambda}$  from combinations of various  $\underline{\lambda}_{\text{soft}}$ , to achieve a macroscopic situation that is also nearly soft – so-called ‘quasi-convexification’. We then sketch the full numerical solution to the problem of general distortions and compare it with experiment.

### 7.2.1 ONE-DIMENSIONAL QUASI-CONVEXIFICATION

In the previous section we have, in effect, presented an example of quasi-convexification of the nematic free energy, considering stripe modulation of the sample only along the  $z$ -axis. This serves as an illustration of a more general problem. Suppose one wants to achieve a deformation  $\underline{\lambda} = \begin{pmatrix} \lambda & 0 & 0 \\ 0 & 1 & 0 \\ 0 & 0 & 1/\lambda \end{pmatrix}$  without paying any energy cost. Without shear, this deformation is only without cost at the deformations  $\lambda = 1$  and for  $\lambda = \sqrt{r}$ , that is at the two positions (of equal energy) in Fig. 6.1, that is at the  $\lambda$  values where the soft plateau starts and finishes in Fig. 6.3. For all intermediate deformations with  $1 < \lambda < \sqrt{r}$ , we have achieved, Fig. 7.2, an overall soft deformation by

splitting into equal volumes with opposite shears,  $\pm\lambda_{xz}$ , and rotation:

$$\begin{aligned}\underline{\underline{\lambda}} &= \begin{pmatrix} \lambda & 0 & 0 \\ 0 & 1 & 0 \\ 0 & 0 & 1/\lambda \end{pmatrix} = \frac{1}{2} \left\{ \begin{pmatrix} \lambda & 0 & \lambda_{xz} \\ 0 & 1 & 0 \\ 0 & 0 & 1/\lambda \end{pmatrix} + \begin{pmatrix} \lambda & 0 & -\lambda_{xz} \\ 0 & 1 & 0 \\ 0 & 0 & 1/\lambda \end{pmatrix} \right\} \\ &= \frac{1}{2} \left\{ \underline{\underline{\lambda}}_{\text{soft}}(+\lambda_{xz}) + \underline{\underline{\lambda}}_{\text{soft}}(-\lambda_{xz}) \right\} \\ \underline{\underline{\lambda}} &= \langle \underline{\underline{\lambda}}_{\text{soft}} \rangle_{\pm\lambda_{xz}}\end{aligned}\quad (7.2)$$

The effectively soft outcome  $\underline{\underline{\lambda}}$  is achieved by a suitably weighted mean of ‘real’ locally soft strains. If we make the microstructure sufficiently fine, then this overall strain  $\underline{\underline{\lambda}}$  has the status of a uniform deformation that is soft, despite having no visible shears associated with it as one might have expected. With this assumption of indefinite fineness (certainly finer than any scale of the problem one will later attempt to address) one has:

$$F_{\text{QC}}(\langle \underline{\underline{\lambda}}_{\text{soft}} \rangle_{\pm\lambda_{xz}}) = \langle F(\underline{\underline{\lambda}}_{\text{soft}}(\lambda_{xz})) \rangle = 0 \quad (7.3)$$

(the additive constant of  $\frac{3}{2}\mu$  being ignored). One ignores the cost of interfacial energy of the narrow regions that separate the individual soft domains. In practical cases there is only a negligible volume of hard deformation associated with the interfaces.

The free energy  $F$  is said to have been *quasi-convexified* to  $F_{\text{QC}}$ . Finally, in a sense the  $F_{\text{QC}}$  points to more general ‘low roads’, elastic trajectories between the initial and the final states of deformation,  $F_A(\lambda)$  and  $F_C(\lambda)$ , of Fig. 6.1. In the soft-deformation expression  $\underline{\underline{\ell}}^{1/2} \cdot \underline{\underline{W}} \cdot \underline{\underline{\ell}}_0^{-1/2}$ , eqn (6.5), we were able to identify an infinite number of such deformations, the cartoon of Fig. 6.3 being a special case where the matrix  $\underline{\underline{W}}$  is simply  $\underline{\underline{W}} = \underline{\underline{\delta}}$ . However with  $F_{\text{QC}}$  one creates more freedom, for instance to eliminate shears from soft modes.

One further preliminary consideration is required; the pairs of deformations  $\underline{\underline{\lambda}}_{\text{soft}}$  must be chosen to be *kinematically compatible*. Deformation gradients  $\underline{\underline{\lambda}}$  displace the material points  $\mathbf{R}_0$  of the initial body to new positions  $\mathbf{R}$  in the target state,  $\mathbf{R} = \underline{\underline{\lambda}} \cdot \mathbf{R}_0$ . Figure 7.2 shows two stripes within the sample, separated by an interface. The accumulated  $x$ -displacement is only that corresponding to the externally imposed  $\lambda$ , while the additional modulation due to local shears averages to zero, in going from the bottom of the lower stripe to the top of the upper stripe. One sees this also in Fig. 7.1 for the Fredericks effect, where there is no overall shear generated between the lower and upper plates which are imposing the overall boundary conditions. Moreover, at the interface between the stripes, the position  $\mathbf{R}$  is given equally by the displacement in going from the top of the upper stripe or from the bottom of the lower stripe - the deformations are compatible. The decomposition of the deformation gradient presented in eqn (7.2) trivially satisfies this condition. In general the  $\underline{\underline{\lambda}}_s$  on the two sides of the interface must be ‘rank-1 connected’, that is, the deformations applied using either  $\underline{\underline{\lambda}}$  on a material point in the interface must agree so that the interface’s deformations are uniquely defined (Bhattacharya, 2003).

The compatibility requirement on the  $\underline{\underline{\lambda}}_s$  of the quasi-convexification arises less trivially already in the simple example (Verwey *et al.*, 1996) where the initial director  $\mathbf{n}_0$  is not perpendicular to the imposed extension  $\lambda$  along  $x$ , but has a pre-tilt angle  $\phi$ , see Fig. 7.6. The concept of soft deformations as a low energy route for director

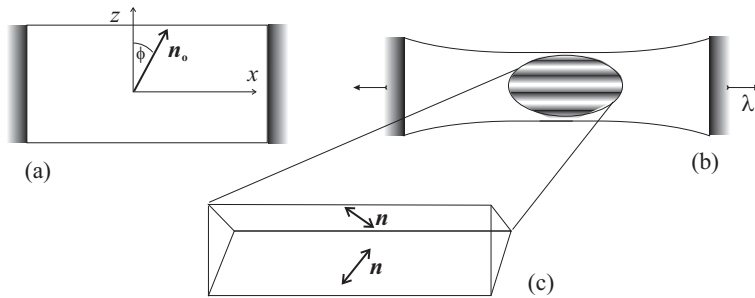


Figure 7.6: A strip of nematic elastomer with initial director,  $\mathbf{n}_0$ , at angle  $\phi$  to the  $z$ -axis (a). On extension by  $\lambda$  along  $x$  it breaks up into a microstructure which avoids macroscopic shear (b). Pairs of stripes suffer soft deformations with director rotations to angles  $\pm\theta$ , and shears,  $\pm\lambda_{xz}$ , such that there is no net  $x$ -displacement on passing through two stripes (c).

re-orientation remains valid. For a uniform system generating only simple shear and the transverse relaxation

$1/\lambda$  in response to the imposed extension, the optimal director rotation to angle  $\theta$  with respect to  $\mathbf{z}$ , and the associated shear  $\lambda_{xz}$ , take the form in alternating ( $\pm$ ) stripes:

$$\sin^2 \theta = \frac{1}{\lambda(r-1)} [r(\lambda^2 - 1) + (r-1) \sin^2 \phi] \quad (7.4)$$

$$\lambda_{xz} = \frac{1}{\lambda[r - (r-1) \sin^2 \phi]} \left( -\lambda^2(r-1) \sin \phi \cos \phi \pm \sqrt{r(\lambda^2 - 1) + (r-1) \sin^2 \phi} \sqrt{r - \lambda^2 - (r-1) \sin^2 \phi} \right). \quad (7.5)$$

Note there are two modes of shear in consecutive stripe domains for each value of  $\sin^2 \theta$ , that is  $\lambda_{xz}^{(+)}$  and  $\lambda_{xz}^{(-)}$  corresponding to director orientation angles  $+\theta$  and  $-\theta$  respectively. Before the deformation is applied ( $\lambda = 1$ ) one has  $\theta = \phi$ , the initial orientation of  $\mathbf{n}_0$ . When director rotation begins, the ‘positive’ domain of shear  $\lambda_{xz}^{(+)} > 0$ , in which the existing director pre-tilt  $\phi$  is in the same direction as the rotation can start its shear deformation continuously from  $\lambda_{xz} = 0$ . However, in order to form the ‘negative’ stripe with shear  $\lambda_{xz}^{(-)} < 0$  of opposite sense, it is necessary to overcome a barrier. Stripes with  $-\theta$  must jump to that state from the initial orientation  $+\phi$ . If the transition takes place immediately as  $\lambda$  exceeds 1, the jump in  $\lambda_{xz}^{(-)}$  takes the value (Verwey *et al.*, 1996):

$$\Delta \lambda_{xz}^{(-)}(\lambda = 1) = -\frac{2(r-1) \sin 2\phi}{r+1 + (r-1) \cos 2\phi}. \quad (7.6)$$

To satisfy the requirement of no net transverse displacement after traversing a pair of stripes, see Fig. 7.6, one needs the connection between the width,  $h$ , of stripes and their shear:

$$h_+ \lambda_{xz}^{(+)} + h_- \lambda_{xz}^{(-)} = 0. \quad (7.7)$$

Thus, as extension begins and  $\lambda_{xz}^{(-)}$  is effectively finite while  $\lambda_{xz}^{(+)}$  is still zero, then the ratio of stripe widths  $h_-/h_+ = -\lambda_{xz}^{(+)}/\lambda_{xz}^{(-)}$  must be zero and increase as  $\lambda$  is greater than 1. However, the relative width of the opposite stripe domains remains different – which would also be reflected in the different intensity of the two pairs of X-ray scattering lobes, cf. Fig. 6.10

The mean deformation is still without shear, on average, but is composed as a mean of the two soft deformations with modified weights, according to their relative volume in the system:

$$\begin{aligned} \underline{\underline{\lambda}} &= \begin{pmatrix} \lambda & 0 & 0 \\ 0 & 1 & 0 \\ 0 & 0 & 1/\lambda \end{pmatrix} = \frac{h_+}{h_+ + h_-} \begin{pmatrix} \lambda & 0 & \lambda_{xz}^{(+)} \\ 0 & 1 & 0 \\ 0 & 0 & 1/\lambda \end{pmatrix} + \frac{h_-}{h_+ + h_-} \begin{pmatrix} \lambda & 0 & \lambda_{xz}^{(-)} \\ 0 & 1 & 0 \\ 0 & 0 & 1/\lambda \end{pmatrix} \\ &\equiv \frac{1}{\lambda_{xz}^{(+)} - \lambda_{xz}^{(-)}} \left\{ \lambda_{xz}^{(+)} \underline{\underline{\lambda}}_{\text{soft}}(\lambda_{xz}^{(-)}) - \lambda_{xz}^{(-)} \underline{\underline{\lambda}}_{\text{soft}}(\lambda_{xz}^{(+)}) \right\} = \langle \underline{\underline{\lambda}}_{\text{soft}} \rangle_{\lambda_{xz}^{(\pm)}}. \end{aligned} \quad (7.8)$$

The quasi-convexified energy is volume-averaged over the energies of the two component distortions of  $\underline{\underline{\lambda}}$ :

$$F_{\text{QC}}(\underline{\underline{\lambda}}) = \frac{1}{\lambda_{xz}^{(+)} - \lambda_{xz}^{(-)}} \left\{ \lambda_{xz}^{(+)} F(\underline{\underline{\lambda}}_{\text{soft}}(\lambda_{xz}^{(-)})) - \lambda_{xz}^{(-)} F(\underline{\underline{\lambda}}_{\text{soft}}(\lambda_{xz}^{(+)})) \right\} = 0. \quad (7.9)$$

The deformation  $\underline{\underline{\lambda}} = \begin{pmatrix} \lambda & 0 & 0 \\ 0 & 1 & 0 \\ 0 & 0 & 1/\lambda \end{pmatrix}$  is still effectively soft since the  $F(\underline{\underline{\lambda}}_{\text{soft}}(\lambda_{xz}^{(\pm)}))$  both vanish, but the details of the microstructure are not as before – the volumes taken up by the two new types of  $\underline{\underline{\lambda}}_{\text{soft}}$  are now different and the interfacial structure problem is modified. The full problem is much more difficult than simply taking an initial director at an angle to the principal stretch. The third dimension becomes involved and sample shape as a whole plays an important role.

### 7.2.2 FULL QUASI-CONVEXIFICATION

So far we have only dealt with planar soft problems. The director has rotated in the  $zx$ -plane and hence there has been no  $y$ -relaxation:  $\lambda_{yy} = 1$ . We may need to make soft imposed deformations that are not restricted to this special value of  $\lambda_{yy}$ . For geometrical reasons (the ideal clamping), we so far only considered simple shears, whereas

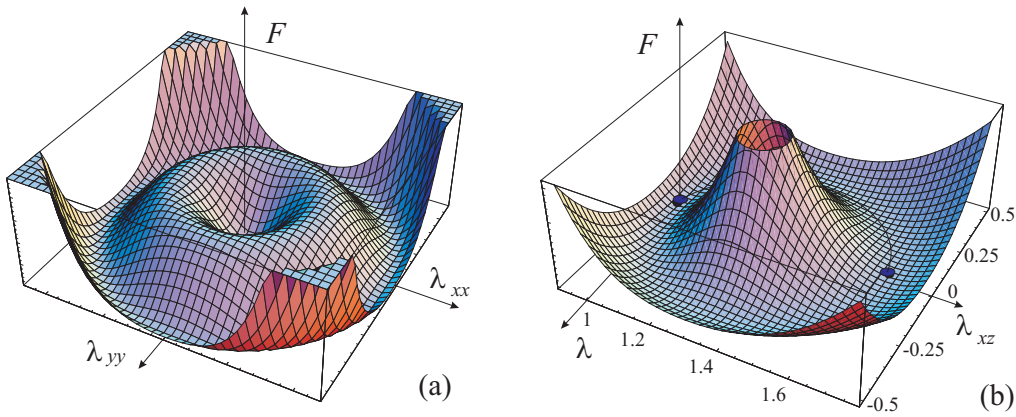


Figure 7.7: Schematic of the free energy density  $F$  against (a) simple extension in two directions perpendicular to  $\mathbf{n}$ , with no shear. At the centre is the minimum associated with no distortion. The minimal values at  $\lambda = \sqrt{r}$  corresponds to soft distortion associated with director rotation by  $90^\circ$ . The concave interval of  $F$  connecting the centre and the ring at  $\sqrt{r}$  can be flattened to zero by quasi-convexification via the creation of microstructure. An example of a continuous soft path around the barrier was given in Fig. 6.3. (b) Soft paths using the component deformations of eqn (7.2) are shown in a plot (S. Conti) using  $\lambda$  and  $\lambda_{xz}$  as variables (with the other in-plane strain  $1/\lambda$  not shown). Two dots and the connecting path correspond to the  $\lambda_{xz}(\lambda)$  curve in Fig. 6.7(b).

the full geometric representation of soft deformations, Fig. (6.3), tells us that more complex local strains may be needed, even for the planar problem. The quasi-convexification problem has been solved in complete generality for ideal nematic elastomers (DeSimone, 1999; DeSimone and Dolzmann, 2002) and applied in a numerical multiscale analysis of the response of a strip with realistic clamps and suffering extension (Conti *et al.*, 2002). Nematic elastomers admit of a fuller analysis of their soft deformations than Martensite and other crystalline transformation problems (Bhattacharya, 2003) since their soft modes are described by the continuous rotations of a director, rather than by discrete crystal symmetries. We sketch the philosophy of the quasi-convexification of nematic elastomers and then examine the response of samples with practical geometries.<sup>1</sup>

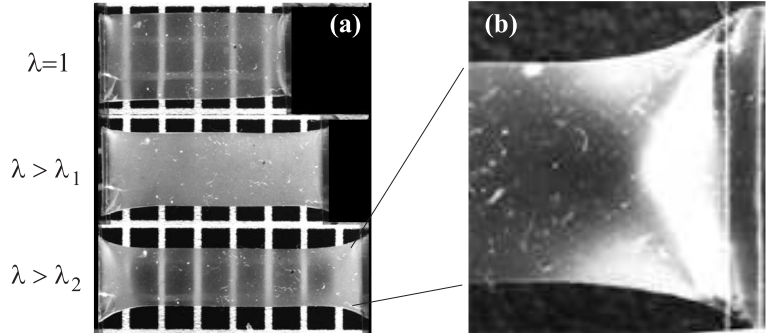
It is difficult to represent the free energy density, even schematically, since it is a function of eight variables (when deforming at constant volume). We attempt this in Fig. 7.7 where we display a free energy density as a function of externally applied extension  $\lambda$  in any of the two directions perpendicular to the initial  $\mathbf{n}$  (but with no shear). The energy has a central minimum at  $(\lambda_{xx}, \lambda_{yy}) = (1, 1)$  representing no distortion,  $F = 0$  on ignoring the  $3\mu/2$  constant. Without sympathetic shear relaxation, the free energy rises on distortion as it would in a classical elastomer. At simple extensions of  $\lambda = \sqrt{r}$  the free energy density is again naturally minimal; it is the rotated and again shear-free state of Fig. 6.1. These two states ( $\lambda = 1$  and  $\sqrt{r}$ ) have the same energy as the large space of soft deformed states which are generally of greater complexity than these simple extensions and contractions. Between the origin and the simple extension of  $\sqrt{r}$ , there is a finite energy cost  $F > 0$  since we do not allow shear in this scheme. It would be obvious in a depiction of  $F$  in higher dimensions that there are soft routes around this barrier, the cartoon of Fig. 6.3 offering one of an infinity of such routes that require shear. One can therefore replace this interval of concavity in  $F$  by  $F_{QC} = 0$  as in eqn (7.9). This introduces inhomogeneous microstructure of no elastic cost, as we have seen in the previous sections. Our earlier, simple examples of convexification corresponded to traversing along one axis only in Fig. 7.7. More complex geometry, including shears induced in more than one direction, is required to quasi-convexify  $F$  in all directions. Outside an ultimate distortion (at most an extension of  $\sqrt{r}$  applied perpendicular to the initial  $\mathbf{n}$ , and less for oblique directions) nothing more can be done – the director is fully aligned with the direction of principal stretch and no mechanism of soft deformation now exists: this elastically hard region is convex and cannot be quasi-convexified away. This is represented by the large strain regions of Fig. 7.7, but is of course much more complex in eight dimensions.

The need for the most general quasi-convexification can be seen from Fig. 7.5. With extension and transverse

<sup>1</sup>We are grateful to A. DeSimone and S. Conti for their help in the material of these sections.

contraction in the bulk of the sample, but not near the clamps, the sample develops curved edges and the local principal stretch is not uniformly along  $x$ ; examples of where this is so are indicated by arrows on the figure. In some regions, especially near the clamps, it may be impossible to find soft combinations of distortions at all – the free energy density may then be quartic or even harder, for instance if  $\lambda_{zz}$  is constrained to be  $\lambda_{zz} \sim 1$  near a completely rigid clamp. On the other hand, the obliquity of the local principal stretching direction may require shears for softness that do not demand inhomogeneous microstructural variation at all: there could be regions of soft response without stripes.

Figure 7.8: (a) The sequence of images illustrating the stretching of an elastomer film. The middle image shows the sample with stripe domains strongly scattering light, the bottom images shows the sample beyond the soft plateau, still retaining scattering regions near the clamps. (b) The expanded image of the clamp region (at  $\lambda > \lambda_2$ ), showing the complicated pattern of areas with local stripe microstructure.



One can see that the precise pattern of deformation depends on the macroscopic shape of the sample, in particular its aspect ratio (length to width ratio). Depending on this shape, oblique stripes will occur in different places at different macroscopic extensions (externally applied  $\lambda$ , distinguishing these from the local extensions in the material) and that the stripe pattern will shift spatially as extension continues. For instance, Fig. 7.8 shows an enhanced view of the clamp region of an elastomer that was stretched well beyond the end of the soft plateau denoted by  $\lambda_2$ , which was determined as  $\lambda_2 = \sqrt{r}\lambda_1$  in Sect. 6.4; however, there are several regions where the stripes remain (seen as white areas, strongly scattering light, in contrast to the transparent areas of uniformly aligned nematic director). If there is a continuous path of regions across the sample that can deform softly, then they will do so first until sufficient are exhausted that the path of soft regions across the sample is broken. The macroscopically soft response will harden due to the non-soft regions through which stress can now pass. Thereafter, other regions of the sample that did not initially have softness available to them will also start deforming. In doing so there is a change of geometry and it is possible that some other regions can then start deforming softly while others are deforming non-softly. Hard and soft deformations can coexist whenever there is a path of non-soft deforming material along the sample so that there is an ultimate continuity of force transmitted along the sample.

### 7.2.3 NUMERICAL AND EXPERIMENTAL STUDIES

A numerical solution of strip elongation (Conti *et al.*, 2002) reveals the non-uniformities that arise because of the clamp constraints and which are intensified when soft deformations in the bulk come to their end. In Fig. 7.9 they show the force against deformation for an ideal elastomer. The ‘affine curve’ corresponds to a model case where no clamp effect is exerted on the stretched elastomer sample. Naturally there is no force until director rotation is complete at  $\lambda_2 = \sqrt{r}$  with  $\theta = \pm\pi/2$ , depending on which stripe one is in. The clamped sample with aspect ratio of 3 can get closer to the ideal soft cut off than that with the aspect ratio = 1 (the square shape), since the former has a relatively smaller volume fraction influenced by the constraints exerted by the clamps. A salutary lesson emerges – the apparent length of the soft region is a function of the macroscopic aspect ratio of the sample. Fortunately experiments discussed before, Sect. 6.4.1, were carried out on samples with large aspect ratios, long rubber strips with aspect ratio  $\sim 10$ -12. This sensitivity to aspect ratio was explored in experiments (Zubarev *et al.*, 1999) and revealed a spatial distribution of microstructure that depended on strain differently in samples of different aspect ratios.

As we have seen in Fig. 7.8, when samples are stretched beyond the onset of hard response,  $\lambda > \lambda_2$ , the stress patterns are non-trivial, especially near the clamps. Figure 7.10 shows larger stresses diagonally towards

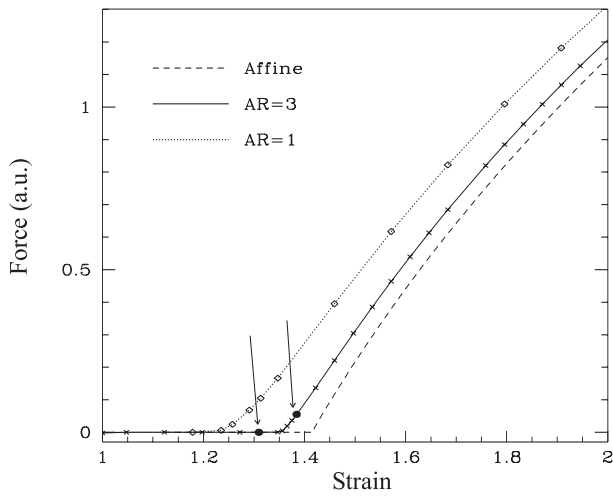


Figure 7.9: Force against extension calculated numerically for an 'affine' sample, with no clamp effect, and for clamped samples of aspect ratio (AR) of 3 and 1, respectively. The anisotropy parameter was taken  $r = 2$ . The two arrows point at the specific extensions examined in Fig. 7.12.

the corners and much less in the central clamp regions, as anticipated in Fig. 7.5. The macroscopic shape is also



Figure 7.10: Spatial distribution of stress is indicated by levels of shading in a sample with  $r = 2$ , of initial aspect ratio = 3, stretched to  $\lambda = 1.38$ , see Fig. 7.9.

rather different from that of a classical elastomer undergoing the same macroscopic extension. The edges near the clamps tend much more directly and with less curvature to the central, straight region. This is a consequence of the microscopic constitutive relation and its macroscopic quasi-convexified form (Conti *et al.*, 2002).

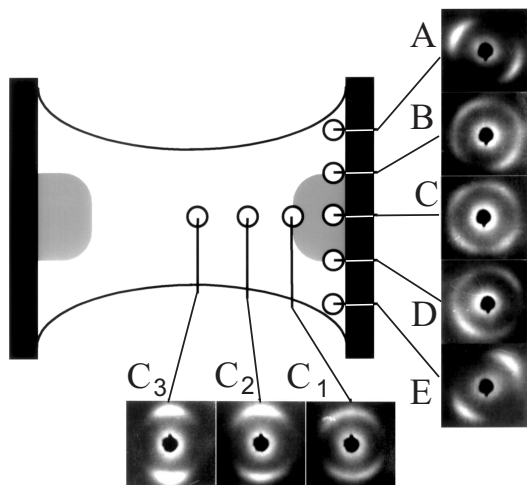
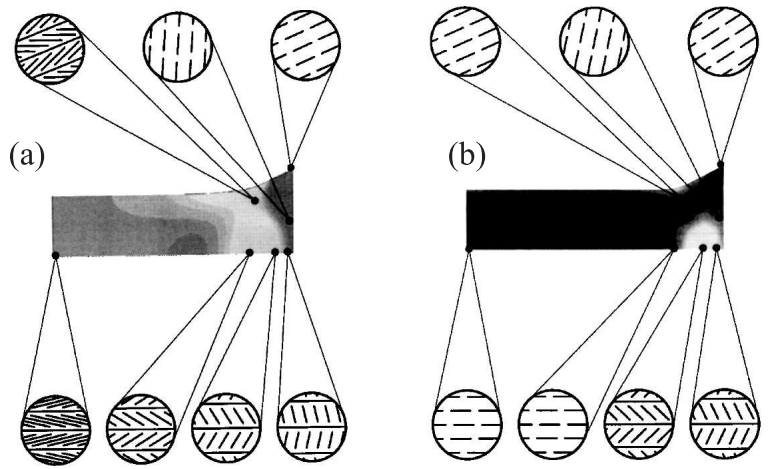


Figure 7.11: Different labelled regions of an extending nematic elastomer with their correspondingly labelled X-ray patterns, indicating the local director orientation.

Inhomogeneous microstructure is evident not only by direct microscopic observation, but also through X-ray scattering. Since the beam area is generally large compared with the width of individual stripes, of several microns, both nematic directions are revealed in the somewhat averaged picture. Figure 7.11 shows X-ray patterns taken from different regions of a sample at a fixed extension (Zubarev *et al.*, 1999). Central regions of the rubber strip (points  $C_2$  and  $C_3$ ) already have their director rotation complete. In the fringes of the clamp region,

where microstructure still exists, point  $C_1$ , the rotation within stripes is not quite complete and so the maxima associated with the directors in neighbouring stripes are not quite coincident, leading to an apparently broadened nematic azimuthal distribution of scattered X-ray intensity. The extreme regions A and E along the rigid clamp have the directors pointing along the maximum extension directions, that is towards the corners and there is no microstructure. At the middle-point C, there are still fully developed stripes with directors at  $\pm\pi/4$  to the extension direction,  $x$ , and thus four azimuthal maxima (see for comparison Fig. 6.10). The X-ray pattern is that of two nematics with orthogonal directors. B and D represent more oblique regions. The distribution of extension and microstructure emerges from the numerical solution of the problem. Figure 7.12(a) shows the microstructure of the top right hand quarter of a stripe with the type of patterns developing at different places shown as insets. The deformation is still soft overall (determined by the stress needed to deform the central region). Closer to the clamp there is reaction but still not hardness at this value  $\lambda = 1.31$ , see Fig. 7.9.

Figure 7.12: Numerical calculations of the distribution of microstructure in a sample of aspect ratio = 3, stretched to (a)  $\lambda = 1.31$ , and (b)  $\lambda = 1.38$ , these strains being labelled in Fig. 7.9. Levels of shading indicate the extent of microstructural development. Director rotation in the stripes at the central clamp region is less than in the bulk which in (a) is undergoing essentially unconstrained soft deformation with the expected director rotation. In (b) the rotation in the bulk is clearly complete and the director apparently uniformly points along  $x$ .



Beyond the hard threshold at  $\lambda = 1.38$ , see Fig. 7.12(b), the director rotation at points along the centre of the sample (bottom of the figure) is as found in experiment, Fig. 7.11. Where the director rotation is complete, that is at  $\theta = \pm\pi/2$ , one might expect a homogeneous director distribution since in a nematic  $\theta = \pi/2$  is equivalent to that at  $\theta = -\pi/2$ . However, neighbouring stripes are separated by narrow inhomogeneous walls. Within such walls there must be directors of intermediate angle that take the director field from  $\theta = \pi/2$  to  $\theta = -\pi/2$  and *vice versa* on making the transition from stripe to stripe. A uniform nematic texture can be made to appear completely dark under suitably oriented cross polarisers. With a dark background, any possible remaining regions of deviating director will appear very bright and will be detected with great sensitivity. One could indeed see bright, unresolvably thin lines where the separation walls between stripes used to be, that were probably the director traversing between the equivalent states  $\theta = \pm\pi/2$  over a short distance,  $w \sim \xi$ , this volume of sample then not being dark under the polarisers.

The effect of initial sample aspect ratio has been seen in the force extension curves, Fig. 7.9, and has also been visualised in experiment. In a square sample (AR=1) one first finds pronounced stripe regions in the middle (the region of highest local extension), which then grow and migrate across the sample towards the clamps, as strain develops (Zubarev *et al.*, 1999). This is qualitatively the sequence of results seen in the numerical solution (Conti *et al.*, 2002), of which Fig. 7.12 (a) and (b) are examples at two strains.

## BIBLIOGRAPHY

---

- Abramchuk, S.S. and Khokhlov, A.R. (1987). *Doklady Akad. Nauk SSSR (Doklady Phys. Chem.)*, **297**, 385. 37
- Ahir, S.V., Tajbakhsh, A.R., and Terentjev, E.M. (2006). *Adv. Func. Mater*, **16**, 556. 39
- Arrighi, V., Higgins, J.S., Weiss, R.A., and Cimecioglu, A.L. (1992). *Macromolecules*, **25**, 5297. 17
- Atkins, R.J. and Fox, N. (1980). *An Introduction to the Theory of Elasticity*. Longman, London. 32
- Ball, J.M. and James, R.D. (1992). *Phil. Trans. Roy. Soc. London A*, **338**, 389. 59
- Ball, R.C., Doi, M., Edwards, S.F., and Warner, M. (1981). *Polymer*, **22**, 1010. 17
- Bhattacharya, K. (2003). *Microstructure of Martensite*. Oxford University Press. 63, 65
- Biggins, J. S., Terentjev, E. M., and Warner, M. (2008). *Phys. Rev. E*, **78**, 041704. 55
- Chandrasekhar, S. (1977). *Liquid Crystals*. Cambridge University Press, Cambridge. 7
- Chang, C.-C., Chien, L.-C., and Meyer, R.B. (1997). *Phys. Rev. E*, **56**, 595. 59
- Clarke, S.M., Hotta, A., Tajbakhsh, A.R., and Terentjev, E.M. (2001). *Phys. Rev. E*, **64**, 061702. 38, 57
- Conti, S., DeSimone, A., and Dolzmann, G. (2002). *J. Mech. Phys. Solids*, **50**, 1431. 60, 65, 66, 67, 68
- Corbett, D. and Warner, M. (2006). *Phys. Rev. Lett.*, **96**, 237802. 41
- Cotton, J.P. and Hardouin, F. (1997). *Prog. Polym. Sci.*, **22**, 795. 22
- Cviklinski, J., Tajbakhsh, A.R., and Terentjev, E.M. (2002). *Eur. Phys. J. E*, **9**, 427. 41
- d'Allest, J.F., Maissa, P., ten Bosch, A., Sixou, P., Blumstein, A., Blumstein, R.B., Teixeira, J., and Noirez, L. (1988). *Phys. Rev. Lett.*, **61**, 2562. 21, 22
- de Gennes, P.-G. (1969). *Phys. Lett.*, **A28**, 725. 37
- de Gennes, P.-G. (1979). *Scaling Concepts in Polymer Physics*. Cornell University Press, Ithaca, N.Y. 15
- de Gennes, P.-G. (1982). In *Polymer Liquid Crystals* (ed. A. Ciferri, W. Krigbaum, and R. Meyer). Academic Press, New York. 45
- de Gennes, P.-G. and Prost, J.P. (1994). *The Physics of Liquid Crystals*. Oxford University Press, Oxford. 7, 9, 12, 13
- Deam, R.T. and Edwards, S.F. (1976). *Phil. Trans. Roy. Soc. A*, **280**, 317. 17
- DeSimone, A. (1999). *Ferroelectrics*, **222**, 275. 60, 65
- DeSimone, A. and Dolzmann, G. (2002). *Arch. Rational Mech. Anal.*, **161**, 181. 65
- Doi, M. and Edwards, S.F. (1986). *Theory of Polymer Dynamics*. Clarendon Press, Oxford. 15
- Eisenbach, C.D. (1978). *Makromol. Chem.*, **179**, 2489. 41
- Finkelmann, H., Greve, A., and Warner, M. (2001a). *Eur. Phys. J. E*, **5**, 281. 38
- Finkelmann, H., Nishikawa, E., Pereira, G.G., and Warner, M. (2001b). *Phys. Rev. Lett.*, **87**, 015501. 40
- Flory, P.J. (1953). *Principles of Polymer Chemistry*. Cornell University Press, Ithaca. 15, 16
- Flory, P.J. (1969). *Statistical Mechanics of Chain Molecules*. Interscience Publishers, N.Y. 15

- Golubovic, L. and Lubensky, T.C. (1989). *Phys. Rev. Lett.*, **63**, 1082. 38
- Gramsbergen, E.F., Longa, L., and de Jeu, W.H. (1986). *Phys. Rep.*, **135**, 195. 11
- Hiraoka, K., Sagano, W., Nose, T., and Finkelmann, H. (2005). *Macromolecules*, **38**, 7352. 6
- Hogan, P.M., Tajbakhsh, A.R., and Terentjev, E.M. (2002). *Phys. Rev. E*, **65**, 041720. 40
- Horn, R.A. and Johnson, C.R. (1991). *Topics in Matrix Analysis*. Cambridge University Press, Cambridge. 32
- Hornreich, R.M. (1985). *Phys. Lett. A*, **109**, 232. 11
- Kundler, I. and Finkelmann, H. (1995). *Macromol. Chem. Rap. Commun.*, **16**, 679. 58
- Kundler, I. and Finkelmann, H. (1998). *Macromol. Chem. Phys.*, **199**, 677. 62
- Küpfer, J. and Finkelmann, H. (1991). *Macromol. Chem. Rap. Commun.*, **12**, 717. 39
- Küpfer, J. and Finkelmann, H. (1994). *Macromol. Chem. Phys.*, **195**, 1353. 57
- Lacey, D., Beattie, H.N., Mitchell, G.R., and Pople, J.A. (1998). *J. Mater. Chem.*, **8**, 53. 39
- Landau, L.D. and Lifshitz, E.M. (1986). *Theory of elasticity*. Pergamon Press, Oxford. 10, 28
- Lecommandoux, S., Noirez, L., Achard, M.F., and Hardouin, F. (1997). *J. de Phys. II*, **7**, 1417. 22
- Lubensky, T.C., Mukhopadhyay, R., Radzikhovsky, L., and Xing, X. (2002). *Phys. Rev. E*, **65**, 011702. 26, 48
- Mitchell, G.R., Davis, F.J., and Guo, W. (1993). *Phys. Rev. Lett.*, **71**, 2947. 43
- Nishikawa, E., Finkelmann, H., and Brand, H.R. (1997). *Macromol. Rap. Commun.*, **18**, 65. 6
- Ogden, R. W. (1972). *Proc. Roy. Soc. A*, **326**, 565. 27
- Ohm, H.G., Kirste, R.G., and Obertur, R.C. (1988). *Macromol. Chem.*, **189**, 1387. 22
- Olmsted, P.D. (1994). *J. de Phys. II*, **4**, 2215. 45
- Percec, V. and Kawasumi, M. (1991). *Macromolecules*, **24**, 6318. 21
- Plate, N.A. and Shibaev, V.P. (1987). *Comb-Shaped Polymers and Liquid Crystals*. Plenum Press, New York. 21
- Popov, Y.O. and Semenov, A.N. (1998). *Eur. Phys. J. B*, **6**, 245. 54
- Skačej, G. and Zannoni, C. (2006). *Eur. Phys. J. E*, **20**, 289. 59
- Stephen, M.J. and Straley, J.P. (1974). *Rev. Mod. Phys.*, **46**, 617. 10
- Tajbakhsh, A.R. and Terentjev, E.M. (2001). *Eur. Phys. J. E*, **6**, 181. 39
- Terentjev, E.M., Warner, M., and Bladon, P. (1994). *J. de Phys. II*, **4**, 667. 59
- Verwey, G.C. and Warner, M. (1997a). *Macromolecules*, **30**, 4189. 54
- Verwey, G.C. and Warner, M. (1997b). *Macromolecules*, **30**, 4196. 54
- Verwey, G.C., Warner, M., and Terentjev, E.M. (1996). *J. de Phys. II*, **6**, 1273. 52, 55, 60, 63, 64
- Warner, M. (1999). *J. Mech. Phys. Solids*, **47**, 1355. 48
- Warner, M., Gelling, K.P., and Vilgis, T.A. (1988). *J. Chem. Phys.*, **88**, 4008. 37
- Warner, M. and Mahadevan, L. (2004). *Phys. Rev. Lett.*, **92**, 134302. 41

Warner, M. and Terentjev, E. M. (2007). *Liquid Crystal Elastomers* (Revised, paperback edition edn). Oxford. 1, 7

Yu, Y., Nakano, M., and Ikeda, T. (2003). *Nature (London)*, **425**, 145. 41

Zubarev, E.R., Kuptsov, S.A., Yuranova, T.I, Talroze, R.V., and Finkelmann, H. (1999). *Liq. Cryst.*, **26**, 1531. 62, 66, 67, 68